UNIVERSITY OF SALERNO

DEPARTMENT OF CHEMISTRY AND BIOLOGY

and

UNIVERSITY OF BASILICATA

DEPARTMENT OF SCIENCE

PhD in Chemistry XXXII Cycle

CHIM/01- Analytical Chemistry

Development and optimization of analytical methods for the analysis of drugs in wastewater samples and chronic aquatic toxicity assessment of the Crustacea Copepoda *Tigriopus fulvus*

PhD Coordinator
Prof. Riccardo Zanasi

Tutor
Prof. Giuliana Bianco

PhD Student
Donatella Coviello

Co-Tutor
Dr. Michela Contursi

Dr. Ermelinda Prato

Dr. Antonio Vassallo

Academic year 2018-2019

Index

List of abbreviation

ASA Acetylsalicylic acid

BE Betaine

CMEs Chemical modified electrodes

CV Cyclic voltammetry

DPV Differential pulse voltammetry

ESI Electrospray ionization

GC Glassy carbon

GO Graphene oxide

HPLC High performance liquid chromatography

IBU Ibuprofen

LTQ Linear trap quadrupole

MS Mass spectrometry

MS/MS Tandem mass spectrometry

NIM Nimesulide

NSAID Non steroidal antiinflammatory drugs

PRX Piroxicam

PA Paracetamol

PVA Polyvinyl alcohol

RPLC Reverse phase liquid chromatography

SEM Scanning electron microscopy

SPE Solid phase electrode

SRM Selected reaction monitoring

XPS X-ray photoelectron spectroscopy

Abstract

Pharmaceutical compounds constitute one of the most important emerging classes of environmental pollutants. Recent studies have discovered their occurrence in environmental samples investigated worldwide, including different types of aqueous matrices. Drugs may be released into water sources and in the effluents from poorly controlled manufacturing or production facilities. In addition, the ubiquitous use of drugs has resulted in their relatively continuous discharge into wastewater, but conventional urban wastewater treatment plants (WWTPs) are not able to efficiently remove most of these pollutants. Thus, pharmaceuticals in surface waters, groundwater and treated water have relatively low concentrations ranging from ng/L to µg/L. This work has the purpose of exploring electrochemical and liquid chromatographic-mass spectrometric techniques for the analysis of several Pharmaceutical and Personal Care Products (PPCPs) and to assess the toxicological effects that some of these drugs have on aquatic organisms, such as *Tigriopus fulvus* (crustacea).

First phase of this study (Part A) covered the development together with electrochemical and spectroscopic characterization of new modified electrodes, i.e. glassy carbon/graphene oxide/polyvinyl alcohol (GC/GO/PVA) and glassy carbon/Betaine/Platinum (GC/BE/Pt) electrodes.

In the Part A of this work two modified electrodes, the first one based on polyvinyl alcohol (PVA) structured with particles of oxidized graphene (GO), and the second one on betaine-Pt on glassy carbon, were developed and characterized by voltammetric and spectroscopic techniques.

Two electrodes were morphologically characterized by Scanning Electron Microscopy (SEM) and superficially by X-Ray Photoelectron Spectroscopy (XPS). Furthermore, in order to evaluate the electroanalytical performance, the new electrode systems have been tested with the selected drugs.

Cyclic voltammetry (CV) and differential pulse voltammetry (DPV), showed that both electrodes have a good response if compared to simple glassy carbon electrodes.

Second phase (Part B) is related to the optimization and validation of an HPLC-MS/MS method for the determination of amoxicillin, erythromycin, clarithromycin, omeprazole, metformin, carbamazepine, acetylsalicylic acid, ibuprofen, diclofenac, naproxen, estradiol and ethinylestradiol in wastewater samples. Firstly, mass spectrometric parameters i.e. ionization mode, capillary temperature, capillary potential and CID energy for tandem mass analysis were optimized. Then, chromatographic parameters, i.e. selection of the chromatographic column, eluents, gradient and flow rate were optimized. Finally, the developed and optimized method has been validated for the analysis of the selected twelve drugs in wastewater samples.

Good linearity (coefficient of determination more than 0.993) and limits of detections in the range 0.0001 µg/L ÷ to 0.7211 µg/L were obtained. No significant matrix effect, evaluated by post extraction addition, was observed. Then, this methodology has been successfully applied to environmental study of pharmaceutical residues occurring in influent and effluent wastewater samples, from the main wastewater treatment plant in Potenza (Basilicata, Southern Italy), showing that for some drugs the purification process is not sufficient to degrade and remove them from the water matrix.

Finally, toxicological effects tests have been carried out to evaluate the effects that carbamazepine and amoxicillin have on aquatic organisms, such as *Tigriopus fulvus* (crustacea). Chronic test of 28 days was carried out on two subsequent generations of *T. fulvus* at a drug concentration actually found in the wastewater samples, i.e. 5 µg/L and 2 µg/L, for carbamazepine and amoxicillin, respectively. The results of the test show that no significative toxic effect of amoxicillin on the first generation of *T. fulvus* was observed, while carbamazepine effects on the number of broods were relevant. Concerning the second generation, amoxicillin once again appears to give no visible toxic effect, while carbamazepine shows toxic effects not only on the number of broods, but also on the number of total nauplii generated. Based on these results, carbamazepine could be considered a potential endocrine disruptor since a delayed reproduction and a reduced fecundity in *T. fulvus* was observed.

Introduction

Pharmaceutical and Personal Care Products (PPCPs) constitute a class of emerging pollutants [1] with high potential to cause harmful effects on the environment and human health. The excessive production of drugs and the increasing consumption of the latter have meant that drug pollution turns out to be one of the problems to be solved in the environmental pollution, especially in water pollution [2]. In detail, it is necessary to keep the pollution of the water under control because drugs are released into the sewage systems and transported to domestic wastewater treatment plants. Indeed, dangerousness of these substances is due to inefficacy of wastewater purification plants to purify water from these molecules; therefore, once they enter the water circle these substances have complete access to every environmental compartment, creating huge problems not only to the flora and to the marine fauna [3-6], but through processes of biomagnification and bioaccumulation also to humans [6,7]. This work has the purpose of exploring electrochemical and liquid chromatographic-mass spectrometric techniques for the analysis of several PPCPs and to assess the toxicological effects that some of these drugs have on aquatic organisms, such as *Tigriopus fulvus* (crustacea).

First phase of this study (Part A) covered the development and electrochemical and spectroscopic characterization of new modified electrodes for the detection of some drugs as paracetamol, ibuprofen, nimesulide, acetylsalicylic acid, piroxicam, vitamin B_1 and vitamin B_6.

Second phase (Part B) is related to the optimization and validation of an HPLC-MS/MS method for the determination of amoxicillin, erythromycin, clarithromycin, omeprazole, metformin, carbamazepine,

acetylsalicylic acid, ibuprofen, diclofenac, naproxen, estradiol and ethinylestradiol in wastewater samples.

Finally, to generate informations on the ecological risks on marine organisms, the chronic effects of two drugs carbamazepine and amoxicillin, alone and in combination, were evaluated across two generations of the Crustacea Copepoda: *Tigriopus fulvus*. These two molecules have been chosen firstly because they are present in wastewater sample analyzed and secondly due to their important pharmacological function, indeed, the first is an antiepileptic, while the second one is an antibiotic, which leads them to be among the drugs most consumed by humans.

References

[1] M. Gavrilescu, K. Demnerovà, J. Aamand, S. Agathos, F. Fava, New biotechnology, 32 1 (2015) 147.

[2] M. Gros, M. Petrovió, D. Barceló, Talanta, 70 4 (2006) 678.

[3] A. J. Ebele, M. Abou-Elwafa Abdallah, S. Harrad, Emerging Contaminants, 3 1 (2017) 1.

[4] C. Mimeault, A. J. Woodhouse, X. S. Miao, C. D. Metcalfe, T. W. Moon, V. L. Trudeau, Aquat. Toxicol. 73 (2005) 44.

[5] G. Vernouillet, P. Eullaffroy, A. Lajeunesse, C. Blaise, F. Gagne, P. Juneau, Chemosphere, 80 (2010) 1062.

[6] Società italiana medicina ambientale “Farmaci e ambiente: l’Ecofarmacovigilanza nel contesto globale.

[7] X. Wu, J. L. Conkle, F. Ernst, J. Gan., Environ. Sci. Technol., 48 (2014) 11286.

Part A

Development and characterization of new electrode materials for the detection of some drugs

This part of the work was developed under the supervision of Prof. I. G. Casella† (*26/10/1959 †04/02/2018) until January 2018.

1. Introduction

The electrode materials based on transition metals, their alloys and / or their oxides-hydroxides are wide used as electrode active materials in various sectors of technologies such as: sensors [1-4], electrochromic devices [5-7], devices for electric condensers [8-10], electrocatalysis systems in heterogeneous phase [11-15], and systems for corrosion prevention [16-18], etc. In the last few years different electrode materials have been developed, through different strategies and with interesting characteristics such as: high degree of electrical conductivity, chemical and electrochemical stability, good charge capacity. Generally, these materials are composed of oxides / hydroxides of Pt, Pd, Ir, Au, Ni, Cu, Co, Rh, Ag, etc., both in single form and in combination between them. Among the different possibilities of film preparation with metal and / or their oxides (sputtering processes, vacuum evaporation, fusion, adsorption, etc.), a significant role is played by the electrochemical deposition procedures, both in anodic and cathodic condition [19]. These electrochemical procedures allow to modulate the composition of the film through the different experimental control variables such as: potentials (E), currents (I), waveforms (E / I) and types of pulse applications (pulsed depositions), times of electrolysis, as well as the composition and pH of the medium. It is also important to be able to design a film with specific morphological characteristics (ie, roughness, shapes and dimensions of the deposit, etc.), modulating not only the applied potential and / or current, but also the temporal methods of application, or use pulsed procedures, which offer wide modulation limits of the surface concentration profile of the species involved in the process. Generally, in electrocatalysis and in particular in electroanalysis, not only the catalytic activity of a specific electrode

material is important, but also the degree of stability of the system over time. In particular in electroanalysis, often due to problems of "surface poisoning" caused by the irreversible absorption of reagents and / or intermediates / reaction products, the amperometric response is subject to poor temporal reproducibility and / or undesirable "memory" effects of the sensor. For this reason, it is necessary to propose electrode materials with marked "anti-poisoning" characteristics, i.e. capable of obtaining constant electrocatalytic performance over time. In order to minimize these passivating phenomena, in the last decades pulsed amperometric strategies have been defined that are able to deal with these undesirable phenomena with sufficient success [20]. At the same time, the availability of electrode systems with good catalytic capacities and adequate anti-poisoning properties is as important as the intrinsic characteristics of the active electrode material and its physical structure. In this sense an intense scientific activity has been developed to obtain both chemical and physical modification of the traditional electrode surfaces based on Au, Pt, Ag (i.e. metallic "bulk") or graphites, through the introduction of electroactive materials consisting of one or more catalytic units (chemically modified electrodes, CMEs) [21,22].

The introduction of multi-dispersed electrocatalytic units in supportive polymeric structures represents another trend of considerable interest; indeed, the concrete possibility of effectively dispersing catalyst particles in three-dimensional (3D) structures represents an essential element about the catalyst's ability to act. Often electrocatalytically active units have been deposited or simply dispersed in both synthetic and natural organic polymers (ie, polypyrroles, polythiophenes, polyanilines, polyaminophenols, nafion, tossflex, PVC, PET, etc.) and characterized as materials of electrochemical interest [21-28]. Many

polymeric structures, in addition to exerting a purely structural character, perform a perm-selective role, thanks to their ionic character, modulating the overall electrochemical behavior of the electrode material in study [27,28]. Thus in the field of electroanalysis, ionic polymeric structures allow to introduce significant elements of analytical selectivity [21, 22, 27,28]. An important and current category of polymeric materials is based on "molecular print technologies" defined as "molecular imprinting electrodes" (MIP), which seem to offer important selectivity contributions in the logic of the new frontiers of CMEs [21, 22, 29, 30]. Following the proposal and characterization of nano-particle electroactive materials, some nanostructured graphite structures (ie, nanotubes, graphenes, etc.) such as single walled carbon nanotubes (SWCNT), multiwalled carbon nanotubes (MWCNT), graphites variously oxidized, etc. have found great interest in different applied technologies [21, 22, 31-34]. In this sense, the current frontiers of research in the study and proposition of new materials of electrochemical interest are directed to the use of carbon-based nanomaterials, where the combination with metal electrocatalysts and polymeric-based supports find wide applicative interests both in the field of purely scientific knowledge than in advanced technologies [35,36,37].

The aim of the first part (Part A) of the present work of thesis concerns the definition of strategies of preparation and characterization of innovative electrode materials of potential interest in various applied technologies, and environmental, pharmaceutical and biological fields. The electrodes, that we developed, have been named: GC/GO/PVA and GC/BE/Pt. To obtain these electrodes we used two different techniques of preparation of CMEs. The electrode GC/GO/PVA was prepared by casting method on glassy carbon electrode (GC); while GC/BE/Pt

electrode was prepared by electrodeposition of Pt particle on a modified graphitic substrate, through an electro-reduction process of Na_2PtCl_6 solution. The behaviour of these electrodes has been studied in detail both from the electrochemical and morphological point of view. Attention was paid to the electroanalytical/amperometric characterization of the sensors concerning the electro-oxidation of some molecules of biological-pharmacological interest. Particularly, GC/GO/PVA was characterized in neutral medium, as electrochemical catalyst for several analgesics drugs. More attention has been devoted to electrocatalytic activities of GC/BE/Pt modified electrode in the electrooxidation of vitamin B group in strong acidic medium.

1.1 Polyvinyl alcohol (PVA)

Polyvinyl alcohol $(C_2H_4O)_n$, (PVA), whose chemical structure is shown in figure 1.1, is a polymer consisting of a chain of carbon atoms to which hydroxyl groups are bound. The presence of this hydroxyl group is responsible for the formation of hydrogen bonds allowing this polymer to assume a significant polar characteristic [38].

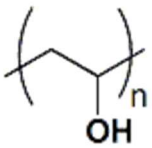

Figure 1.1: Chemical structure of PVA.

PVA is a white granular powder, soluble in water, insoluble in various organic solvents and capable of maintaining most of its properties when subjected to heat treatments (> 100°C) [39]. It has a density of 1.19-1.3 g/l, a melting temperature of 230°C and a flame temperature of 75°C.

This polymer has an important biocompatible character, it is used in medicine to perform sutures [40], in surgical sponges, in catheter coatings, to develop implants for the replacement of degraded hyaline cartilage following osteoarthritis, for the development of meniscal prostheses [41] and for the development of tissues necessary for the construction of heart valves [42]. PVA also has a moderate nature of biodegradability [41]. It is also used with various chemotherapeutic agents in order to improve the pharmacokinetics of the active ingredient [43] and when added to enzymatic histochemical incubation it allows an accurate localization of the enzymatic activity in the cell [44]. In contactology it is used in the manufacture of contact lenses and tear drops [45], since it is able to form a distributed and persistent aqueous film on the cornea. Other applications concern the pharmaceutical and cosmetic fields, in which it is used in cleaning creams, shaving creams and facial masks [46]. Its use also extends to other sectors such as textiles, construction, packaging, automotive, adhesive and paper production industries. In particular it is used in textiles for the production of non-wovens in which the fibers have randomly oriented structures; some examples are found in the manufacture of bags and surgical gowns [46]. In the construction industry it is used as a reinforcement of cements and concretes [46]. From the PVA can be manufactured containers for oils, greases, paints and to protect some metals from aggressive gases [46]. In the automotive industry it is used as a reinforcement in tires and as a precursor of polyvinyl butyral (PVB), which is used in the manufacture of automotive safety glasses [46]. It is also used for the production of various types of paper, such as coated, release and inkjet [39], while in the production of adhesives it serves as a thickener in different types of glues [47].

1.2 Graphene oxide (GO)

Graphene is a two-dimensional allotropic form of carbon, consisting of a hexagonal lattice structure, defined as a honeycomb, in which the distance C - C is 1.42 Å, that is in a single lattice all the carbon atoms are sp^2 hybridized. Graphene is the structure at the base of all the other graphitic allotropic carbon states, such as graphite, nanotubes and fullerene [48], represented in figure 1.2.

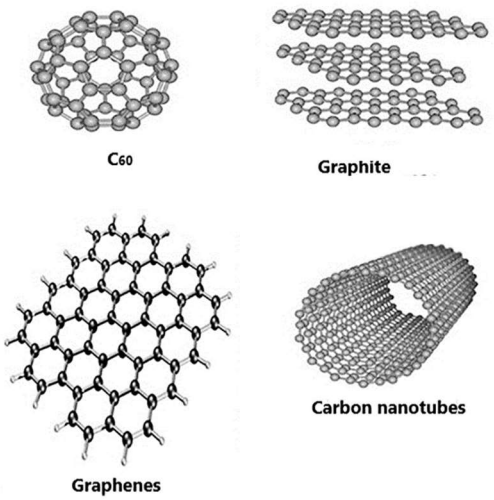

Figure 1.2: Graphitic allotropic forms of carbon.

The discovery of graphene took place in 2004 and allowed the two physicists A. Gejm and K. Novoselov to win the Nobel Prize in Physics in 2010. This material has the mechanical strength of the diamond and the flexibility of plastic materials. It is currently considered a valid basic element in "post-silicon" electronics. Potential applications include, among other things: electronics (eg flexible "touch screen" displays), storage and power generation (eg solar cells, batteries, supercapacitors, etc.), sensors and devices in the medical field [49]. Generally, GO is

obtained through two steps: graphite oxidation to obtain graphite oxide and then, exfoliation processes to obtain lamellar layers or "simple layer" sheets of GO. There are four types of oxygenated functional groups present on the lattice: epoxide (-O-), hydroxide (-OH), carbonyl (C = O) and carboxyl (-COOH); generally the first two are on the basal plane, while the other two are on the edges of the lamella [50]. An example of GO is shown in figure 1.3.

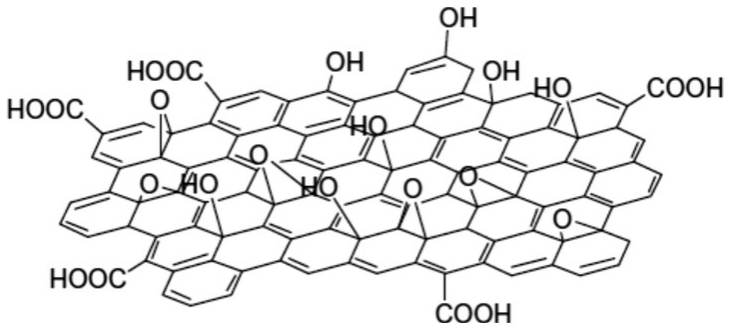

Figure 1.3: Example of graphene oxide (GO).

The increase in the interlamellar distance (with respect to graphite) leads to a decrease in the attractive forces between the lamellas accentuated by the decrease in electronic currents, indeed, the carbon atoms linked to oxygen present a state of intermediate hybridization between sp^2 and sp^3. The conjugate system typical of graphite is responsible for high conductivity (~ 100 S/cm in graphite) and therefore the presence of oxygen atoms leads to a decrease in the conductivity itself. The GO can behave as a conductor for low oxygen contents, as an insulating species with high oxidation (theoretical maximum of 50%), or as a semiconductor for the latter intermediate levels. The oxygen atoms assume a partial negative charge; therefore, it is possible to classify as

an extrinsic p-doped semiconductor. The loss of regular distance of the lamellas also cause the loss of metallic brightness typical of graphite.
The applications of the GO are varied; in dentistry it is used as a bacteria inhibitor [51], in the oncology sector it is used because it is able to neutralize cancer stem cells, without damaging healthy ones. Recent studies suggest that GO is able to inhibit the formation of "ball-tumors" in breast, pancreas, lung, brain, ovary and prostate cancer. It has been observed that the GO leaflets prevent cancer stem cells from forming tumors – sphere [52]. In addition, the GO, if properly functionalized, can be used for the transport of chemotherapy drugs to target organs [53]. Unlike graphene and CNTs, the GO has an easy dispersibility in water as in other organic solvents, due to the presence of oxygen atoms. For this reason, it is able to disperse in the aqueous medium, so it can act as a surfactant and allow insoluble materials to be dispersed rather than forming aggregate structures [54]. This material is less conductive but more transparent than graphene, so it can be better used for the production of transparent conductive films, in fact it can be deposited essentially on any substrate assuming a conducting character. This kind of coating is used in "flexible" electronics, in solar cells, in liquid crystal devices, in chemical sensors and as a substitute for ITO (Indium tin-oxide), currently used for touch screens. The GO combined with polymers forms nanocomposites, causing a change in the properties of the starting polymer. Thanks to its extensive surface area this material is to be considered useful as electrode material in batteries and double-lattice capacitors, in fuel cells and also in solar panel structures [55]. The development of a low-cost, high-performance Li-ion battery containing GO dates back to April 2014. The project (University of Southern California, USA), involved the use of a silicon anode and a cathode

structured from sulfur powder covered with GO containing ions – Li [56].

1.3 Betaine (BE)

Betaine, also referred to as trimethylglycine, oxyneurine and glycine – betaine, is a naturally occurring human nutrient that was first discovered in sugar beets and was later found in several microorganisms, marine invertebrates, plants and animals. Chemically, it is a neutral methyl derivative of glycine with a positively charge tri – methylammonium group and a negatively charged carboxyl group, as report in figure 1.4

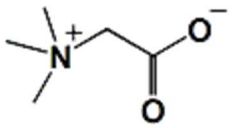

Figure 1.4: Chemical structure of betaine.

Betaine helps to maintain the normal physiological functions of vital organs like heart, liver, brain and kidneys. It acts as an osmolyte and as a methyl donor, whereby it plays an important role in the methionine cycle. Lack of betaine in the diet can result in hypomethylation, elevated homocysteine and reduced S-adenosylmethionine (SAM) concentration, resulting in perturbed methionine metabolism, liver steatosis and increase the predisposition to stroke, cardiovascular disorders, Alzheimer's and atypical DNA methylation leading to carcinogenesis [57]. In the electrochemical field, recent specialized literature proposes the use of choline and betaine as electrode modifiers for the preparation of modified electrodes by electrodeposition of metallic species catalytically active in electroanalytical and electrosynthetic contexts (Au, Pt, Pd, Zn, Sn, etc.) [58].

In this work, it was considered useful to investigate the use of betaine to modify the surface of graphite electrodes in order to make them more receptive substrates for the subsequent electrodeposition of active platinum particles [59].

1.4 Target molecules: Paracetamol

Paracetamol (PA), whose chemical structure is showed in figure 1.5, is an analgesic and antipyretic drug widely used for pain relief and fever reduction [60,61].

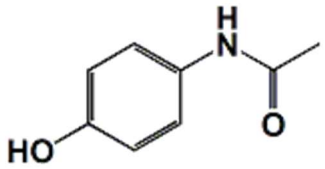

Figure 1.5: Chemical structure of paracetamol.

Thanks to its stability in aqueous solutions it is particularly suitable for pediatric use [62]. Although it is a drug widely administered worldwide, the mechanism of action with which paracetamol reaches antipyretic and analgesic effects is still a subject of debate today. Based on its analgesic and antipyretic effects, similar to those of acetylsalicylic acid, it has been hypothesized that paracetamol acts through the cyclooxygenase pathway [62]. Alternative mechanisms of action include: the central serotonergic mechanism through the activation of the serotoninergic inhibitory pathway of pain [62,63]; inhibition of the L-arginine – nitric oxide pathway mediated through N-methyl-D-aspartate (NMDA) [62,64] and the production of active metabolites which have an effect on cannabinoid receptors [62,65]. At therapeutic dosages paracetamol is generally well tolerated [60], however at high doses it is extremely hepatotoxic [66].

1.5 Target molecules: Nonsteroidal anti-inflammatory drugs (NSAID)

Non-steroidal anti-inflammatory drugs (NSAIDs) are a group of drugs of different chemical composition and different therapeutic potentials having a minimum of three common features: identical basic pharmacological properties, similar basic mechanism of action as well as similar adverse effects. Moreover, all drugs in this group exhibit acidic character, indeed pKa values are in the range of 3–5 (acids of medium strength). NSAID molecules contain hydrophilic groups (carboxylic or enolic group) and lipophilic ones (aromatic ring, halogen atoms). In accordance with their acidic character, NSAIDs occur in the gastric juice in the protonated (lipophilic) form. Also, in the small intestine, there are conditions favourable for absorption of weak acids. NSAIDs are classified according to their chemical structure into the following groups: salicylic acid derivatives (i.e. acetylsalicylic acid, salicylamid, sodium salicylate); pyrazolone derivatives (i.e. phenylbutazone, propyphenazone); indoleacetic acid derivatives (i.e. indomethacin, sulindac); phenylacetic acid derivatives (i.e. diclofenac); propionate acid derivatives (i.e. ibuprofen, naproxen, ketoprofen, tiaprofenic acid); enolic acid derivatives (i.e. piroxicam, meloxicam, tenoxicam); antranil acid derivatives (i.e. mefenamic acid, flufenamic acid); nicotinic acid derivatives (i.e. niflumic acid); pyranocarboxylic acid derivatives (etodolac); pyrrolepyrroles (ketorolac); coxibes (i.e. celecoxib, etoricoxib); naphtylbutanone derivatives (nabumetone); sulphonamides (nimesulide); benzoxazocine derivatives (nefopam) [67]. Non-steroidal anti-inflammatory drugs (NSAIDs) are among the most commonly prescribed agents worldwide to treat a variety of pain-related conditions, including arthritis and other rheumatic diseases [68]. In addition,

epidemiological studies have shown that long-term use of NSAIDs reduces the risk of developing Alzheimer's disease and delays its onset [69].

1.5.1 Acetylsalicylic acid

Acetylsalicylic acid (ASA), shown in figure 1.6, known as aspirin, is a pharmaceutical product with anti-inflammatory, analgesic, and antipyretic qualities.

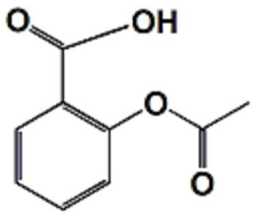

Figure 1.6: Chemical structure of acetylsalicylic acid.

ASA is widely used in curing fever and minor pain [68] and is also great effective in Alzheimer's disease [70-72], cancer [73] and cardiovascular disease [70,74,75] thanks to anticoagulant properties [68,76]. Acetylsalicylic acid exerts its anti-inflammatory, analgesic, antipyretic and anti-platelet aggregation action by inhibiting COX-1 and COX-2 [77]. The most frequent side effects observed when taking this molecule are related to disorders of the gastrointestinal tract, this because the inhibition of COX by this drug results in loss of the cytoprotective effects of PGE2 on the gastric mucosa [78].

1.5.2 Piroxicam

Piroxicam (PRX), figure 1.7, is non-steroidal anti-inflammatory drug (NSAID) belongs to a family of Oxicam [79].

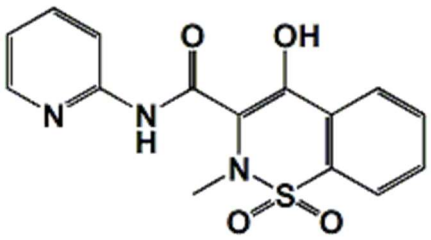

Figure 1.7: Chemical structure of piroxicam

It is used to reduce pain, inflammation, and stiffness caused by osteoarthritis and rheumatoid arthritis [68, 79, 80]. Anti-inflammatory activity of piroxicam is due to the reversible inhibition of COX-1 resulting in disruption and production of prostaglandins [79]. Piroxicam also inhibits the migration of leucocytes in to sites of inflammation and prevents the formation of thromboxane A2, an aggregating agent, by the platelets. It is well absorbed following oral administration however its use has been associated with a number of undesirable side effects on the stomach and kidneys in addition to gastric mucosal damage [79, 81]. These side effects can be avoided by topical administration of the drug [79].

1.5.3 Nimesulide

Nimesulide (NIM), figure 1.8, is a non-steroidal anti-inflammatory drug with good antipyretic and analgesic properties [82,83].

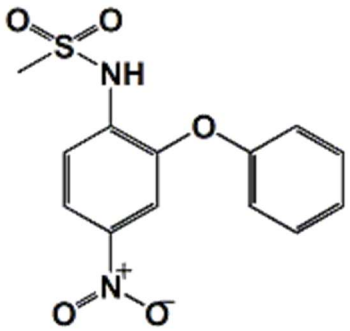

Figure 1.8: Chemical structure of nimesulide.

This substance is employed in pharmaceutical formulations to help in controlling and/or preventing diseases and are widely used in the treatment of rheumatoid arthritis [83], osteoarthritis, inflammation of the genitourinary system, otorhinolaryngological diseases, odontostomatological practice and postoperative pain [82]. Nimesulide is a unique NSAID, not only due to its chemical structure, indeed it has a sulfoanilidic group instead of the carboxylic one [76], but also for its ability to specifically inhibit COX-2, thus exerting milder effects on the gastric mucosa [84]. Regarding its mechanism of action, nimesulide not only inhibits COX-2, but also inhibits the release of oxidants from activated neutrophils, decreases histamine release from mast cells and inhibits the production of the platelet activating factor by human basophils [85]. On the other hand, the excess use of nimesulide causes acute side effects related to gastrointestinal (abdominal discomfort, heartburn, abdominal cramps, nausea, vomiting and diarrhoea), central nervous (headache, dizziness and drowsiness) and genitourinary (blood in urine, decrease in urination and kidney failure) systems [82].

1.5.4 Ibuprofen

Ibuprofen (IBU), figure 1.9, is the third most popular drug in the world, non-prescription, non-steroidal drug [86] used as an anti-inflammatory analgesic and antipyretic drug with anti-inflammatory effects and it is used for the treatment of pain or inflammation caused by conditions such as rheumatoid arthritis, degenerative joint diseases and menstrual cramps [61,66], migraine, muscle aches, tooth aches and osteoarthritis [86].

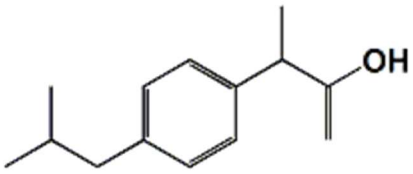

Figure 1.9: Chemical structure of ibuprofen.

Ibuprofen, today, is one of the safest drugs for the treatment of pain, inflammation and fever. Compared to aspirin and paracetamol it is more effective, in smaller doses, in the treatment of many painful conditions, it also has a greater a wider range of tolerability [87]. Ibuprofen inhibits both constitutive COX1, which is responsible for the production of prostanoids that control a wide range of physiological functions (blood flow, gastric and renal function), and inducible COX-2, which is responsible for the synthesis of prostanoids that produce inflammation and pain [88]. Just the inhibition of COX-1 is at the origin of the side effects of this molecule. Moreover, in 2015 the European Medicines Agency provided data showing a slight increase in the risk of myocardial infarction and stroke in patients taking high doses of ibuprofen [89].

1.6 Target molecules: Vitamin B group

Vitamins are micronutrients that are essential for the metabolism of all living organisms. They are found as precursors of intracellular coenzymes that are necessary to regulate vital biochemical reactions in the cell. Vitamin B complex is a water-soluble vitamin class that plays an important role in cell metabolism. Eight vitamins which are different from each other in terms of their chemical composition and pharmacological properties create thus family [90]: thiamine (B_1), riboflavin (B_2), niacin (B_3), pyridoxine (B_6), pantothenic acid (B_5), biotin (B_7 or H), folate (B_{11}–B_9 or M) and cobalamin (B_{12}). Each B-group vitamin is chemically different and acts in synergy to maintain the body's homeostasis by playing major roles in metabolic processes such as energy production and red blood cell formation [91]. In this work, vitamin B_1 and vitamin B_6 were used as target molecules.

1.6.1 Vitamin B_1

Thiamine or vitamin B_1 consist of a thiazole/thiazolium ring linked by a methylene bridge to an aminopyrimidine ring [90], as shown in figure 1.10.

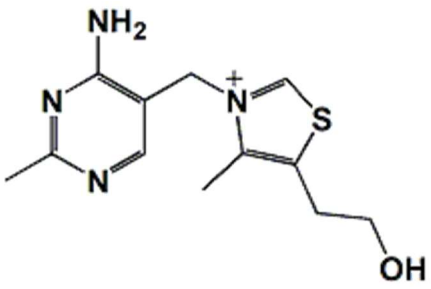

Figure1.10: Chemical structure of vitamin B_1.

Thiamine is present in limited quantities in almost all foods and in large amount in pork and offal. Bread and cereals are eaten whole or vitaminized, because thiamine is contained in the germ and in the bran of wheat, in the pulp of rice and in that part of all the cereals that is eliminated during the grinding to dare these foods a lighter color and finer consistency. A diet rich in brewer's yeast, wheat germ, molasses and bran, provides the whole human body with sufficient thiamine and helps prevent the accumulation of fatty deposits in the artery walls. Also known as a "moral vitamin" due to its relationship with a healthy nervous system and its beneficial action on mental attitude, thiamine also relates to individual learning ability. It is necessary for the growth of children and it is important for improving muscle tone. Thiamine is essential to stabilize the appetite as it improves the assimilation of food during digestion, particularly of starches, sugars and alcohol. The lack of vitamin B_1 causes damage to the nervous and cardiovascular system and also a general state of physical exhaustion, weight loss derived from an increasing difficulty in ingesting food accompanied by strong salivation and vomiting. Vitamin B_1 deficiency can also cause cardiac changes, neurological disorders, pupil dilation and hypersensitivity phenomena of the spine. In their extreme phase, vascular and nervous system injuries caused by vitamin B_1 deficiency can lead to semi-coma and following death [92].

1.6.2 Vitamin B_6

Pyridoxine or vitamin B_6 is a pyridine derivative [93], as it can be observed in figure 1.11.

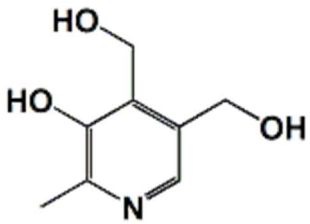

Figure 1.11: Chemical structure of vitamin B_6.

Pyridoxal phosphate, which is the active form of vitamin B_6, is involved, as a coenzyme, in numerous metabolic transformations of amino acids [94], including decarboxylation, transamination and racemization, and it is also involved in some enzymatic steps in the metabolism of amino acids containing sulfur and hydroxyl groups. All living organisms require vitamin B_6 and they must either synthesize it or, like humans, derive it from nutrients [95]. Pyridoxine is present in the liver, meats, cereals and wholemeal bread, soybeans and vegetables. When cooking food, significant amounts are lost. Pyridoxine is also sensitive to ultraviolet radiation and oxidation. When an individual is fed a diet deficient in pyridoxine convulsive effects may occur that the administration of vitamin B6 is able to inhibit.

2. Principles of Analytical techniques

2.1 Electroanalytical techniques

Electrode reaction are heterogeneous chemical processes that involve one or more steps with transfer of charge across the electrochemical interface to or from the electrode. The difference from other heterogeneous chemical reactions is that the kinetics are, not only dependent on the concentrations of the reacting species and the temperature, but they are also strongly influenced by the gradient of electrical potential at the interface.

Considering the following reduction semireaction:

$$Ox + ne \rightleftarrows Red \qquad (2.1)$$

This process consists of various intermediate steps, the sum of which will lead to the conversion of the oxidized species into the reduced one, both in solution. Generally, the reaction rate on the electrode, and therefore the resulting current, will be controlled by the slower "step" rate of the following possible processes [96]:

- mass transport to the electrode that can occur by migration, convection and diffusion. An example is the transfer of the Ox or Red species from the solution to the electrode and / or vice versa;
- charge transfer on the electrode surface;
- chemical reactions associated with electron transfer, in which the oxidant, the reducing agent or any reaction intermediates are involved;
- other surface processes: adsorption, desorption, crystallization, electrodeposition, etc.

Among these, the step to achieve mass transfer to/from the electrode provides direct information on the analytical concentration of the species involved in the redox process. In figure 2.1, shown below, it is schematically represented what happens in solution near an electrode.

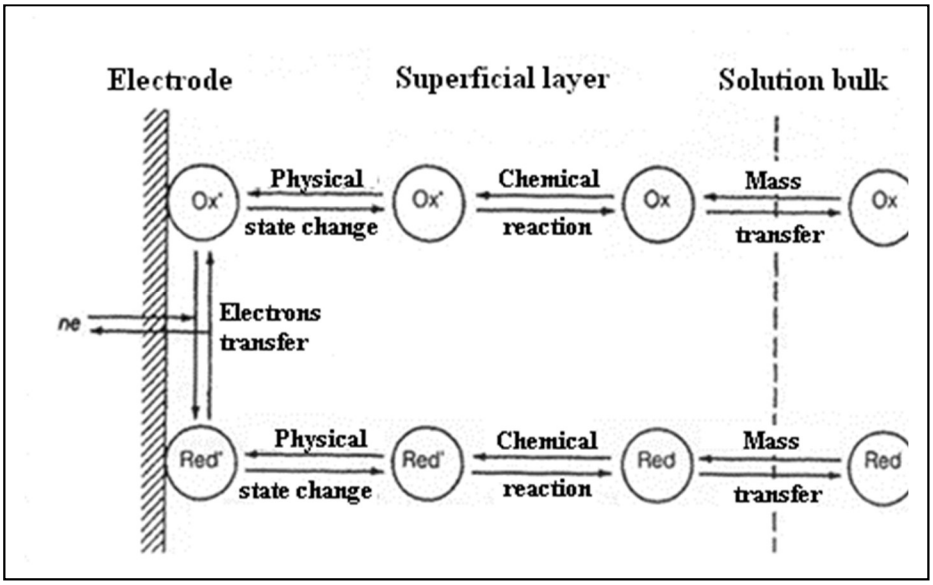

Figure 2.1: Schematic representation of what happens near electrode surface.

The reactions to take into account are:

$$Ox_{bulk} \rightarrow Ox_{electrode} \tag{2.2}$$

$$Ox_{electrode} + ne^- \rightleftarrows Red_{electrode} \tag{2.3}$$

$$Red_{electrode} \rightarrow Red_{bulk} \tag{2.4}$$

If the reactions (2.2) and (2.4) are slower than (2.3) the global reaction rate of the reaction (2.1) will be controlled by mass transfer, so we obtain concentration polarization. In this case, under diffusive conditions, the current will be constant and independent from the applied potential, it will depend on the concentration of the analyte. The mass transfer can be verified in three ways: diffusion, movement according to

concentration gradient; migration, movement of the charged species induced by the applied electric field; and convection, i.e. movement induced by mechanical agitation or temperature gradient. On the other hand, if the reaction (2.3) is the slowest of the others, the reaction rate will be controlled by the electronic transfer and we will talk about the process confined to the electrode; the current will be a function of the electrode potential and its correlation with the concentration will be of a complex nature.

Considering the reaction (2.3) and assuming that mass transport is fast enough to operate in the absence of concentration polarization; the overall rate of the reaction (2.3) will be:

$$v = v_f - v_b = K_f C_o^s - K_b C_r^s \tag{3.5}$$

where

v_f = rate of reduction reaction;

v_b = rate of oxidation reaction;

K_f = heterogeneous rate constant of reduction reaction;

K_b = heterogeneous rate constant of oxidation reaction;

C_o^s = oxidant concentration on electrode surface;

C_r^s = reductant concentration on electrode surface.

Reaction rate can be expressed in differential form:

$$\frac{dN_r}{dt} = \frac{-dN_0}{dt} = K_f C_o^s - K_b C_r^s \tag{2.6}$$

where:

N = number of moles involved in the oxidation – reduction reaction per area unit;

$\frac{dN}{dt}$ = conversion rate per area unit.

Measured current on the electrode will be linked to the conversion rate of the oxidant species to reductant one, as showed in equation 2.7:

$$I = nFA\left(\frac{dN_o}{dt}\right) \tag{2.7}$$

where

n = number of electron involved in oxido – reduction reaction;

F = Faraday constant (96485 C mol^{-1});

A = surface area of electrode.

From (2.6) and (2.7) it follows that:

$$I = nFA(K_f C_0^s - K_b C_r^s) \tag{2.8}$$

If $K_f C_0^s = K_b C_r^s$ system is in equilibrium and the resulting current will be zero;

if $K_f C_0^s > K_b C_r^s$ reduction reaction prevails and there will be a cathodic current, I_c;

if $K_f C_0^s < K_b C_r^s$ oxidation reaction prevails and there will be an anodic current, I_a.

Rate constant K_f e K_b are proportional to $e^{\frac{-\Delta G^{\neq}}{RT}}$, where $\Delta G^{\neq}$ is Gibbs energy (free energy) of activation for the reduction or oxidation reaction, T is absolute temperature and R is universal constant.

Gibbs energy of activation for reduction process is:

$$\Delta G_f^{\neq} = \Delta G_0^{\neq} - \alpha nF(E - E^o) \quad (2.9)$$

on the other hand, for oxidation process is:

$$\Delta G_f^{\neq} = \Delta G_0^{\neq} - (1 - \alpha)nF(E - E^o) \quad (2.10)$$

From (2.9) and (2.10) it is evident that there is a relationship between the potential applied to the electrode and the free energy barrier for the considered redox process. The term α, defined as an electronic transfer coefficient, is related to the degree of symmetry of the "activated complex" and has values between 0 and 1. Hence, from (2.9) and (2.10) the rate constants are redefined as follows:

$$K_f = K_0^{\left[\frac{-\alpha nF(E-E^0)}{RT}\right]} \quad (2.11)$$

$$K_b = K_0^{\left[\frac{-(1-\alpha)nF(E-E^0)}{RT}\right]} \quad (2.12)$$

with

K_0= standard rate constant of the system, that is K_f e K_b values when E = E^0.

In conclusion it can be stated that the total current given by

$$I = I_c + I_a \quad (2.13)$$

will be function of the potential, as shown in the following equation:

$$I = nFAK^0 \left\{ C_O^s \left[\frac{-\alpha nF(E-E^0)}{RT} \right] - C_R^s \left[\frac{(1-\alpha)nF(E-E^0)}{RT} \right] \right\} \qquad (2.14)$$

Below, in figure 2.2, the relationship between current and potential is reported. As can be observed, in non-diffusive conditions, the current is always linked to the applied electrode potential, as well as to the concentrations of the active species.

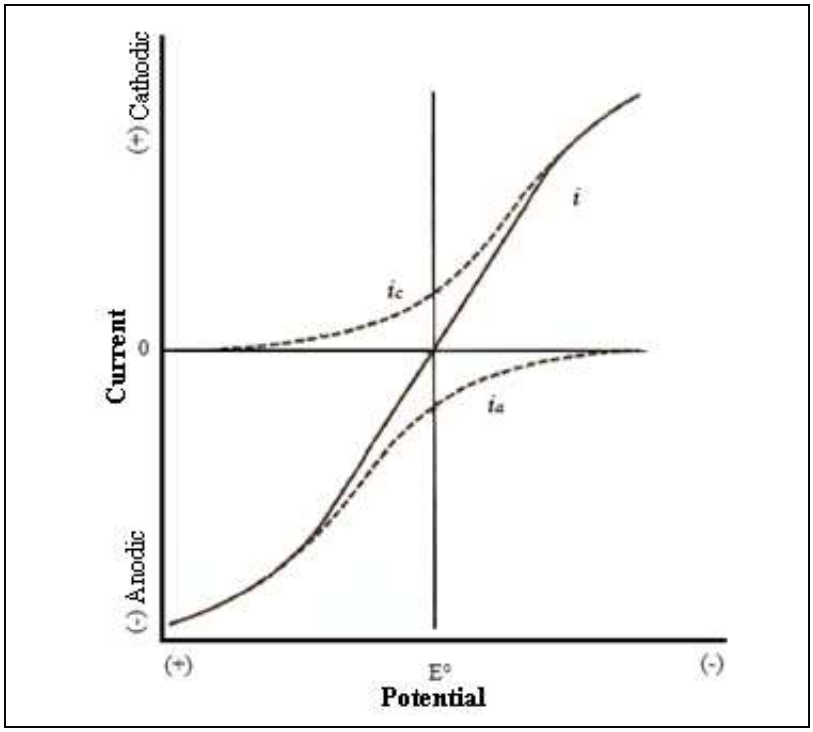

Figure 2.2: Current – potential relation for electrodic processes.

2.1.1 Voltammetry

Voltammetry is electrochemical method that records the current produced as a function of a potential applied to an electrolysis cell. For a generic reversible process, it will be:

$$Ox + ne^- \rightleftarrows Red \qquad (2.15)$$

The concentrations of the electroactive species on the electrode surface are related to the potential applied to the cell according to the Nernst equation:

$$E = E^{0'} + \frac{RT}{nF} \ln \frac{C_O^S}{C_R^S} \qquad (2.16)$$

where

E = electrodic potenzial;

$E^{0'}$ = standard electrodic potenzial, characteristic for each semi-reaction;

R = gas constant (8.314 $JK^{-1}mol^{-1}$);

T = temperature;

n = number of electrons exchanged in the process;

F = Faraday constant (96.485 C mol);

C_O^S = concentration of oxidized species;

C_R^S = concentration of reduced species.

Applying to the system a potential $E < E^{0'}$, for a generic time t; from (2.16) it will be observed that the reaction evolves in the sense of reduction and that $C_O^s \rightarrow 0$, while the concentration of oxidant in the solution (C_{Ob}) will remain constant; we deduce the formation of a

concentration gradient in proximity of the electrode surface, which will be responsible for the transport by diffusion of the Ox species from the solution to the electrode surface. The concentration gradients of the electro-active species in the electrode/solution interface are represented by concentration/distance profiles from the electrode itself, as shown in figure 2.3.

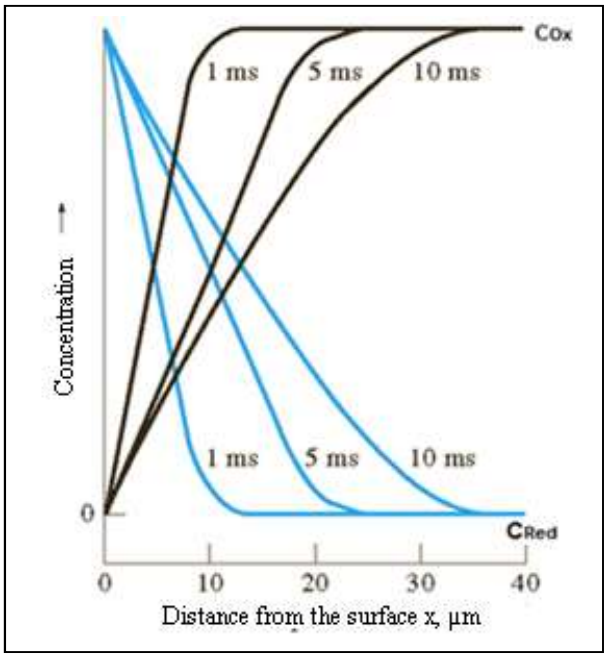

Figure 2.3: Concentration/distance profiles from the electrode related to the reaction $Ox + ne^- \rightarrow Red$ under diffusive control and for values of applied potential $E<E^{0'}$.

Figure 2.3 shows that, in the absence of agitation and as the electrolysis time increases, the concentration gradient becomes more and more extended. The electrolysis current represents a quantitative measure of the transport speed of the Ox species towards the electrode surface; therefore, it will be possible to write:

$$I = nFAD_O \frac{\delta C_o}{\delta x} \qquad (2.17)$$

where

I = current;

n = number of electrons involved in the reaction;

F = Faraday constant;

A = electrode superficial area;

D_O = diffusion coefficient of the species Ox;

$(\delta Co)/\delta x$ = transport rate of the species Ox, with C_O concentration of Ox and x surface distance from the electrode.

In stationary conditions the diffusion is restricted to the electrode-solution interface, called the Nernst diffusion layer (δ), in which the solution is totally stagnant and the transport occurs by diffusion only, as shown in figure 2.4.

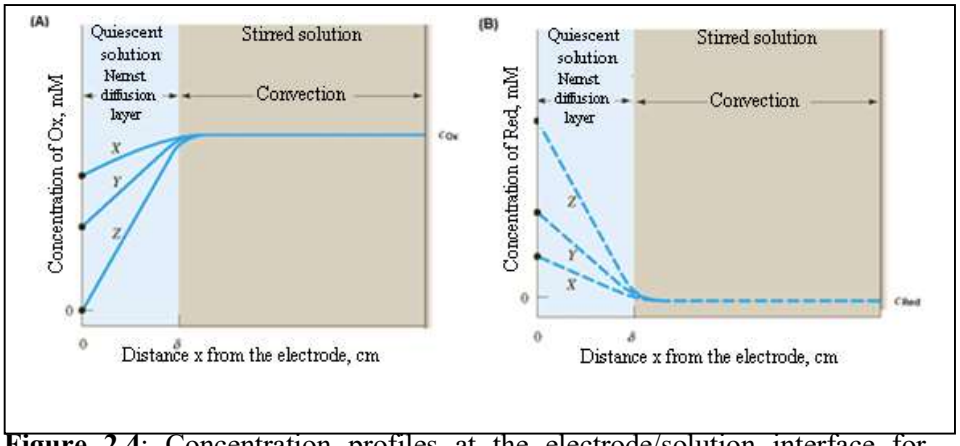

Figure 2.4: Concentration profiles at the electrode/solution interface for electrolysis $Ox + ne^- \rightarrow Red$, for a solution placed under agitation and for three potential values.

As can be seen from Figure 2.4, at time X the equilibrium concentration of Ox at the electrode surface has been reduced to about 80% of its initial value and the equilibrium concentration of Red is increased by an equivalent quantity; at time Y the equilibrium concentrations of the two species at the surface are almost the same and equal to $C_{Ox}/2$ and at the time Z and beyond the surface concentration of Ox approaches zero and that of Red approaches the initial concentration of Ox. At more negative potentials of Z, substantially all the Ox ions entering the surface layer are immediately reduced to Red. The value (δCo)/δx represents the slope relative to the initial section of the concentration profile shown in figure 3.4. This value can be approximated to $\frac{(C_O - C_O^s)}{\delta}$. It follows that (2.17) becomes:

$$I = \left(\frac{nFAD_O}{\delta}\right)\left(C_O - C_O^S\right) = K_O\left(C_O - C_O^S\right) \qquad (2.18)$$

The equation (2.18) shows that, for a fixed value of the thickness δ, with decreasing C_O^s the current increases until the surface concentration of Ox tends to zero. In these conditions the current value becomes independent from the applied potential and we can talk about cathodic current limit:

$$I_{l,c} = K_O C_O \qquad (2.19)$$

Similarly, for anodic processes, we can define the total current and the anodic limit current as follows:

$$I = \left(\frac{nFAD_R}{\delta}\right)(C_R - C_R^s) = K_R(C_R - C_R^s) \qquad (2.20)$$

$$I_{l,a} = K_R C_R \tag{2.21}$$

From equations (2.18,2.19,2.20 and 2.21), by making the appropriate substitutions we will obtain:

$$C_O^s = \frac{(I_{l,c} - I)}{K_O} \tag{2.22}$$

$$C_R^s = \frac{(I_{l,a} - I)}{K_R} \tag{2.23}$$

from which:

$$E = E^{o\prime} - \left(\frac{RT}{nF}\right) \ln\left(\frac{K_O}{K_R}\right) + \left(\frac{RT}{nF}\right) \ln\left(\frac{I_{l,c} - I}{I_{l,a} - I}\right) \tag{2.24}$$

From equation (2.24) it is possible to define a fundamental parameter: the half-wave potential ($E_{1/2}$), which represents the potential corresponding to a current equal to $I = (I_{l,c} + I_{l,a})/2$.

$$E_{1/2} = E^{o\prime} - \left(\frac{RT}{nF}\right) \ln\left(\frac{K_O}{K_R}\right) \tag{2.25}$$

from which

$$E_{1/2} = E^{o\prime} - \left(\frac{RT}{nF}\right) \ln\left(\frac{D_O}{D_R}\right) \tag{2.26}$$

The equation (2.24) can therefore be rewritten as follows:

$$E = E_{1/2} + \left(\frac{RT}{nF}\right) \ln\left[\frac{(I_{l,c} - I)}{(I - I_{l,a})}\right] \tag{2.27}$$

Assuming that the diffusion coefficients of the reduced and oxidized species are equal, the half-wave potential can be assimilated to the potential E° of the specific redox pair; therefore, it is possible to state that the half-wave potential is a characteristic quantity of the redox pair under examination (E°) [97].

2.1.2 Cyclic voltammetry (CV)

Cyclic voltammetry (CV) is one of the most widely used electrochemical techniques for acquiring qualitative/quantitative information on redox processes, since it is able to give a rapid view of the potentials and relative currents, characteristic of the electroactive species involved in a given process. A generic CV experiment consists in applying, between the working electrode and the reference immersed in a solution at rest, a potential having a triangular waveform, like the one shown in figure 2.5.

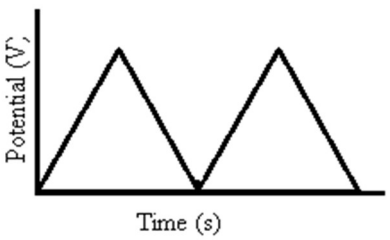

Figure 2.5: Signal of excitation potential - time in CV.

During the potential scan, the potentiostat records the current deriving from the application of the potential; the resulting graph, current - potential (E-I), is called a cyclic voltammogram. An example of a cyclic voltammogram, for a generic redox reaction, is shown in figure 2.6.

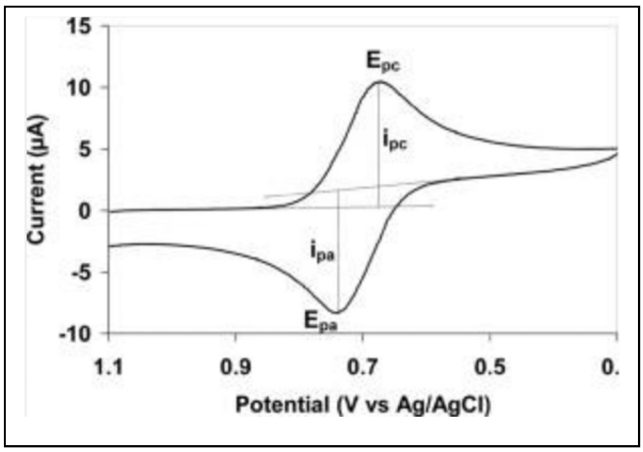

Figure 2.6: Example of a cyclic voltammogram for a generic reaction Ox + e- ⇄ Red.

From figure 2.6, we observe that only oxidized species, Ox, is present at the beginning of scan and that a potential scan is applied towards decreasing values, starting from a potential value to which no reduction reaction occurs. As soon as the applied potential reaches the characteristic value E° of the redox process, the increase of a cathodic current begins to register, until a peak appears. After passing the potential region where the reduction process takes place, the potential direction is reversed. During the reverse scan, the Red molecules (generated in the first half-cycle and accumulated near the surface) are oxidized again to Ox and an anode current develops, which will have its maximum at the characteristic potential value of the oxidation reaction.
Important parameters, to be considered, are the two peak currents (cathodic current peak I_{pc}, anodic current peak I_{pa}), the two peak potentials (cathodic potential peak E_{pc}, anodic potential peak E_{pa}) and the half-wave potential $E_{1/2} = (E_{pa} + E_{pc})/2$. For a reversible process and in diffusive conditions, the charge transfer is fast enough to allow the reagent and the product to be present at the equilibrium concentration on

the electrode surface. Under these conditions $E_{1/2} \approx E°'$ will occur and electrode transfer is the only process that occurs at the electrode, the ratio between the intensities of the peak currents tends to the unit ($I_{pa}/I_{pc} \approx 1$). For reversible processes, controlled by diffusion, the peak current is given by the Randles-Sevcik equation:

$$I = Kn^{3/2}AD^{1/2}Cv^{1/2} \qquad (2.28)$$

where

K = Randles – Sevcik constant (2.69×10^5);

N = electrons exchanged in redox process;

A = electrode area;

C = concentration;

D = diffusion coefficient;

v = potential scan rate, V/s.

From equation (2.28) it can be seen that the current is directly proportional to the concentration of the electroactive species and to the square root of the scanning speed of the potential. It obviously also depends on the diffusion coefficient of the species (D), as from the area of the electrode (A) and on the number of electrons involved in the process (n).

For processes with different degrees of electrochemical irreversibility, the voltammogram shows separation of the peak potentials ΔEp (E_{pc} and E_{pa}) depending on the scanning speed (ν) and on the analyte concentrations. The values of the peak currents (I_{pa} and I_{pc}) will be lower than those obtained under conditions of total reversibility. Peak currents will be given by expressions of the type:

$$I = f(2.99 \cdot 10^5)n(\alpha n_a)^{1/2}ACD^{1/2}v^{1/2} \quad (2.29)$$

where

α = electronic transfer coefficient;

n_a = number of electrons involved in the electronic transfer stage;

f = correlation factor.

The CV is used to study the chemical-physical behavior of electro-active molecules at the solution electrode interface, where reagents and products can be involved in adsorption-desorption processes. An ideal Nernstian type behavior of species confined to the electrode manifests itself through voltammetric peaks of symmetrical shape and the difference in peak potentials (E_{pc} - E_{pa}) tending to zero. The peak current is directly proportional to the surface concentration (Γ (mol cm^{-1})) and to the scanning speed:

$$I = \frac{n^2F^2\Gamma Av}{4RT} \quad (2.30)$$

The peak area, or the amount of charge consumed during the reduction, can be used to calculate the surface concentration of the electroactive molecule:

$$\Gamma = \frac{Q}{nFA} \quad (2.31)$$

Thanks to all the information of qualitative and quantitative nature, the CV can be used to study the behavior and performance of electrodes and/or electrode materials for the various possible applications in

different technological application contexts. In this sense, chemically modified electrodes (CMEs) are studied and characterized by using voltammetric techniques in CV.

2.1.3 Differential pulse voltammetry (DPV)

Differential pulse voltammetry (DPV) consists in applying a periodic series of voltage pulses of constant duration and amplitude. The current intensity is measured immediately before the impulse is opened and immediately before the end of the same. The current difference measured between these two points is represented graphically in figure 2.7.

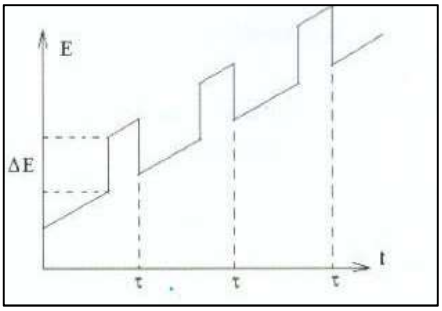

Figure 2.7: Waveform in DPV.

The first sampled current is instrumentally subtracted from the second one and a current difference is obtained, which, if it is reported on a system of cartesian axis as a function of the potential applied, generates a voltammogram, as showed in figure 2.8.

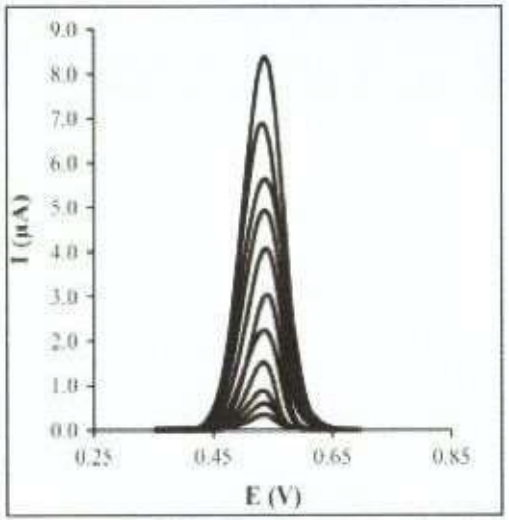

Figure 2.8: Voltammogram obtained by DPV.

DPV is an extremely useful technique for measuring traces of both organic and inorganic molecules having an electroactive character.

2.1.4 Chronoamperometry

Chronoamperometry is a technique particularly suited to electroanalysis which involves the use of a controlled potential applied to a stationary electrode placed in a non - stirred solution and with which the dependence of the current on time is measured. Figure 2.9 shows the signal potential excitation - time of analysis (a) and the current response - time of analysis (b).

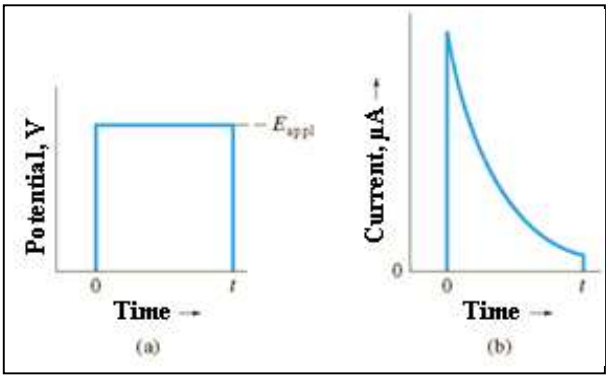

Figure 2.9: Example of signal potential excitation - time (a), current variation - time in a generic experiment chronoamperometric (b).

From figure 2.9 (b), it is observed that at the beginning the current increases instantaneously to a current value necessary to convert all the reagents on the electrode surface in the products, according to what is dictated by the applied potential. Immediately afterwards, the current decreases more or less rapidly depending on the diffusion conditions of the electroactive species involved.

Under these experimental conditions, not stirred solution and stationary electrode, mass transport can be easily controlled by diffusion alone, this implies a gradual expansion of the diffusion layer, associated with reagent depletion, and therefore with increasing time there is therefore a decrease of the current recorded. The current, in diffusive conditions, will be correlated with the concentration of the reagent in solution and at the time of electrolysis, according to the Cottrell equation:

$$I = \frac{nFACD^{1/2}}{\pi^{1/2}t^{1/2}} = kCt^{-1/2} \qquad (2.32)$$

where

D = diffusion coefficient;

C = concentration of the redox species in solution;

t = application time of the potential.

The current decreases with the square root of time.

From these experiments, important chemical-physical parameters can be determined such as D, n, A, etc.

The chronoamperometric response, recorded under stirring conditions is shown in figure 2.10.

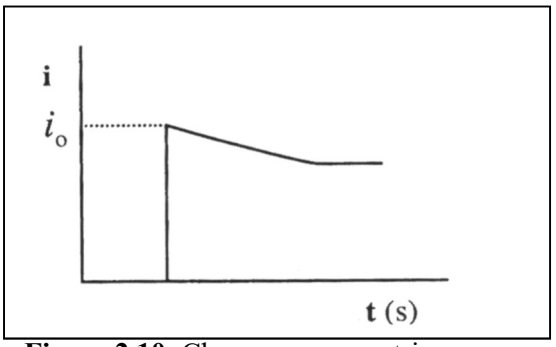

Figure 2.10: Chronoamperometric response of a solution kept under constant agitation.

As can be seen from Figure 2.10, in this case the current rises from zero up to the value i_0, as soon as the potential is applied and remains almost constant for the whole time of electrolysis. Its average value is obviously related to the C, A, n, degree of agitation and degree of electrochemical reversibility of the system. Often, the formation of poisoning species on the electrode surface can lead to significant decreases in currents, up to their total suppression; these are passivated electrode systems.

2.2 Spectroscopic technique

2.2.1 X–ray photoelectron spectroscopy (XPS)

When a radiation impacts the matter, it absorbs some of the energy carried by the radiation. This absorption process can lead to electronic transitions of the system. Generally, since these are quantized processes, the energy absorbed will be equal to the energy difference between the final state and the initial state of the transition itself. Part of the energy, however, will be transported by the electrons involved in the transition in the form of kinetic energy of the same (KE) [98,99]. Measuring this energy, it will be possible to trace the energy of the orbital from which a specific electron has been expelled, through the report 2.34:

$$BEv = h\nu - KE \tag{2.34}$$

where
BEv = binding energy of the electron with respect to the vacuum;
hν = energy of the incident radiation;
KE = kinetic energy of the emitted electron.

In XPS spectroscopy, where radiation is used in the X-ray range, the latter is able to allow electronic transitions involving the expulsion of electrons from the most internal orbitals of an atom. By measuring the escape velocity of the emitted electrons (KE), it is possible to go back to the energy of the core level from which electrons come (BE), through the relation 2.34. This last report, if correctly expressed, must contain additional terms related to the interaction of the electron in the emission phase from the sample:

$$BE_v = h\nu - KE - (\Phi_{SP} - \Phi_C) \quad (2.35)$$

where
$(\Phi_{SP} - \Phi_C)$ = contact potential, given by the difference between the work function of the spectrometer (Φ_{SP}) and the sample (Φ_C).

As can be seen from equation 2.35 the BE_v depends both on the work function of the spectrometer and on that of the sample, so, to simplify everything we define the bond energy calculated with respect to the Fermi level (BE_F).

$$BE_F = BE_v - \Phi_C \quad (2.36)$$

and then we come to the following expression:

$$BE_F = h\nu - KE - \Phi_{SP} \quad (2.37)$$

If we take into account electrostatic loading of the sample, we will have:

$$BE_F = h\nu - KE - (\Phi_{SP} + S) \quad (2.38)$$

where
S = corrective term (also called electrostatic loading of the sample).
It takes into account the formation on the surface of the sample of a positive charge, following the emission of electrons, which tends to attract the latter, causing a slowing down and therefore a decrease in their kinetic energy. For conductive samples this term is negligible. For non-conductive or semiconductor samples, the term will be non-negligible.

The experimental evaluation of this term is conducted through a calibration method using samples whose BE_F is exactly known. Signal C1s relative to the graphitic carbon, whose BE_F is exactly known (284.6 eV), often is considered as internal reference signal.

Further variations in experimental BE values, compared to those reported in the literature, are due to "chemical shift" and electronic relaxation energy. The chemical shift is a phenomenon in which the kinetic energy of a photoelectron varies due to the interactions with its own chemical environment. This contribution depends on the Madelung potential, and on the polarity of the atomic bonds that determine a variation of the electronic intensity on the atom and therefore variations of the binding energy. The electronic relaxation energy consists of two parts: an atomic contribution, R^a, and an extra-atomic contribution, R^{ea}. The first depends on the atomic number and the core orbital involved in the photoemission process; it is due to the contraction of the most external electric charges through the core holes. The second one (R^{ea}) is due to the relaxation energy associated with the rest of the system, that is the flow of electron density from the surrounding environment towards the ionized atom in the core level. Considering these two contributions, BE can be rewritten as follows:

$$BE_F = k + k_q + V_M - R^a - R^{ea} \qquad (2.39)$$

$V_M = \sum_j (q_j/R_j)$ where q_j is the charge of all other atoms, R_j is their distance from the atom from which the core electron escaped;

k = term related to the Hartree - Fock energy of the core electron in the free atom;

q = valence charge;

k_q = contribution of the core potential resulting from the removal of an electron of valence, can be approximated by the integral of Slater that holds in consideration of the interaction between core and valence electrons;

R^a = atomic contribution to relaxation energy;

R^{ea} = extra-atomic contribution to the energy of relaxation.

Thanks to equation (2.39), it is possible to attribute to each experimental BE value a certain chemical state of the element under examination and therefore, it allows to obtain useful qualitative information on the chemical environment of the sample under examination.

The spectrum obtained from an XPS analysis consists of various contributions (peaks), which can be divided into primary and secondary peaks. The primary peaks are:

- Photoelectronic peaks derive from the coupling of the spin (s) moment with the orbital angular momentum of the electron (l). If $l > 0$ the electron, which is expelled from this orbital, can "choose" between two final states characterized by different value of the quantum number associated to the total angular momentum of the electron (j) that is $j = l + s$, therefore given that the values that can be assumed by s are ± 1/2 we will have $j = l + 1/2$ and j = l - 1/2. It will be observed a doublet consisting of two peaks in which the relative intensity ratio will be given by the ratio of the multiplicities $(2j + 1)$ of the states:

$$\frac{\left[2\left(l+\frac{1}{2}\right)\right]}{\left[2\left(l-\frac{1}{2}\right)\right]}$$

For 2p orbitals this ratio will be 2 : 1.

- Auger peaks are generated following a relaxation process to which the atom is subjected after it has lost an electron. When an electron is ejected from the atom it leaves a hole which, due to the "waterfall" effect, will be filled by the electrons of the outer layers. There are therefore two processes of relaxation, competitive between them:
  - X-ray fluorescence: emission of a hυ radiation, whose energy will be due to the difference in energy between the starting orbital and the arrival of an electron subject to relaxation.
  - Auger electron emission: emission of an electron coming from the same orbital or an orbital higher than the starting electron subject to the relaxation.

The probability of one or the other process occurring is shown in figure 2.11.

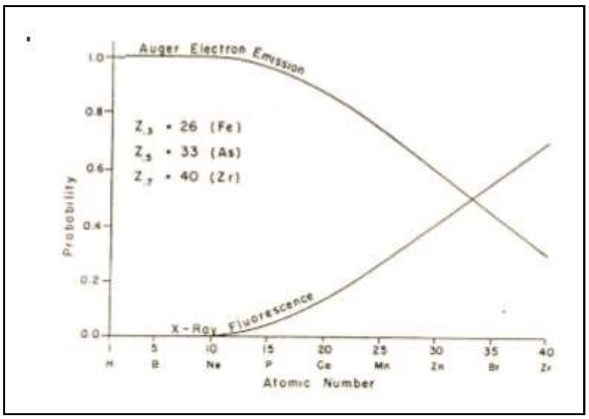

Figure 2.11: Variation of relaxation processes in relation to the atomic number of the element.

As can be seen, for light atoms ($Z < 30$) the most probable process is the emission of an Auger electron, while if Z increases the fluorescence process becomes more probable.

The secondary peaks are the following:

- The **satellite peaks** derive from the use of a non-monochromatic source, therefore the radiation, not being monochromatic, will produce secondary photoelectrons with lower intensity than primary ones.
- **Ghost peaks** are due to the excitation of the impurity present in the source. Causes that determine the presence of ghost peaks are due to the exhaustion of the anode of the source, the oxidation of the anode, etc.
- **Multi-splitting** occurs when elements with more unpaired electrons are present in the valence level. Indeed, if $l = 0$ (orbital s) the electron remained after the photoelectron emission can has spin equal to ± ½ and we can couple with the spin of the unpaired valence electrons giving two final states $s = \pm ½$. If, instead, the ionized orbital has $l > 0$, the situation becomes more complicated due to the numerous final states that can interact with each other, giving rise to a series of peaks or in some cases, to a widening of the main peak.
- The **shake-up** and **shake-off** peaks are due to the photoelectron which excites a valence electron (shake-up) or ionizes it (shake-off) losing energy; it will have signals at lower values of kinetic energy than the main peak of the same element.

In addition to the primary and secondary peaks in an XPS spectrum we find a background signal due to two factors:

- Photoelectrons that are emitted with an initial kinetic energy E_i, but that arrive at the detector with a kinetic energy $E < E_i$. The energy loss is due to the shocks that the electrons undergo in the path between the sample and the detector.

- Bremstralung radiation due to common X-ray sources;

Using the intensity of photoelectronic peaks it is possible to carry out quantitative analyses of the species identified, considering the direct proportionality between the quantity present in the sample and the area of the recorded peak. The relation that connects the intensity of the peak to the amount of compound present, for a solid sample, is as follows:

$$I = F\,D\,\sigma\,L\,\lambda\,T \tag{2.40}$$

where
I = peak intensity;
F = constant that depends on the intensity of the source radiation;
D = atomic density of the sample;
σ = cross section that depends on the energy of the source;
L = angular emission anisotropy which depends on the particular orbital;
λ = mean free path of an electron;
T = spectrophotometer transmission function.

It is important to have standard samples, through which determine the experimental parameters: σ L λ T. In the literature, there are databases containing precisely these data, commonly defined as relative sensitivity factors. By arbitrarily setting the fluorine sensitivity factor 1s as unitary, the sensitivity factor of each element can be evaluated experimentally using a comparison procedure.

2.2.2 Scanning electron microscopy (SEM)

Scanning electron microscopy (SEM) exploits the interaction between the surface of the sample and an electron beam in order to provide morphological and topographical information of the same [99]. The physical principle of this technique is based on inelastic collisions, in which occurs a loss of kinetic energy from electrons. The lost energy is transformed into potential energy through excitation of the electronic and vibrational states or through ionization processes. The ionization of electronic levels generates secondary electrons, which travel through the solid, losing their kinetic energy; only the electrons that are produced on the surface are emitted in the vacuum and collected by the detector. By analyzing the secondary electrons, a topographic and morphological image of the sample is obtained [100]. Moreover, when the electrons leave the atom, they generate an electronic hole in the orbital, from which they were emitted, generating a process of relaxation of the atom, a phenomenon in which the electrons of higher orbitals go to fill the formed hole, producing energy. This energy will be issued in the form of:

- Photons that can have low energy (visible range). This effect is called cathodoluminescence.
- X-rays if they have high energy and will be collected by an EDS (X-ray energy dispersion detector) or WDS (X-ray wavelength dispersion detector) detector.
- Auger electrons that are the basis of Auger electron spectroscopy.

The use of an electron beam, in place of a photonic beam, has two fundamental advantages: intense analytical signal due to the use of

electrons having a high cross section of interaction with the atoms affected, and high resolution signals.

3. Experimental section

3.1 Reagents and materials

To prepare the dispersion of PVA/GO we used polyvinyl alcohol (Aldrich, mw:130.000, 99% hydrolyzate) and graphene oxide (Aldrich, powder, 15-20 sheets, 4 – 10% edge – oxidized). To prepare the electrode GC/BE/Pt we used betaine (Sigma Aldrich, ≥ 98%), KCl (Sigma Aldrich, ≥ 99%) and $Na_2PtCl_6 \cdot 6\ H_2O$ (Sigma Aldrich, 98%). The solutions used to test the electrodes have been prepared with NaOH (Sigma Aldrich, ≥ 98%), $K_2HPO_4 \cdot 3H_2O$ (Sigma Aldrich, ≥ 99%), KH_2PO_4 (Sigma Aldrich, ≥ 99%), H_2SO_4 (Sigma Aldrich, 95 – 98%), acetylsalicylic acid (Sigma Aldrich, ≥ 99%), ibuprofen (Sigma Aldrich), nimesulide (Sigma Aldrich), paracetamol (Sigma Aldrich), piroxicam (Farmalabor). Counter electrodes and reference electrodes were supplied by AMEL (Milano). All the solutions were prepared in deionized and bidistilled water (Milli-Q Gradient Millipore/Elix 5).

3.2 Apparatus

3.2.1 Electrochemical analysis

Voltammetric and amperometric analysis were conducted with an Autolab PGSTAT 30 galvanostat potentiometer (Metrohm, Holland), showed in figure 3.1A.

Figure 3.1: PGSTAT 30 potentiostat / galvanostat with measurement cell and acquisition system.

The potentiostat/galvanostat is governed by a dedicated GPES software (software package version 4.9, Metrohom). The electrolysis and measurement cell is configured with three electrodes as shown in figure 3.1B: a saturated calomel reference electrode (SCE), an auxiliary electrode (or counter electrode) of Pt and a graphite-based working electrode (GC), suitably modified during the course of the work. During the measurements the potential at the working electrode was made to vary according to the reference electrode; while the resulting current was measured between the working electrode and the counter electrode. This three-electrode cell configuration is necessary to minimize the ohmic drop on the working electrode and stabilize the potential on the reference electrode.

3.2.2 X-ray photoelectron spectroscopy (XPS)

In this work XPS analyzes were conducted with two different spectrometers: Leybold LH X1, as regards the characterization of the GC/GO/PVA electrode, and the Phoibos 100-MCD 5, as regards the GC/BE/Pt electrode.

The components of the instrument are:

X-ray source: consisting of a pair of tungsten filaments (in figure 3.3 represented by filament 1 and filament 2) which are heated by Joule effect by applying an adequate potential difference to the extremes. This induces the emission of electrons which, in the collision with the anode, will generate photoelectrons in the X-ray spectral range. The anode can consist of Mg and/or Al; so it can generate photoelectrons from Mg or Al.

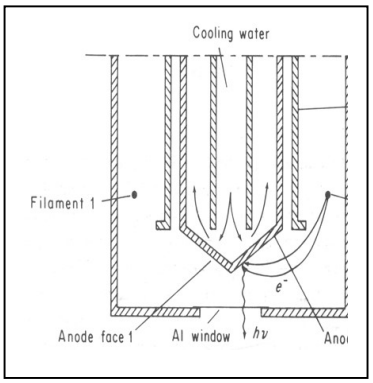

Figure 3.3: Internal structure of X-ray source.

Pre-analysis room is a chamber in which the sample is initially placed and where a pre-vacuum is made up to about 10^{-8} mbar.

Analysis room where the sample analysis is performed. The analysis is carried out in ultra-high vacuum (UHV) conditions, at about 10^{-9} mBar. These vacuum conditions are necessary because the free path of the electrons, emitted by the sample, must be as free as possible from collisions with possible particles, thus preserving their initial kinetic energy.

Vacuum pumps: a turbomolecular pump and a rotary pump are generally mounted for the pre-chamber; instead, as far as the analysis room is concerned, there is a rotary pump, a turbomolecular.

Analyzer: it measures the kinetic energies of the electrons leaked from the superficial atoms, previously hit by X-rays coming from the source. The analyzer used in this work is concentric (CHA). An example of CHA is shown in figure 3.4 A and B.

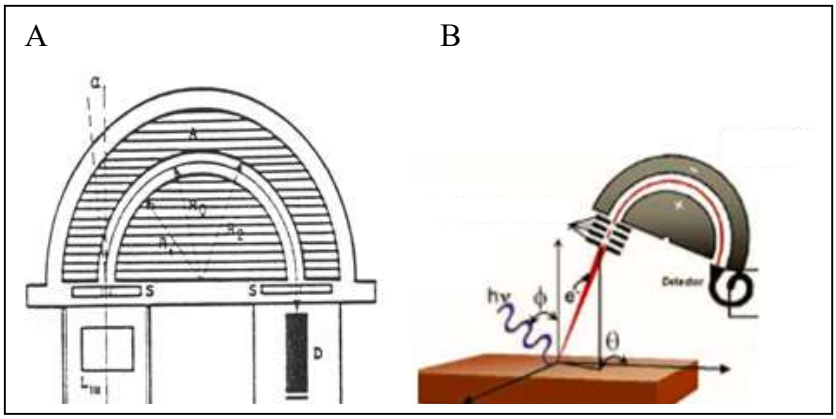

Figure 3.4: Concentric analyzer (CHA) (A) and magnification of the hemispherical capacitor of a CHA (B).

The CHA consists of an electrostatic lens and a hemispherical condenser. The lens is composed of a series of cylinders with different electrostatic potentials. These allow to collect the electrons emitted within a certain angle and convey them to the inlet of the hemispherical condenser. In order to obtain a better spectral resolution, the electrostatic lens can delay the electrons by varying, in a controlled way, the kinetic energy with which they reach the entrance of the electrostatic condenser. The kinetic energy of the electrons at the entrance of the hemispherical condenser will therefore be given by:

$$E^0 = \frac{E_S}{B}$$

where

B = delay factor applied by the electrostatic lens;

E_S = energy with which the electrons were emitted from the sample;

E^0 = electron energy at the electrostatic capacitor input.

The hemispherical condenser consists of two hemispherical metal plates, to which a variable potential difference is applied. The trajectory of the electrons inside the capacitor plates depends both on the value of this potential difference and on the kinetic energy of the electrons themselves. Only the electrons characterized by a precise value of kinetic energy E^0 are deflected on the exit slit, while all the others are lost hitting against the framework.

Signal amplifier is different between the two machines used. In the Leybold spectrometer is an electro-multiplier with 16 dynodes and its operation is based on a secondary emission process (electro-multiplication). It consists of a glass tube, inside which a vacuum was made and in which there is an anode and several electrodes that make up the dynodes. The electrons escaping from the analyzer hit a dynode (cathode) allowing the emission of secondary electrons that are focused towards the next dynode. These dynodes are covered with high secondary emission coefficient material and placed at ever more positive potentials. The first electron emitted acquires kinetic energy thanks to the electric field present; when this electron hits the first electrode it causes the emission of several electrons with lower energy, these will impact the second dynode producing other electrons and so on. In this way a “waterfall” effect will be generated, thanks to which a significant

amplification of the signal is obtained. A diagram of the operation of an electro-multiplier is shown in figure 3.5.

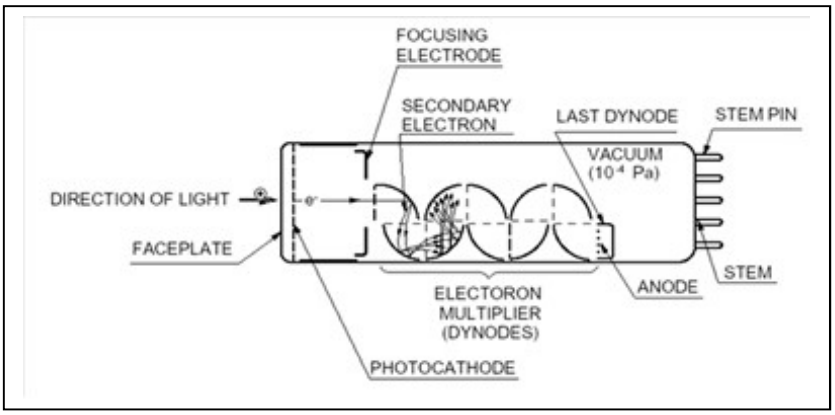

Figure 3.5: Dynode series electromultiplier.

The PHOIBOS spectrometer is equipped with a Channel electron multiplier (channeltron or CEM). It is a high gain device for the detection of energetic particles such as electrons, ions or radiation. The CEM consists of a small one curved glass tube whose interior walls are covered with a high material resistance, as shown in figure 3.6. The resistant material becomes a continuous dynode when a potential is applied between the ends of the tube. The intensity obtained with this type of detector is much higher than the classic photomultiplier.

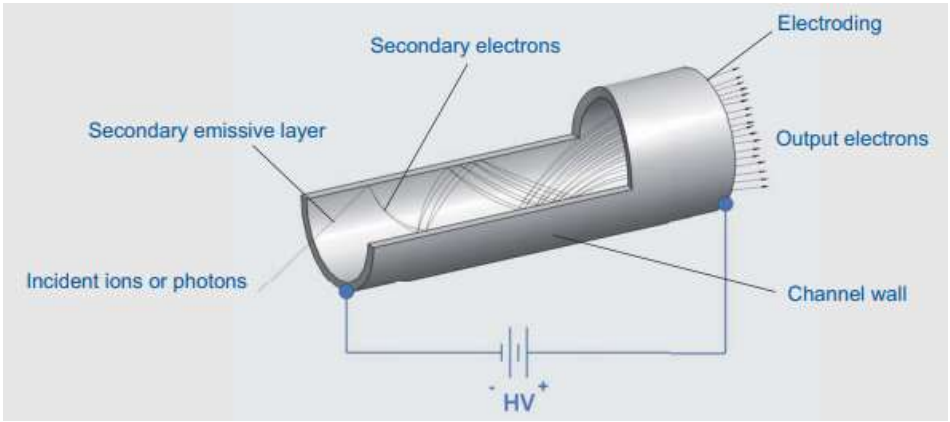

Figure 3.6: Channel electron multiplier.

Spectra processing system: XPS signal processing was done with a program developed in this University (NEWGOOGLY), which uses model curves obtained from a "mixing" of a Lorenzian and a Gaussian which go to "fit" the experimental XPS curve. The parameters of the respective elaborated curves, such as: binding energy, full width at half maximum (FWHM) and the relative areas, corrected with their own sensitivity coefficients, constitute the essence of XPS processing.

3.2.3 Scanning Electron Microscopy (SEM)

The surface images were obtained with an electron scanning microscope (SEM) of the Philips ESEM series XL 30. Figure 3.7 shows the section of the column of a SEM instrument.

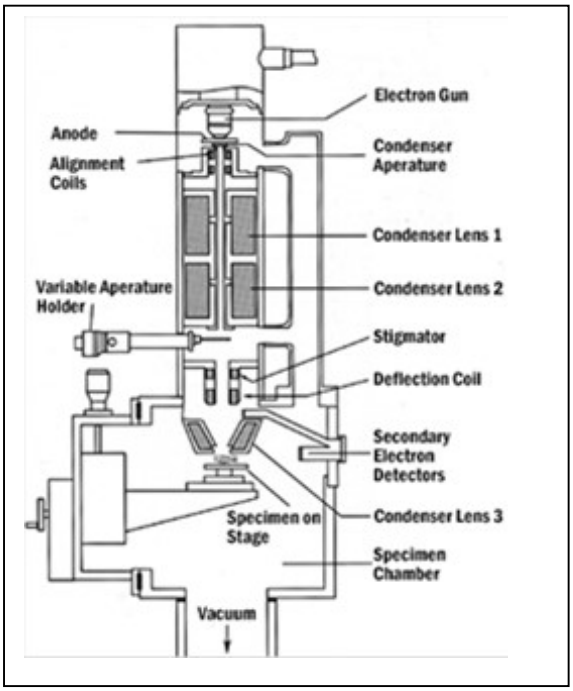

Figure 3.7: Section of a SEM column.

The fundamental components of SEM analysis instrument are:

Emitter, in which an electron beam is produced starting from a tungsten source, or, as in the present case, LaB_6. The source, through the application of a potential difference, is heated by Joule effect and emits electrons that constitute the electron beam.

Vacuum system is necessary to minimize electron-gas interactions. The pressures that will occur in the different areas of the microscope will be: 10^{-5} mbar in the emitter part, less than 10^{-3} mbar in the column part

between emitter and analysis chamber and approximately 10^{-3} mbar in the chamber analysis. To obtain these values, different pumps type (rotary, turbomolecular and ionic) are used.

Analysis room is equipped with a table for samples that can move in the three directions of the space, can rotate 360° along its vertical axis and be inclined up to 90°.

Detector EDS, showed in figure 3.8, is a detector in X-ray energy dispersion.

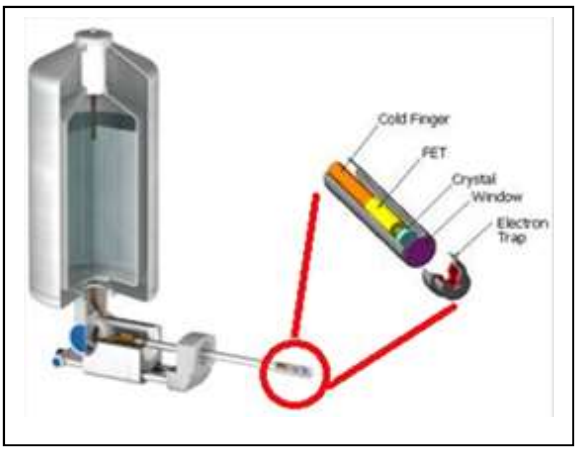

Figure 3.8: Detector in energy dispersion of X-rays (EDS).

This detector consists of a Si crystal doped with Li, coated at both ends with a conductive layer of Au and kept in high vacuum and at a temperature of -192°C with liquid nitrogen.

3.3 Electrode preparation

3.3.1 GC/GO/PVA electrode

Polyvinyl alcohol (PVA) based film structured with oxidized graphene particles (GO) was prepared through a "casting" process. On the surface of glassy carbon (GC) after normal mechanical cleaning operations (treatment on cloth with Al_2O_3 powder and washing with H_2O) 10 µL of a PVA/GO emulsion were added. The different solutions used for the casting were prepared by taking different quantities of an aqueous dispersion of GO (20 mg/5 mL) and an aqueous solution of PVA (0.004 g/mL). While the GO aqueous dispersion was prepared with 20 mg of GO and 5 mL of water, aqueous PVA solution was obtained by dissolving 0.1 g of PVA in 25 mL of water and placing it in a sonicator for about two hours at 80°C. Following the casting, the electrode was placed in an oven at 50°C for 10 minutes [36,37].

3.3.2 GC/BE/Pt

On the surface of glassy carbon (GC) after normal mechanical cleaning operations (treatment on cloth with Al_2O_3 powder and washing with H_2O) was electrodeposited a betaine (BE) film by cyclic voltammetry, from a phosphate buffer solution at pH=7 containing betaine 1.5 mM and KCl 10 mM, using a potential range between -1.7 V ÷ 1.8 V vs SCE, 20 mV/s, 6 cycles. After betaine deposition, the electrode was activated in H_2SO_4 0.2 M solution and finally, platinum was electrodeposited under voltammetric conditions between 0.4 V ÷ 0.1 V vs. SCE, 50 mV/s, 30 cycles in 2.0 mM of Na_2PtCl_6 solution.

4. Results and discussions

4.1 GC/GO/PVA electrode

4.1.1 Electrochemical characterization

Polyvinyl alcohol film (PVA) structured with graphene oxide particles (GO) was prepared as described in chapter 2-3, based on a procedure recently developed in the laboratory [36,37]. After the preparation phase, the GC/GO/PVA electrode was subjected to an electrochemical treatment by cyclic voltammetry, cycling the potential between 0 V and 1.5 V vs SCE for 50 cycles at 100 mV/s in a phosphate buffer solution (PBS) at pH 7. Figure 4.1 shows the comparison of the voltammetric profile of the electrode, obtained respectively before and after the electrochemical treatment.

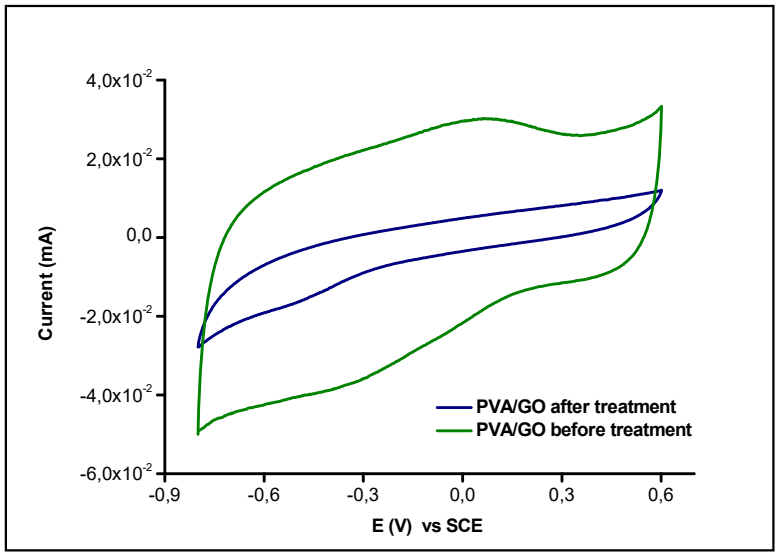

Figure 4.1: Voltammetric profile of the electrode GC/GO/PVA before and after electrochemical treatment. Potential range (-0.8V÷0.6V), 0.1 V/s, 5 cycles in PBS pH 7.

From figure 4.1 it can be observed that, following the electrochemical treatment, there has been a decrease in the capacitive current over the

whole range of potential applied. It is hypothesized that this treatment is attributable to the reduction of the electrode substrate tested.

The present investigation is focused on the electrochemical characterization of the electrode GC/GO/PVA by electrochemical, X-ray photoelectron spectroscopy (XPS) and scanning electron microscopy (SEM) techniques. The electrochemical properties of GC/GO/PVA were defined in phosphate buffer solution toward the oxidation of some important molecules such as paracetamol, acetylsalicylic acid, ibuprofen, piroxicam, and nimesulide.

In figure 4.2 we can observe the voltammetric response of GC/GO/PVA electrode (A) and GC electrode (B) in presence of increasing concentrations of paracetamol.

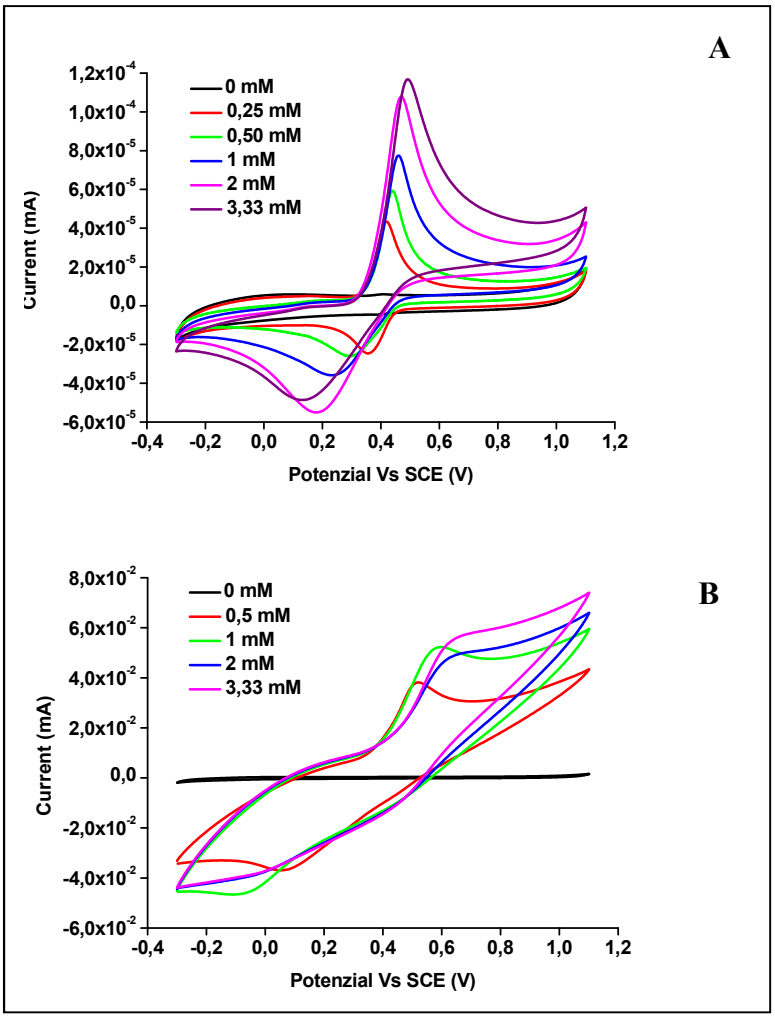

Figures 4.2: Voltammetric profiles of GC/GO/PVA system (A) and GC electrode (B) in the presence of increasing concentrations of paracetamol. Support electrolyte PBS (pH 7), potential range -0.3 V ÷ 1.1 V, scan rate 0.1 V/s, cycles number 5.

The GC/GO/PVA electrode, figures 4.2 A shows a cathodic peak at about 0.3 V, and an anodic peak at about 0.4 V vs SCE, which grows linearly with increasing paracetamol concentration. Also GC electrode, figure 4.2 B, presents an activity in the oxidation of this molecule, but the anodic and cathodic peaks are less defined than those of the modified electrode. Although both electrodes show a ΔEp (Epa - Epc) dependent

on the concentration of paracetamol, for the modified electrode this dependence is minor, therefore it is possible to affirm that in the modified electrode there is a greater degree of electrochemical reversibility compared to the GC electrode.

In the presence of acetylsalicylic acid, the voltammetric responses shown in figures 4.3 were obtained.

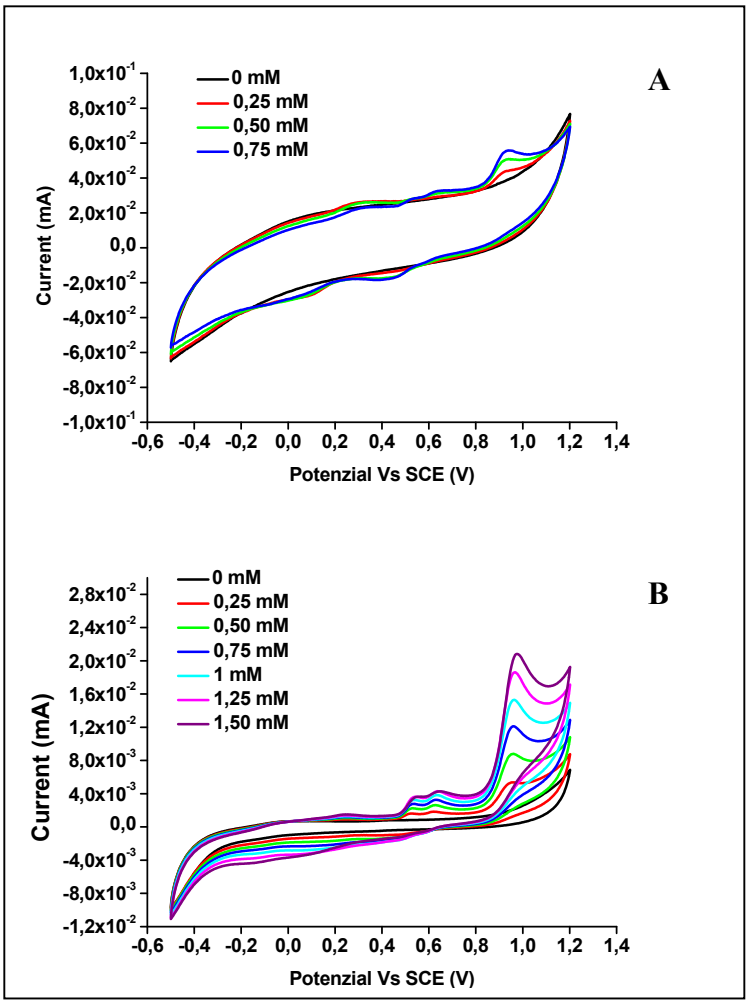

Figures 4.3: Voltammetric profiles of GC/GO/PVA system (A) and GC electrode (B) in the presence of increasing concentrations of acetylsalicylic acid. Support electrolyte PBS (pH 7), potential range -0.5 V ÷ 1.2 V, scan rate 0.1 V/s, cycles number 5.

As can be seen from figure 4.3 A, the GC/GO/PVA electrode has only one well defined oxidation wave at 0.9 V vs SCE whose intensity increases linearly with the concentration of the analyte. On the other hand, the GC electrode, figure 4.3 B, has three oxidation waves at 0.5 V,

0.7 V and 0.9 V respectively. However, in both cases the activity of electrocatalysis towards this target molecule still seems to present areas of overlapping of potentials with oxygen discharge.

The next molecule we tested is piroxicam, shown in figure 4.4.

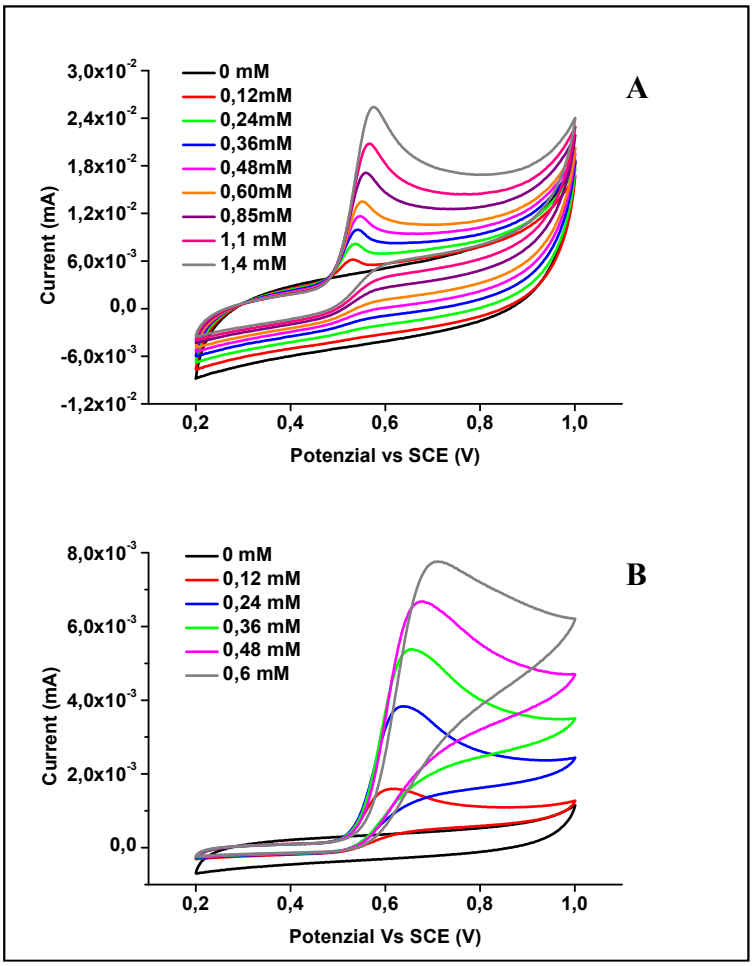

Figures 4.4: Voltammetric profiles of GC/GO/PVA system (A) and GC electrode (B) in the presence of increasing concentrations of piroxicam. Support electrolyte PBS (pH 7), potential range 0.2 V ÷ 1.0 V, scan rate 0.1 V/s, cycles number 5.

As regards the voltammetric profile obtained with the GC/GO/PVA electrode, figures 4.4 A, there is a large oxidation wave, which has its maximum for potentials of about 0.5 V vs SCE. Also the GC electrode

is active towards the oxidation of piroxicam, figures 4.4 B, in fact a very wide wave can be observed with apex at about 0.6 V and that increasing the concentration of the analyte is increasingly overlapping with the oxygen discharge.

The forth molecule we tested is Nimesulide, shown in figure 4.5.

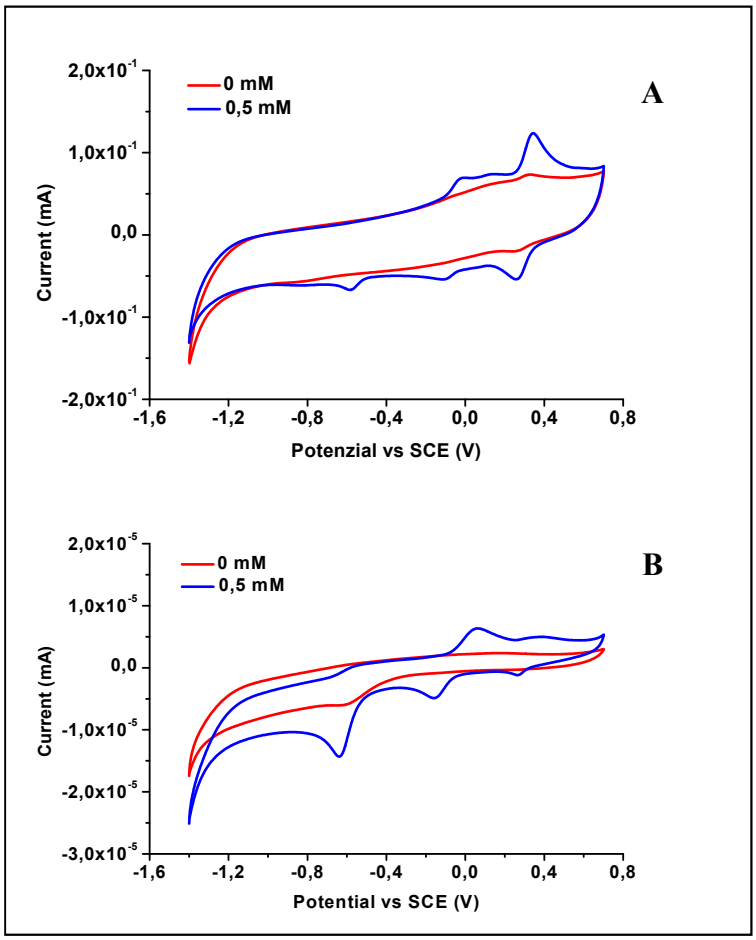

Figures 4.5: Voltammetric profiles of GC/GO/PVA system (A) and GC electrode (B) in absence and in presence of 0.5 mM of nimesulide. Support electrolyte PBS (pH 7), potential range -1.4 V ÷ 0.7 V, scan rate 0.1 V/s, cycles number 5.

Figures 4.5 A and B respectively show the behavior in cyclic voltammetry of the GC/GO/PVA and GC electrode in the presence of

nimesulide. It is clear that in both cases we have a complex electrochemical behavior. In both cases we have the presence of two waves in oxidation and three in reduction, however the relative and absolute intensities of the same are different. In fact, in the case of the modified electrode we have a signal intensity of about five orders of magnitude greater than GC electrode. Unfortunately, it was not possible to study the electrode behavior related to concentration additions higher than 0.5 mM because at higher concentrations than this value nimesulide in PBS solutions (pH7) precipitates.

The last molecules we analyzed is ibuprofen, figure 4.6.

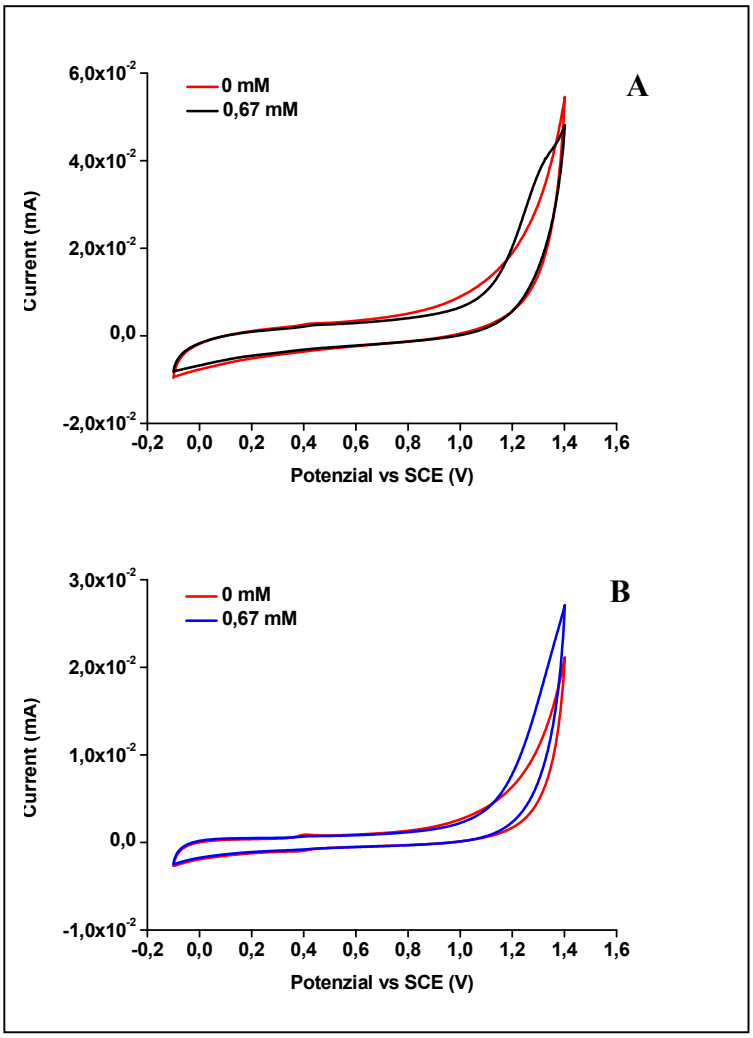

Figures 4.6: Voltammetric profiles of GC/GO/PVA system (A) and GC electrode (B) in absence and in presence of 0.67mM of ibuprofen. Support electrolyte PBS (pH 7), potential range -0.1 V ÷ 1.4 V, scan rate 0.1 V/s, cycles number 5.

For this molecule the behavior of the two electrodes tested is similar. Indeed, in both cases, in the whole range of potentials studied, a redox pair is not observed but it is present a single oxidation wave for potentials greater than 1.3 V that overlaps with the oxygen discharge. It was not

possible to test higher concentrations of analyte with cyclic voltammetry since the electrode was already very close to saturation level.

Following cyclic voltammetry study, we tested the electrode performance using differential pulse voltammetry (DPV). This technique makes it possible to measure currents with a low content of capacitive currents [101], which makes it possible to detect much lower concentrations of the molecules studied. In this work we used the waveform showed in figure 4.7. This waveform was suggested by Metrohom with the related management software [102,103].

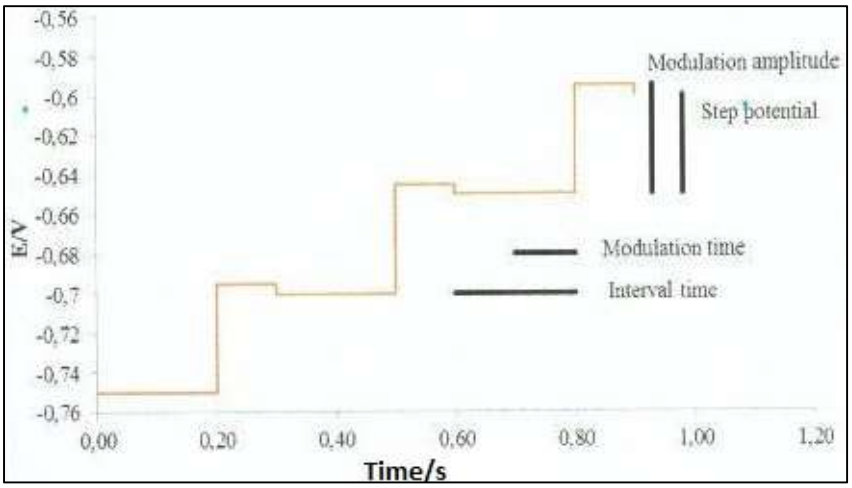

Figure 4.7: Waveform used in this work. Interval time 0.2 s, modulation time 0.1 s, step potential 0.0051V and modulation amplitude 0.05505V.

Figures 4.8 – 4.12 shows the DPV profile acquired with the GC/GO/PVA electrode in the presence of molecules studied.

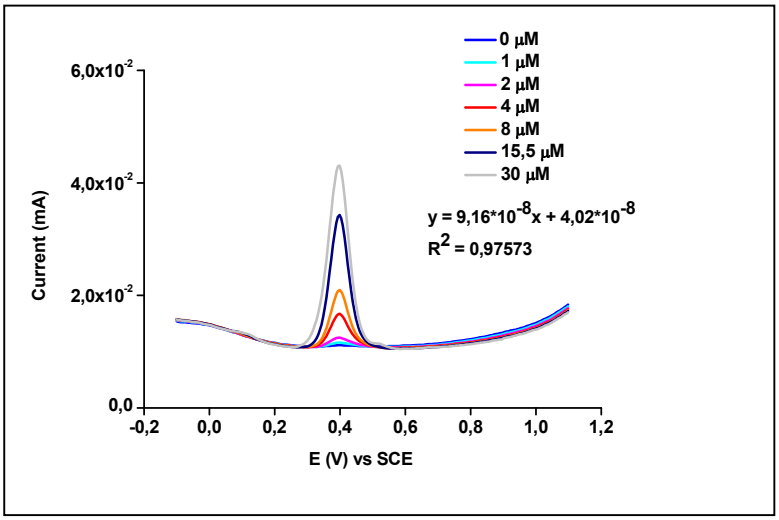

Figure 4.8: DPV profiles of GC/GO/PVA system in the presence of increasing concentrations of paracetamol. Support electrolyte PBS (pH 7), potential range -0.1 V ÷ 1.1 V, waveform showed in figure 4.7.

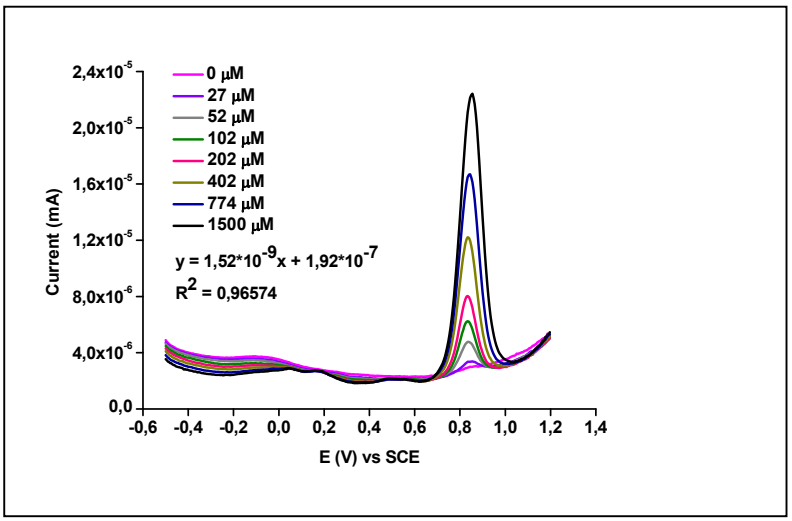

Figure 4.9: DPV profiles of GC/GO/PVA system in the presence of increasing concentrations of acetyl salicylic acid. Support electrolyte PBS (pH 7), potential range -0.5 V ÷ 1.2 V, waveform showed in figure 4.7.

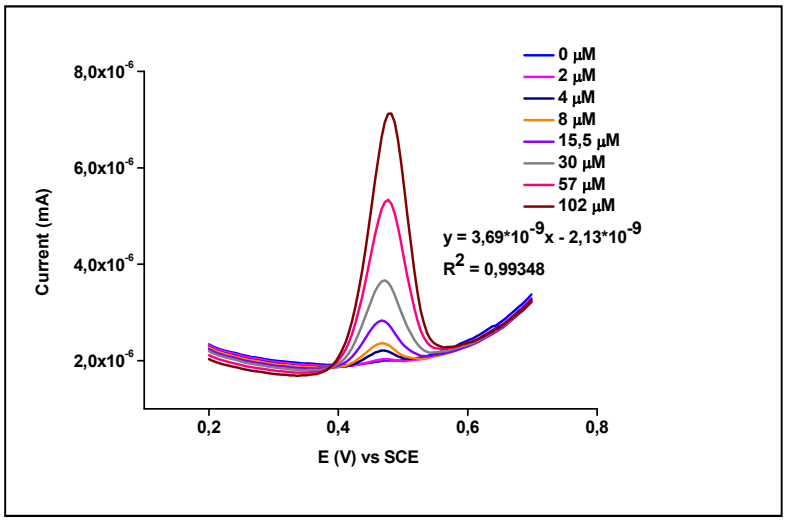

Figure 4.10: DPV profiles of GC/GO/PVA system in the presence of increasing concentrations of piroxicam. Support electrolyte PBS (pH 7), potential range 0.2 V ÷ 0.7 V, waveform showed in figure 4.7.

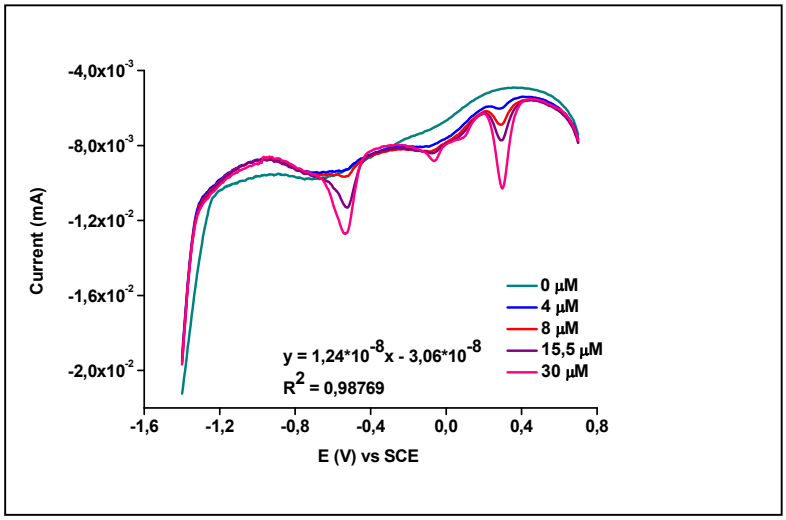

Figure 4.11: DPV profiles of GC/GO/PVA system in the presence of increasing concentrations of nimesulide. Support electrolyte PBS (pH 7), potential range -1.4 V ÷ 0.7 V, waveform showed in figure 4.7.

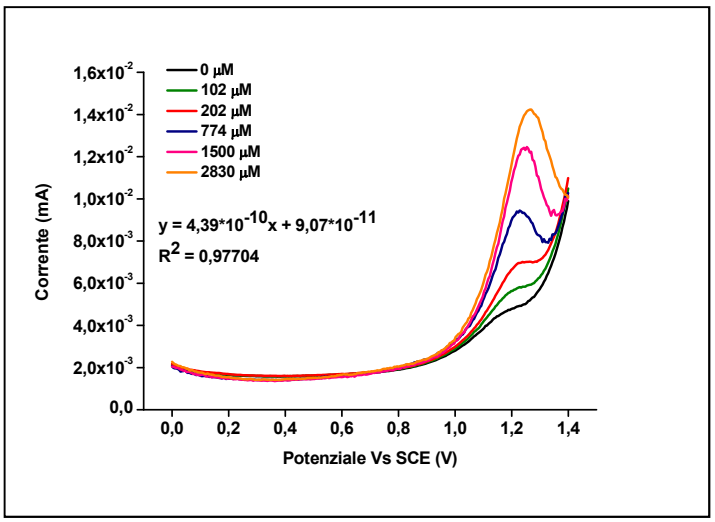

Figure 4.12: DPV profiles of GC/GO/PVA system in the presence of increasing concentrations of ibuprofen. Support electrolyte PBS (pH 7), potential range 0 V ÷ 1.4 V, waveform showed in figure 4.7.

As can be seen from the figures 4.8 – 4.12, well-defined oxidation peaks are obtained. Furthermore, the resulting calibration plots show a good linear signal-concentration correlation for all the analyzed molecule with correlation coefficients better than 0.966.

4.1.2 SEM analysis

Scanning electron microscopy (SEM) can provide valid indications about the superficial morphological state of electrode materials both freshly prepared and following prolonged use in different application contexts. In general, the superficial distribution of a catalyst plays an essential role in defining the relative performances, as the degree of adhesion and allocation on a surface substrate play important roles in defining its physical and chemical properties.

Figure 4.13 shows a SEM image relating to a graphitic surface covered with a PVA film.

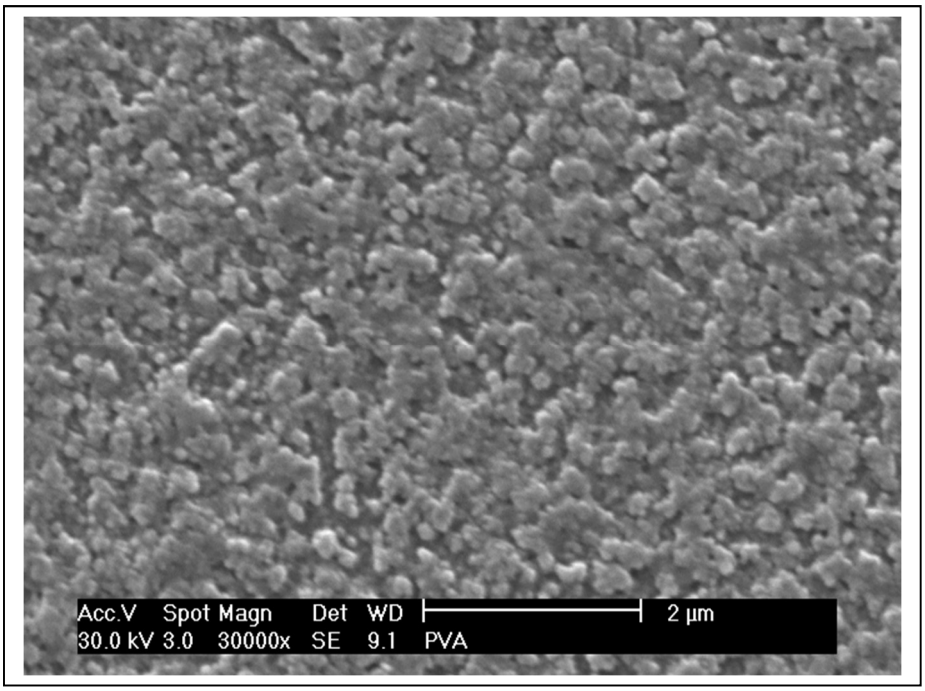

Figure 4.13: Morphology of the PVA film deposited on GC by procedure of casting.

The surface of the PVA shows a high degree of surface roughness, with the film distributed over the entire surface to form agglomerated structures variable in both shapes and sizes. Furthermore, PVA film shows a high degree of porosity, thus offering a high exposed surface. PVA films, with SEM images very similar to the figure 4.13, were obtained through casting procedures on graphite from solutions prepared with 15% of PVA in H_2O / DMSO (20:80) and kept at 140 °C for 2 h and then crystallization at -20 °C [104].

Figures 4.14 A and B show the dispersion of graphene particles, before and after electrochemical treatment, in aggregate forms and joined together by the polymeric matrix of the PVA.

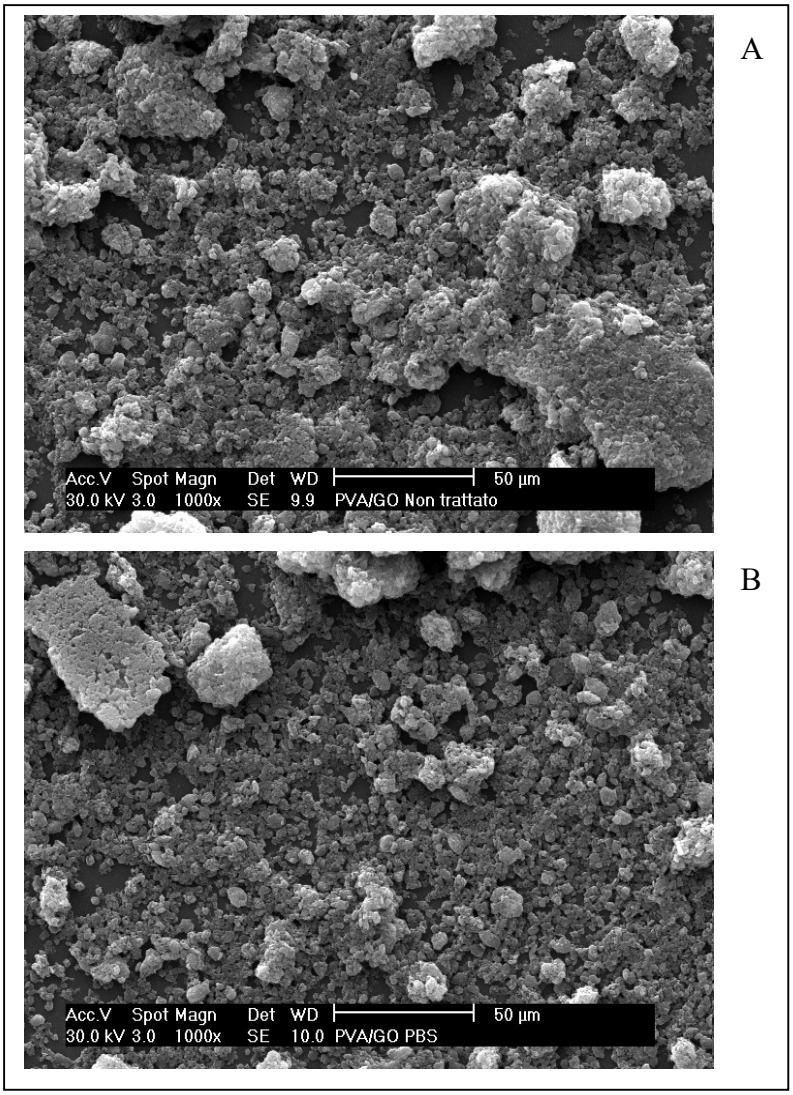

Figure 4.14: Morphology of the PVA/GO film deposited on GC by casting, before (A) and after (B) electrochemical treatment.

The graphene particles appear as tiled structures, defined in the literature as “nanoplatelets”; they have very uneven thicknesses and shapes with high degrees of aggregation between them. From the comparison of figures 4.7 and 4.8 it can be deduced that the PVA/GO deposit, obtained with emulsions containing about 80% GO, shows a total disappearance

of the initial form of the PVA polymer, to the advantage of thickened tile structures of GO forming irregular conglomerates. Comparing figures 4.8 A and B it can be observed that no substantial variation of the substrate has occurred, in both samples there are inhomogeneous lamellar structures and a good degree of aggregation of the components is maintained, even after strong electrochemical stress.

4.1.3 XPS analysis

XPS (X-ray Photoelectron spectroscopy) analysis is particularly useful for defining the surface chemical composition of electrode substrates. In this regard, two systems have been analyzed and compared, such as: PVA and PVA/GO. The XPS analysis was carried out by studying in detail the spectral regions of C1s and O1s, through a comparative approach of the respective spectroscopic signals. The different signals considered were fitted using curves of the Gaussian/Lorenzian type and the stoichiometric ratios of the highlighted species were obtained using the respective sensitivity factors [105-107]. The form of the spectroscopic signals as well as that of the relative secondary structures (shake-up signals) have been defined according to that has already been attributed by the specialist literature [107].

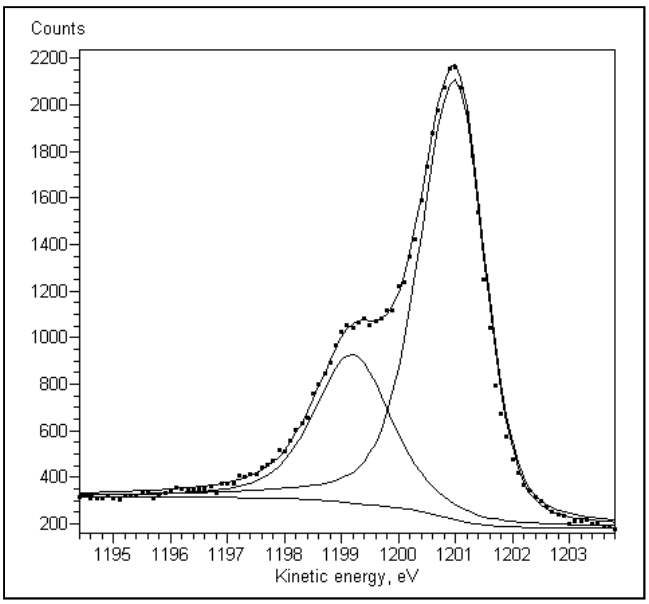

Figure 4.15: C1s spectrum of PVA/GO before electrochemical treatment.

Figure 4.15 shows the C1s region relative to the PVA/GO film before electrochemical treatment. It is evident, besides the graphitic signal (CH) centered at about 284.6 eV, the intense signal at ca. 286.3 ± 0.2 eV, attributed to the hydroxyl carbon (C-OH) [107-109] deriving mainly from the alcohol groups of the PVA. Subsequently, the XPS analysis was also conducted for the GC/GO/PVA electrode after electrochemical treatment, figure 4.10.

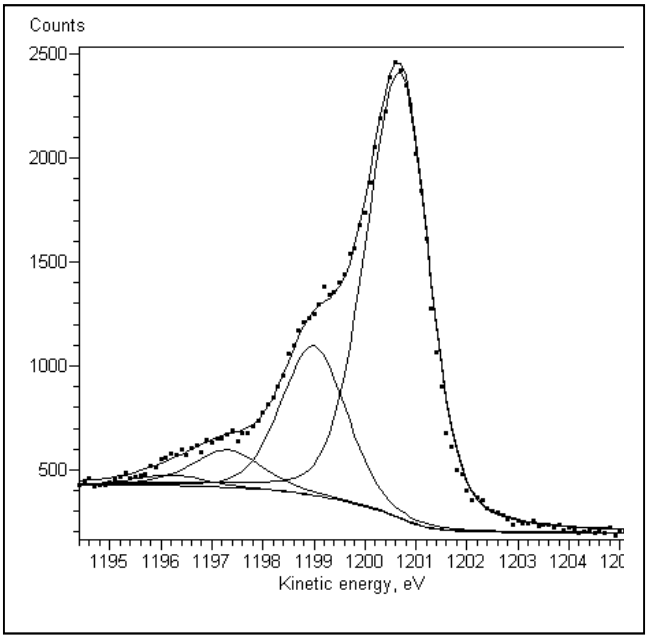

Figure 4.16: C1s spectrum of PVA/GO after electrochemical treatment.

As can be seen from figure 4.16, in addition to the graphitic and alcoholic signals, two other signals have appeared, with higher binding energies (B.E.), which are generally attributed to the oxidized carbon species such as: C = O and COOH.

The O1s signal, showed in figure 4.17, can be "fitted" by three distinct contributions with B.E. attributable to different oxygenated carbon groups, although the exact assignment is quite complicated by the mutual overlapping of the signals.

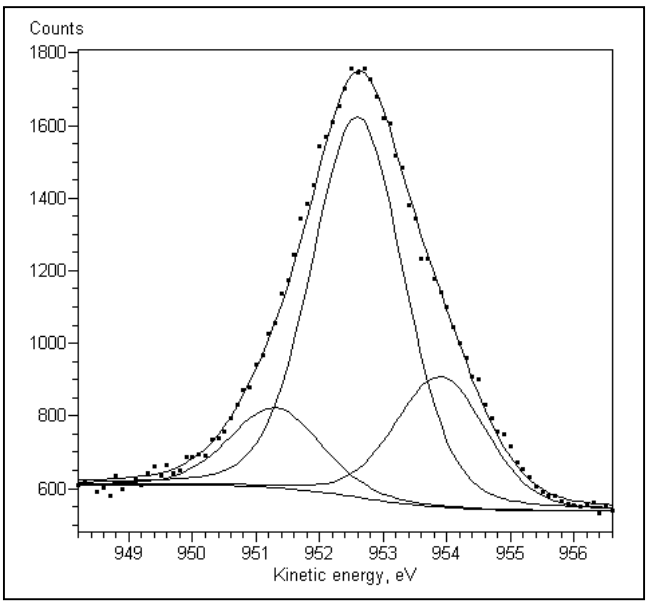

Figure 4.17: O1s spectrum of PVA/GO after electrochemical treatment.

4.2 GC/BE/Pt electrode

4.2.1 Electrochemical characterization

The GC/BE/Pt electrode was prepared as described in paragraphs 2-3. Figure 4.18 shows the behavior of the GC/BE/Pt electrode: the complex system of redox waves in the hydrogen area (between 0.0 V and - 0.3 V vs SCE), due to the processes of oxidation/reduction of hydrogen adsorbed on Pt particles [110-115], while waves at about 0.5 V and 0.6 V are due to the formation of Pt at high oxidation states (i.e., I and / or III) and their relative reduction to metallic Pt [111-116].

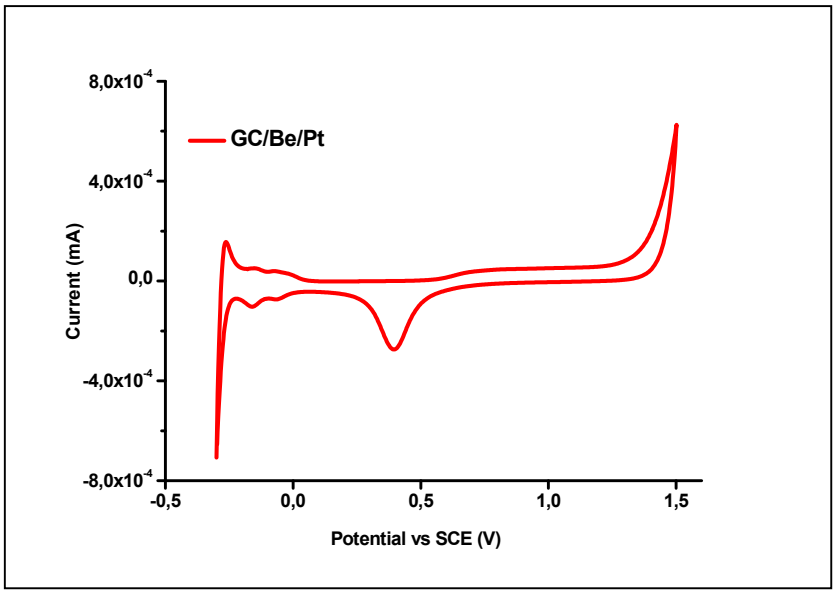

Figure 4.18: Voltammetric profile of GC/BE/Pt electrode.
Potential range (-0.3 V÷1.5 V), 0.1 V/s, 5 cycles in H_2SO_4 0.2 M.

As expected, general profile of the GC/ BE/Pt system is very similar to that of Pt, as showed in figure 4.19.

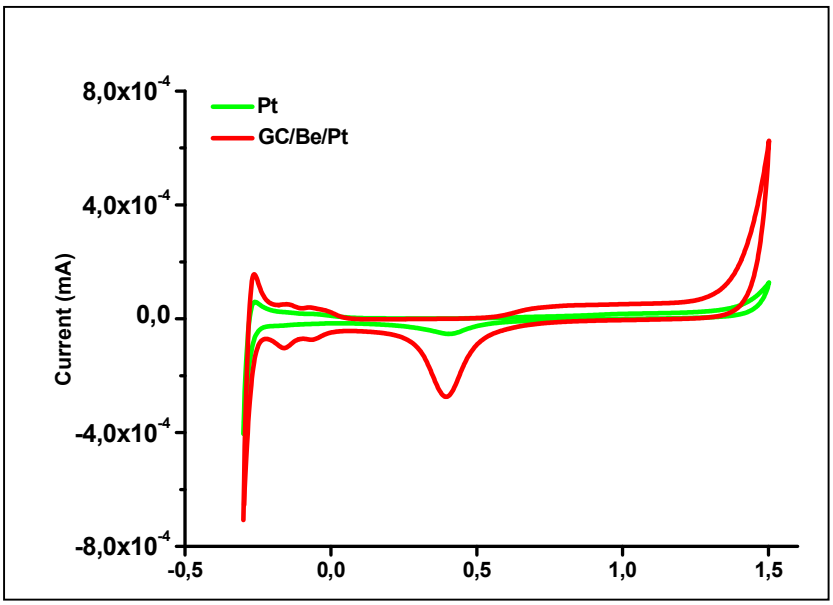

Figure 4.19: Voltammetric profile of GC/BE/Pt electrode and Pt electrode.
Potential range (-0.3 V÷1.5 V), 0.1 V/s, 5 cycles in H_2SO_4 0.2 M.

From the direct comparison between the classical Pt electrode with the modified GC/BE/Pt electrode; it clearly emerges that although the profile is very similar between the two electrodes, the currents involved are deeply different in intensity. The GC/BE/Pt electrode shows throughout the region investigated, intensity of charge greater than 300% compared to the traditional Pt electrode, having a similar geometric area. Probably, the surface polydispersion of platinum particles produces a significant increase in the exposed active area, producing consequently, for the same geometric area (apparent electrode area), a significant increase in the real electrode area (roughness factor).

The GC/BE/Pt electrode, prepared as described above, was characterized in an acid environment (H_2SO_4 0.2 M). It shows a good mechanical and electrochemical stability in the range of potential investigated between -0.3 V and 1.5 V (SCE). As shown in Figures 4.18 and 4.19, the voltammetric profile of the GC/BE/Pt electrode highlights a large region of potentials where platinum performs its traditional electrochemical performance such as: the hydrogen region, through the classic and complex redox processes; the region of platinum transition (Pt^0/Pt (I)/Pt (IV)) between 0.1 V and 1.1 V, that is the formation of platinum at the different oxidation states; finally the massive discharge of the medium to high potentials through the oxidation of H_2O and relative formation of O_2, at potentials greater than 1.3 V [111-113].

In this work the electroanalytical performance of the GC/BE/Pt electrode as amperometric sensor for the determination of vitamins B_1 and B_6 were tested.

Figure 4.20 shows the voltammetric behavior of the GC/BE/Pt sensor towards the oxidation of vitamin B_6 in H_2SO_4 0.2 M.

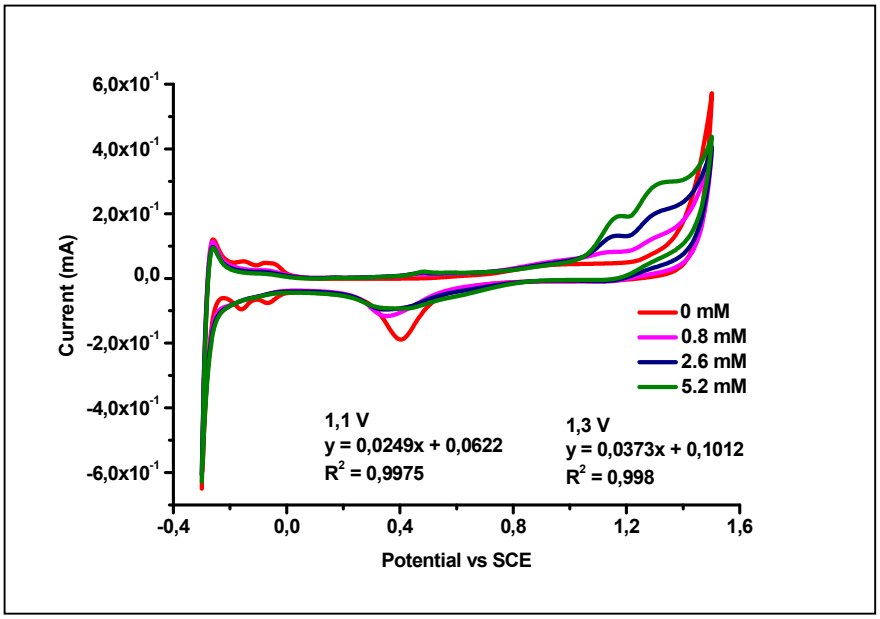

Figure 4.20: Voltammetric profiles of GC/GO/PVA electrode in presence of increasing concentrations of vitamin B_6. Potential range (-0.3V÷1.5V), 0.1 V/s, 5 cycles in H_2SO_4 0.2 M.

Various additions of vitamin B_6 show an increase in the currents of a complex oxidation wave between 1.0 V and 1.5 V, partially also affecting the discharge region of the medium. Moreover, even in presence of trace amounts of analyte, there is a clear contraction of the Pt reduction signal, in addition to the partial disappearance of the complex system of redox waves in hydrogen potential area. Decrease of the characteristic signals of platinum voltammetric behavior is an indication of the presence of phenomena of irreversible adsorption of the analyte or of some of its reaction product on the active sites of the Pt. However, although there are evident phenomena of irreversible adsorption of the analyte or its reaction products, the complex

voltammetric response for applied potentials > 1.0 V is proportional to the concentration of vitamin B_6.

Figure 4.21 shows the voltammetric response of a GC electrode not modified in the presence of vitamin B_6.

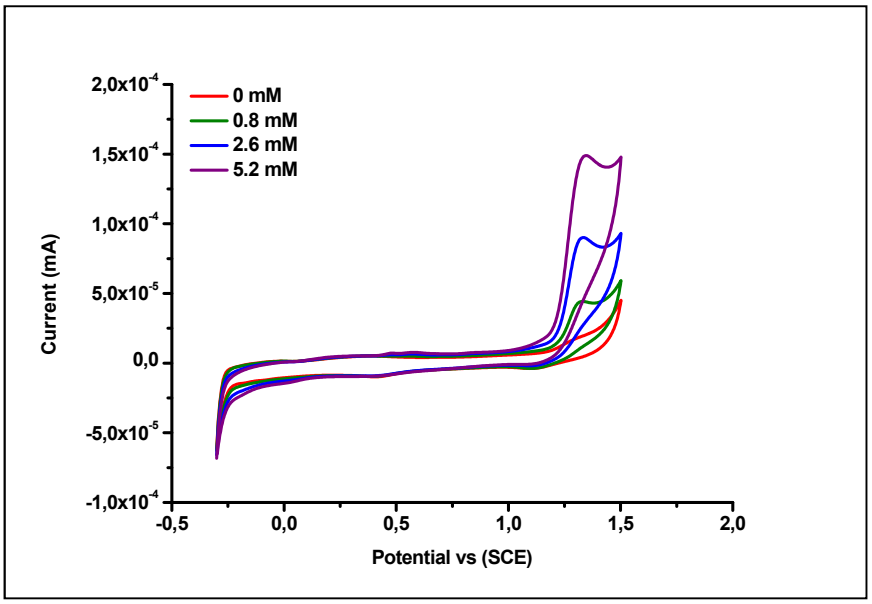

Figure 4.21: Voltammetric profiles of GC electrode in presence of increasing concentrations of vitamin B_6. Potential range (-0.3V÷1.5V), 0.1 V/s, 5 cycles in H_2SO_4 0.2 M.

It is observed that graphite (GC) is able to oxidize vitamin B_6, however there are appreciable currents only for potentials greater than 1.2 V. It is therefore clear that the presence of the BE/Pt system on the electrode surface allows to "anticipate" the potentials of electro-oxidation.

Figure 4.22, instead, shows the voltammetric behavior of the electrode GC/BE/Pt in presence of increasing concentrations of vitamin B_1. In this case, an evident redox system is observed at potentials just above 1.0 V vs. SCE, where a reduction wave also appears, although little resolved and low current intensity.

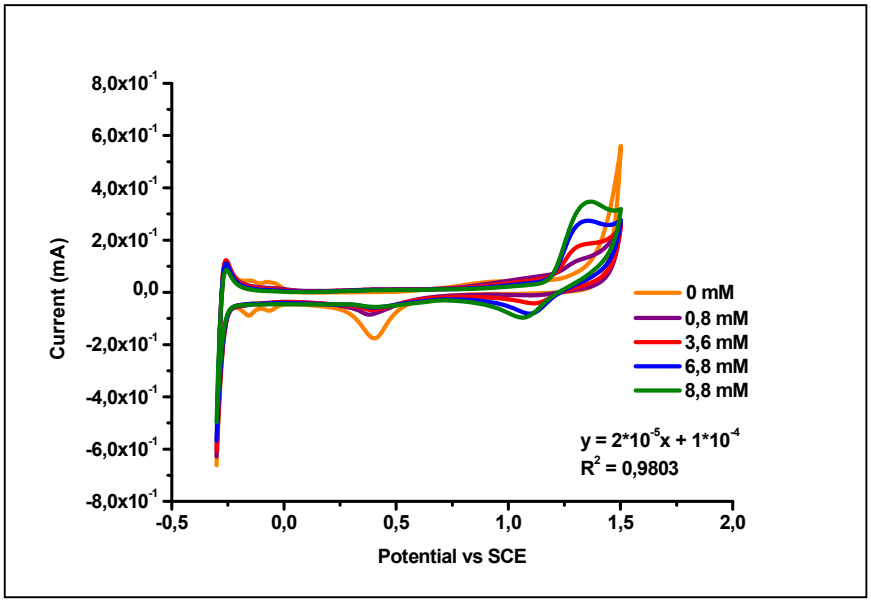

Figure 4.22: Voltammetric profiles of GC electrode in presence of increasing concentrations of vitamin B_1. Potential range (-0.3V÷1.5V), 0.1 V/s, 5 cycles in H_2SO_4 0.2 M.

Also in this case, a good linearity signal vs. concentration is observed with coefficient of correlation of 0.98.

In order to understand some analytical performances, particularly useful for potential amperometric applications, the electrode system GC/BE/Pt was tested in conditions of constant applied potential in the presence of increasing concentrations of analyte.

Figure 4.23 shows a typical amperometric comparison between the electrodes GC and GC/BE/Pt in the presence of consecutive additions of vitamin B_1. The electrode systems were subjected to a constant applied potential of 1.3 V.

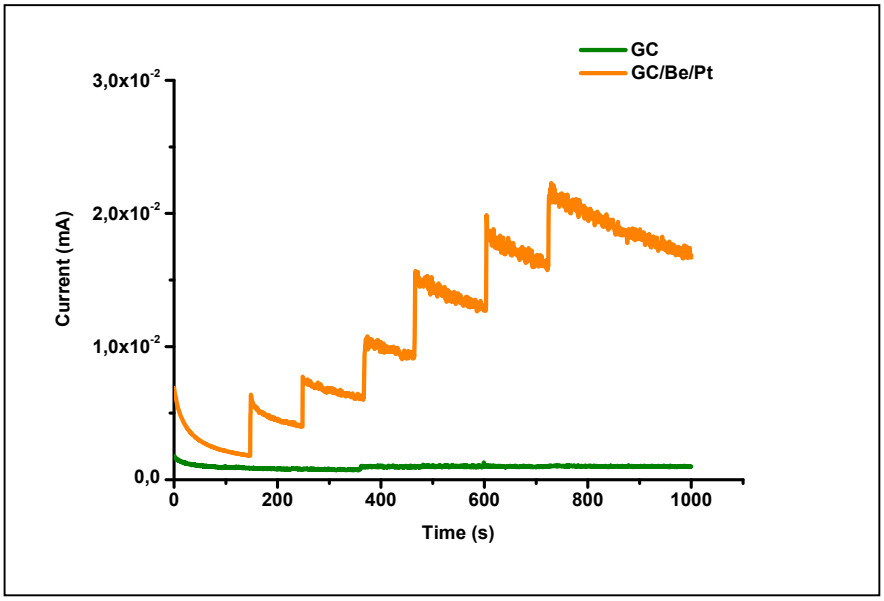

Figure 4.23: Chronoamperometric comparison between GC and GC/BE/Pt electrode in presence of increasing concentration of vitamin B_1. Potential applied 1.3V in H_2SO_4 0.2 M.

As can be seen from Figure 4.23, the GC/BE/Pt system shows a significant and clear amperometric response in presence of increasing concentration (mM) of analyte, although significant decrease of the signal with time can be observed.

Amperometric conditions used seem to indicate an obvious phenomenon of superficial poisoning of the sensor object of studio, caused by the formation of probable products of the oxidation reaction and/or caused by the absorption of the vitamin itself. Often, systems platinum-based electrodes, are subject to important effects of superficial poisoning caused by irreversible adsorption of the analyte or its oxidation products on the active sites of the system [20,112,113,116,117], so much to require the use of potential pulsed amperometric techniques, known as PAD (Pulsed Amperometry Detection) [20]. Interesting it is, however, to observe the comparison with the amperometric signal of the system

GC electrode not modified: the amperometric response following the adding the same vitamin concentrations, shows no significant contributions of oxidation current.

Figure 4.24 shows the amperometric determination of vitamin B_6.

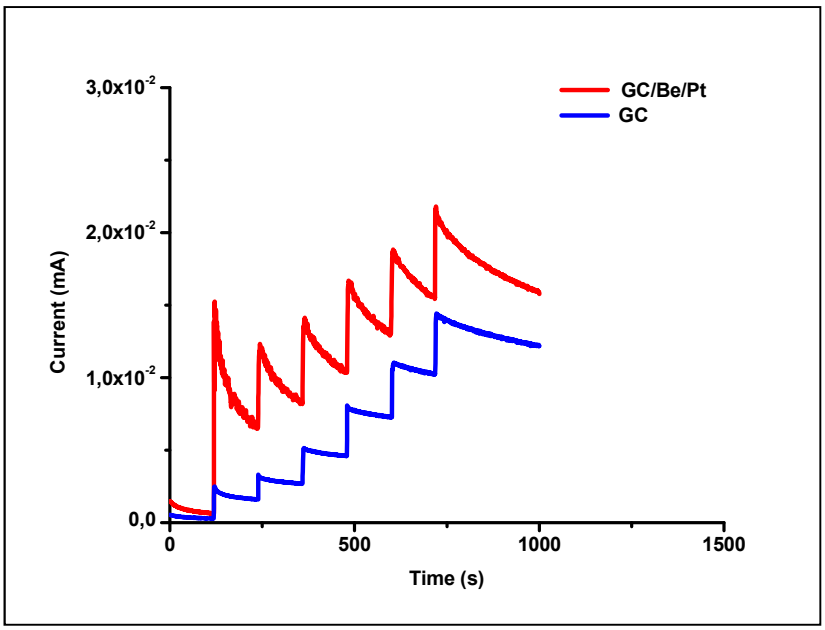

Figure 4.24: Chronoamperometric comparison between GC and GC/BE/Pt electrode in presence of increasing concentration of vitamin B_6. Potential applied 1.3 V in H_2SO_4 0.2 M.

Also in this case, the GC/BE/Pt electrode has current values visibly higher than the GC electrode system. It is however well evident as the GC/BE/Pt system has sensitive effects of superficial poisoning during the measurement process. It is evident that the presence of platinum on the electrode surface increases the undesired phenomena of superficial poisoning of the system.

4.2.2 SEM analysis

In order to have useful information about the morphological properties of BE/Pt deposit on the graphitic surface, a detailed SEM analysis was carried out on newly prepared GC/BE/Pt electrodes and after intense electrochemical treatment through the continuous looping of the potential in H_2SO_4 0.2 M for 200 scans.

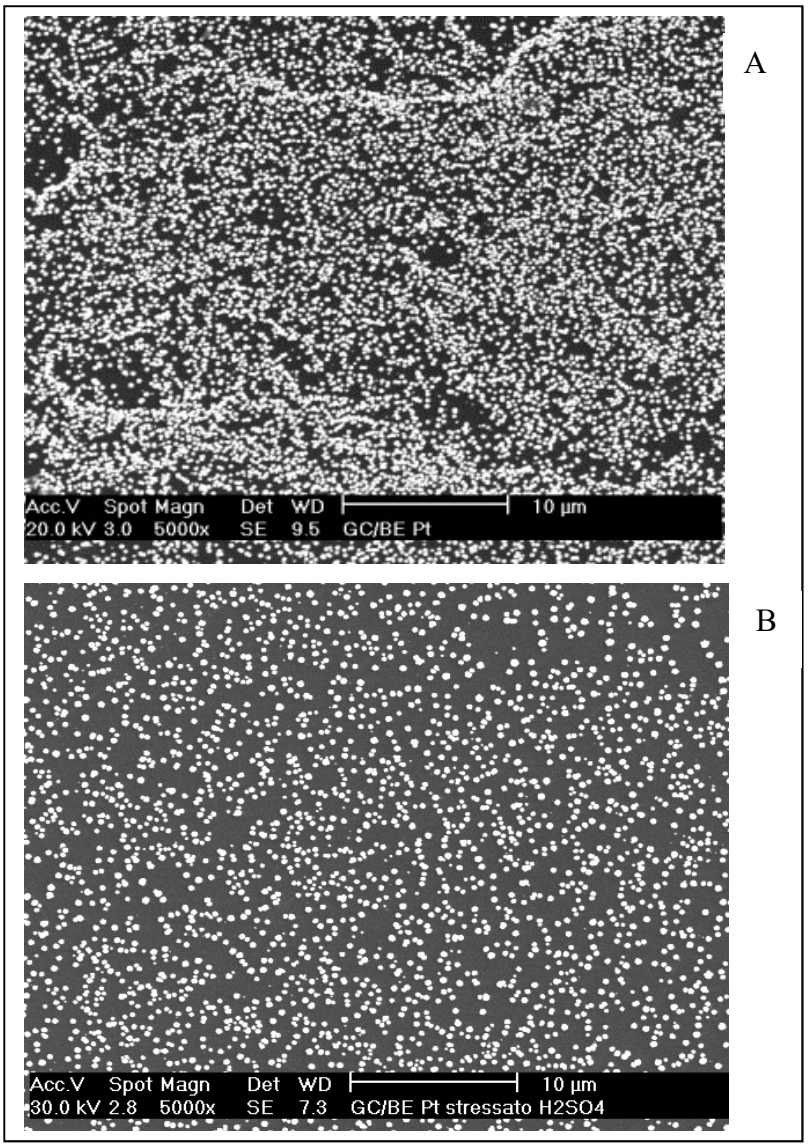

Figure 4.25: SEM images of GC/BE/Pt electrode before (A) and after (B) electrochemical stress in H_2SO_4 0.2 M.

Figure 4.25 A shows an image of freshly prepared GC/BE/Pt electrode: the electrode surface appears homogeneously covered with Pt particles having mainly globular type structure. Figure 4.25 B shows the surface image of the GC/BE/Pt electrode after prolonged treatment (200 scans) in H_2SO_4 0.2 M. Emerges a sensible decrease of the surface density of the polydisperse particles of Pt, although the shape and the dimensions result completely similar to that observed before the electrochemical treatment in acidic solution. The prolonged voltammetric treatment of the GC/BE/Pt electrode system in an acid environment, seems to show overall, after an initial phase of dissolution of Pt globules not adherent to the electrode surface, a good degree of physical stability, and the maintenance of an optimal degree of surface polydispersion of catalytic units. The high degree of surface polydispersion of the catalyst, as observed by SEM analysis, seems to agree with the voltammetric data, where the GC/BE/Pt electrode carries out a redox activity of approximately 300% compared to traditional metal Pt electrode having similar geometric dimensions to that of GC/BE/Pt.

4.2.3 XPS analysis

In order to better characterize the developed GC/BE/Pt system we performed an XPS characterization. First of all, because in literature there are no references relating to the XPS analysis on betaine to better attribute the signals recorded by the analysis of our electrode, we performed the acquisition of the betaine standard, acquiring the C1s, O1s and N1s regions.

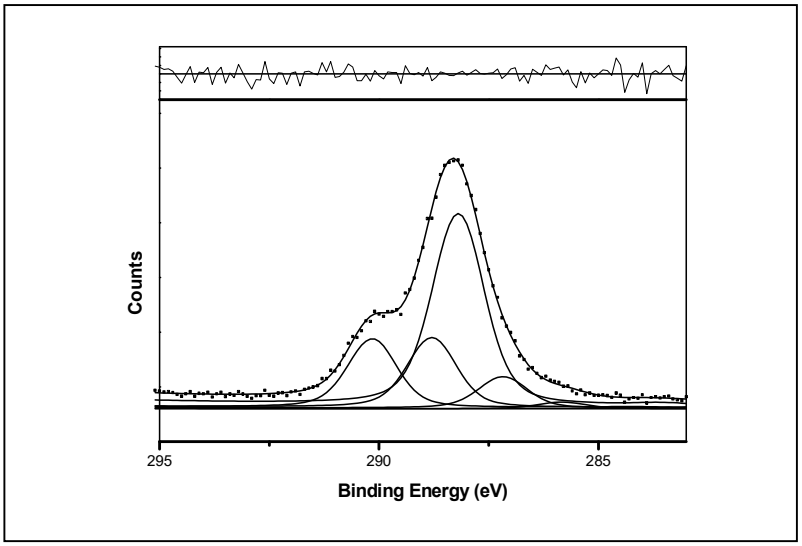

Figure 4.26: C1s spectrum of betaine standard.

Figure 4.26 shows the C1s region of the betaine standard. The signal was fitted by 4 contributions: the first was attributed to an impurity, the second one at 286.3 eV to the three methyl groups bound to nitrogen, the third signal at 286.9 eV to C in alpha to the carboxyl group, while the last one at 288.2 eV to COO^- group.

In figure 4.27 was reported the O1s region.

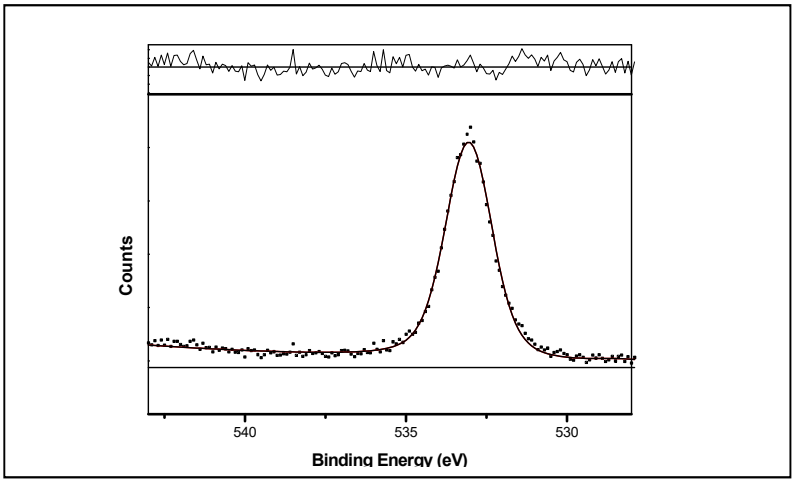

Figure 4.27: O1s spectrum of betaine standard.

The O1s region was fitted with a single peak, attributable to the oxygens belonging to the carboxyl.

N1s region, as shown in figure 4.28, was fitted with 2 peaks, the first at 399.8 eV attributable to a neutral NR_3 amine, which in our case will be $N(CH_3)_3$ [119,120]; while the second one at 402.7 eV attributable to a nitrogen of a quaternary amine, which in our case will be precisely the nitrogen of betaine $(CH_3)_3N^+CH_2COOH$. The presence of the non-charged form of nitrogen could be attributed to a betaine degradation process that occurs following exposure to X-rays.

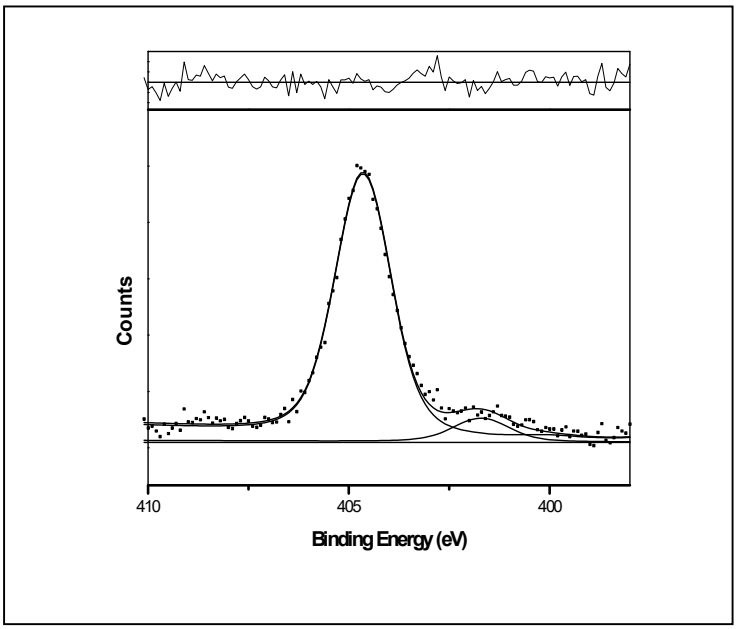

Figure 4.28: N1s spectrum of betaine standard.

Next, in figure 4.29, the C1s region of GC/BE/Pt system is shown. The signal was dense with six components, whose positions are compatible with those found in the case of the betaine standard and with the various oxidation states of the graphite (support on which betaine and then Pt were deposited first).

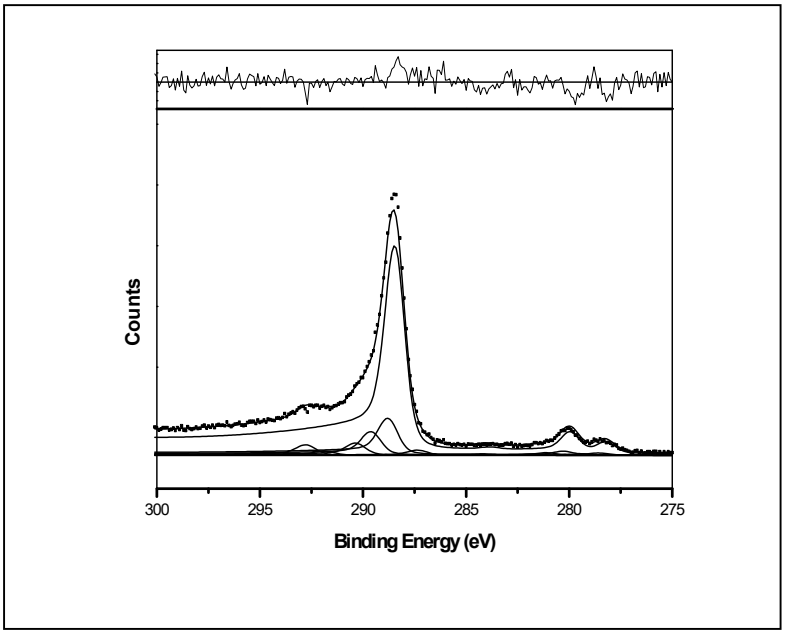

Figure 4.29: C1s spectrum of GC/BE/Pt system.

N1s region, figure 4.30, was fitted with 3 peaks. The first two, respectively at 403.5 eV and 399.9 eV attributable to NR_4^+ and NR_3, as in the case of the betaine standard, while the third one at 398.9 attributable to an N-Pt bond [121].

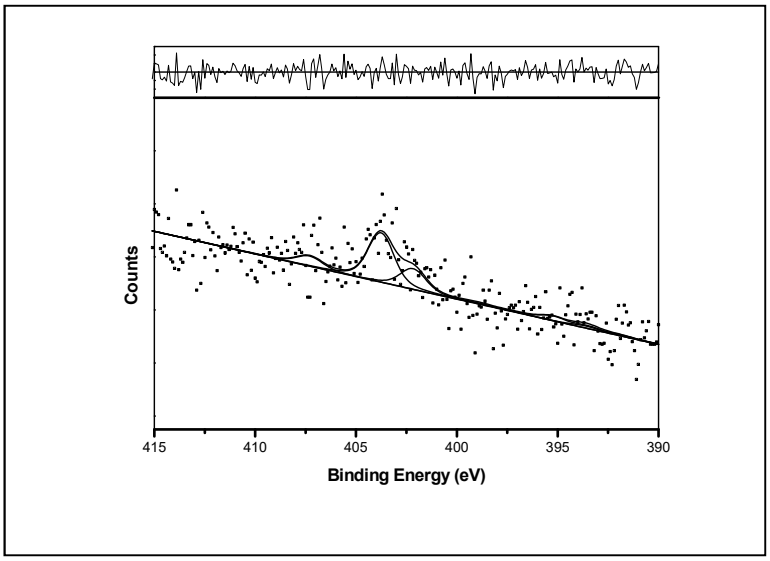

Figure 4.30: N1s spectrum of GC/BE/Pt system.

Unlike, however, of the betaine standard in figures 4.28, in the nitrogen of the GC/BE/Pt system the most intense peak is that of NR_3, which suggests that the betaine has rearranged in order to form a link with the graphite support; while on the other side some betaine molecules have formed bonds with Pt (II) atoms on which the globular particles of Pt^0 have grown, as we can well observe from SEM images.

Finally, we report the region of Pt4f, figures 4.31.

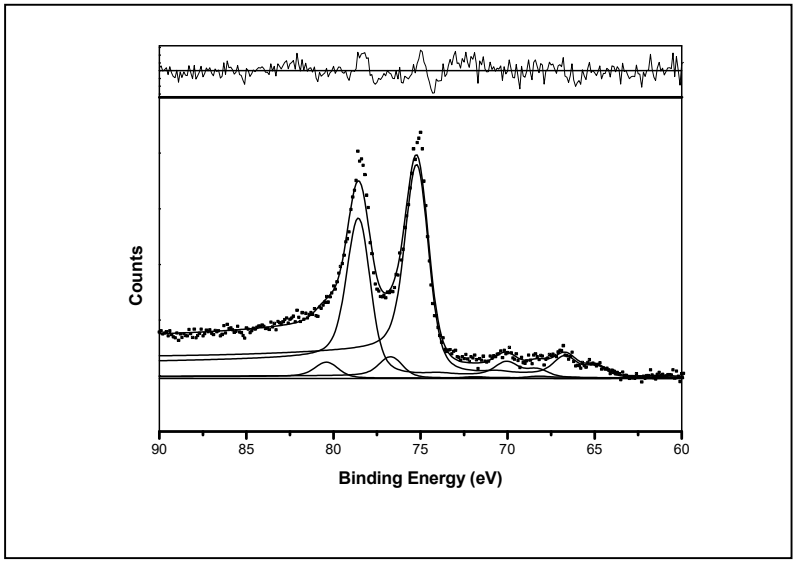

Figure 4.31: Pt4f spectrum of GC/BE/Pt system.

From the figure we can observe two double doublets, available at 71.3 eV and 72.5 eV respectively. The first is imputable to Pt^0, while the second one is Pt-N bonded.

Conclusion

In part A of this work the main purpose was the definition of an experimentally preparation and voltammetric and spectroscopic characterization of two modified electrodes: an electrode material based on polyvinyl alcohol (PVA) structured with particles of oxidized graphene (GO) called GC/GO/PVA, and a modified electrode betaine-Pt based bound on the electrodic surface of glassy carbon, called GC/BE/Pt. For the GC/GO/PVA electrode the morphological characterization (SEM characterization) allowed to observe a PVA film distributed over the entire graphitic surface in which the particles of graphene are dispersed in aggregate forms, moreover the film shows a high degree of porosity, thus offering a high exposed surface. From XPS characterization it can be deduced the presence of carbon atoms with different oxidation states, compatibly with the structure of the polymer and graphite oxide. The electrochemical characterization involved the use of voltammetric techniques, not only cyclic, but also pulsed (DPV).

The electrode was tested as an electrochemical sensor for the determination of some molecules classified as emerging pollutants. The voltammetric investigations have highlighted a good electrocatalytic character of the GO/PVA substrate for the oxidoreduction in a neutral environment (phosphate buffer solution pH 7) of paracetamol, ibuprofen, acetylsalicylic acid, piroxicam and nimesulide. DPV analysis, thanks to decrease of the capacitive currents, showed interesting analytical performances of the GC/GO/PVA sensor, in wide ranges of potentials usable for analytical purposes. Calibration lines, for potentials investigated have shown good correlations and good limits of revelation, generally attested at μM levels.

As regards the GC/BE/Pt electrode, it has been demonstrated that the use of betaine represents an element of strategic importance in the preparation of the electrode active material: indeed, the surface modification of graphite effectively allows for electro-depositing meso/nano particles of Pt in the region of potentials between 0.4 V and 0.1 V, that is to obtain adequate surface loads of platinum in the region of potentials greater than the massive discharge of H_2. Therefore, the use of betaine allows to define and modulate better electrodeposition conditions of platinum species on traditional electrode substrates. The morphological surface analysis of the electrode material under study (SEM analysis), allowed to highlight an effectively polydispersed BE/Pt structure on the electrode surface where the Pt catalyst appears in stable globular form also following prolonged electrochemical stress. As regards XPS characterization, it is evident the formation of a betaine Pt-N bond and the presence of Pt^0. The electrodic system was then tested in an environment of H_2SO_4 0.2 M with the anodic oxidation of vitamins B_1 and B_6, offering good electroanalytical performance, especially with respect to the behavior of the unmodified GC system. The chronoamperometric analysis reported a more intense response to the modified electrode, although it also showed significant signs of superficial poisoning of the sensor object of study.

References

[1] M. Wang, S. Yao, M. Madou, Sens. & Actuators, B 81 (2002) 313.

[2] A. N. Bezbaruah, T. C. Zhang, Anal. Chem., 74 (2002) 5726.

[3] G. Hanrahan, D. G. Patil, J. Wang, J. Environ. Monit., 6 (2004) 657.

[4] J. Gabel, W. Vonau, U. Guth, Ionics, 9 (2003) 176.

[5] L.M. Schiavone, W.C. Dautremont-Smith, G. Beni, J.L. Shay, Appl. Phys. Lett., 35 (1979) 823.

[6] Y. Sato, K. Ono, T. Kobayashi, H. Wakabayashi, H. Yamanaka, J. Electrochem. Soc., 134 (1987) 570.

[7] M. Ristova, R. Neskovska, V. Mirčeski, Solar Energy Mater. Solar Cells, 91 (2007) 1361.

[8] Y. U. Jeong, A. Manthiram, J. Electrochem. Soc., 149 (2002) 1419.

[9] J. P. Zheng, Electrochem. Solid-State Lett., 2 (1999) 359.

[10] K. R. Prasad, N. Miura, Electrochem. Comm., 6 (2004) 1004.

[11] M. Chigane, M. Ishikawa, Electrochim. Acta, 42 (10) (1997) 1515.

[12] I. Arul Raj, K.I. Vasu, J. Appl. Electrochem., 20 (1990) 32.

[13] D. R. Rosseinsky, R.J. Mortimer, J. Electroanal. Chem., 151 (1983) 133.

[14] L. D. Burke, M. McRann, J. Electroanal. Chem., 125 (1981) 387.

[15] M. Kankeo, T. Okada, J. Electroanal. Chem., 255 (1988) 45.

[16] A. L. Yerokhin, X. Nie, A. Leyland, A. Matthews, Surf. And Coatings Tech., 130 (2000) 195.

[17] R.W. Revie, H.H. Uhlig, “Corrosion and corrosion control. An introduction to corrosion science and engineering.”, Wiley

Interscience, J. Wiley & Sons, Hoboken, USA (2008).

[18] X. Cao, R. Vassen, W. Fischer, F. Tietz, W. Jungen, D. Stover, Adv. Mat., 15 (2003) 1438.

[19] M. Paunovic, M. Schlesinger, Fundamental of electrochemical Deposition, J. Wiley & Sons Inc., Pennington, (USA) 2006.

[20] W.R. La Course, Pulsed electrochemical detection in high performance liquid chromatography, Wiley & Sons, New York, USA (1997).

[21] R.W. Murray, Molecular design of electrode surfaces. Techniques of chemistry, Vol. 22, Wiley & Sons, New York, USA (1992).

[22] R.W. Murray, A.J. Bard, Chemically modified electrodes in electroanalytical chemistry, Marcel Dekker, New York, USA (1984).

[23] F.T.A. Vork, L.J.J. Janssen, E. Barendrecht, Electrochim. Acta, 12 (1986) 1569.

[24] L.Z. Fan, J. Maier, Electrochem. Comm., 8 (2006) 937.

[25] M.J. Croissant, T. Napporn, J.-M. Léger, C. Lamy, Electrochim. Acta, 43 (1998) 2447.

[26] H. Laborde, J.M. Léger, C. Lamy, J. Appl. Electrochem., 24 (1994) 219.

[27] J. Li, F. Ye, L. Chen, T. Wang, J. Li, X. Wang, J. Power Sources, 186 (2009) 320.

[28] H.S. White, J. Leddy, A.J. Bard, JACS, 104 (1982) 4811.

[29] R. Shoji, T. Takeuchi, I. Kubo, Anal. Chem., 75 (2003) 4882.

[30] T. Alizadeh, M. R. Ganjali, M. Zare, P. Norouzi, Electrochim. Acta, 55 (2010) 1568.

[31] F. Léonard, The physics of carbon nanotube devices, W. Andrew Inc. New York, USA (2009).

[32] S. Yamashita, Y. Saito, J. H. Choi, Carbon nanotubes and graphene for photonic applications, Woodhead Publishing Series in Electronic and Optical Materials, Oxford, UK (2013).

[33] J. M. Marulanda, Carbon Nanotubes Applications on Electron Devices, Publisher: InTech, (DOI: 10.5772/977).

[34] R.C. Alkire, P.N. Bartlett, J. Lipkowski, Electrochemistry of Carbon Electrodes, 16 Ed., Wiley-VCH, Germany (2015).

[35] I. G. Casella, D. Gioia, M. Rutilo, Sens. Actuators B: Chemical, 255 3 (2018) 3533.

[36] D. Coviello, M. Contursi, R. Toniolo, I. G. Casella, J. Electroanal. Chem., 791 (2017) 117.

[37] D. Coviello, I. G. Casella, Electrochim. Acta, 261 (2018) 104.

[38] S. Rajendran, M. Sivakumar, R. Subadevi, J. Power Sources, 124 (2003) 225.

[39] N. Board, "Modern Technology of Resins & their Applications", Asia Pacific Business Press Inc., India (2002).

[40] R. Kronenthal, Z. Oser, E. Martin, Polymers in Medicine and Surgery, Springer Science & Business Media, NY (2013).

[41] G. Orlando, J. P. Lerut, S. Soker, R. J. Stratta, Regenerative Medicine Applications in Organ Transplantation, Academic Press, UK (2013).

[42] V. Nedovic, R. Willaert, Applications of Cell Immobilisation Biotechnology, Springer Science & Business Media, Netherlands (2005).

[43] G. Hanks, N. I. Cherny, N. A. Christakis, M. Fallon, S. Kaasa, R. K. Portenoy, D. C. Currov, Oxford Textbook of Palliative Medicine, Oxford University Press, Oxford (2005).

[44] L. M. Mcmanus, R. N. Mitchell, Pathobiology of Human Disease: A dynamic Encyclopedia of Disease Mechanism, Academic Press, USA (2014).

[45] C. Azzolini, F. Carta, S. Gandolfi, G. Marchini, U. Menchini, F. Simonelli, C.E. Traverso, Clinica dell'apparato visivo, Edra Masson, Milano (2014).

[46] NPCS Board of Consultants & Engineers, Handbook on Textile Auxiliaries, Dye and Dye Intermediates Technology, Asia Pacific Business Press Inc., India (2009).

[47] A. Pizzi, Wood Adhesive: Chemistry and Technology, CRC Press, NY (1989).

[48] A. Tiwari, M. Syvajarvi, Graphene Materials: Fundamentals and Emerging Applications, John Wiley & Sons, USA (2015).

[49] S. Ray, Applications of Graphene and Graphene – Oxide based Nanomaterials, Elsevier, USA (2015).

[50] D. Jiang, Z. Chen., Graphene Chemistry: Theoretical Perspective, John Wiley & Sons, UK (2013).

[51] J. He, X. Zhu, Z. Qi, C. Wang, X. Mao, C. Zhu, Z. He, M. Li, Z. Tang, ACS Appl. Mater. Interfaces, 7 (2015) 5605.

[52] M. Fiorillo, A. F. Verre, M. Iliut, M. Peiris-Pegés, B. Ozsvari, R. Gandara, A. R. Cappello, F. Sotgia, A. Vijayaraghven, M. P. Lisanti, Oncotarget, 6 (2015) 3553.

[53] X. Yang, Y. Wang, X. Huang, Y. Ma, Y. Huang, R. Yang, H. Duan, Y. Chen, J. Mater. Chem., 21 (2011) 3448.

[54] J. Kim, L. J. Cote, F. Kim, W. Yuan, K. R. Shull, J. Huan, J. of Am. Chem. Soc., 132 (2010) 8180.

[55] Y. Zhu, S. Murali, W Cai, X. Li, J. W. Suk, J. R. Potts, R. S. Ruoff, Adv. Mat., 22 (2010) 5226.

[56] www.graphene-info.com/graphene-batteries.

[57] V. R. Preedy, Food & Nutritional components in focus betaine, chemistry, analysis, function and effects, RSC Publishing, UK (2015).

[58] P.Wang, Z. Mai, Z. Dei, Y. Li, X. Zou, Bionsens. Bioelectron., 24 (2012) 3242.

[59] J. Li, H. Xie, J. Appl. Electrochem., 42 (2012) 271.

[60] B. G. Katsung, S. B. Masters, A. J. Trevor, Farmacologia generale e clinica, VIII Ed. Piccin, Padova, (2011).

[61] A. B. Lima, L. M. F. C. Torres, C. F. R. C. Guimarães, R. M. Verly, L. M. da Silva, Á. D. Carvalho J., W. T. P. dos Santos, J. Braz. Chem. Soc., 25 3 (2014) 478.

[62] B. J. Anderson, Pediatr. Anesth., 18 (2008) 915.

[63] A. Tjolsen, A. Lund, K. Hole, European Journal of Pharmacology, 193 (1991) 193.

[64] R. Bjorkman, K.M. Hallman, J. Hedner, T. Hedner, M. Henning, Pain, 57 (1994) 259.

[65] A. Ottati, S. Leone, M. Sandrini, A. Ferrari, A. Bertolini, Eu. J. Pharmacol. 531 (2006) 280.

[66] R. R. Cunha, S. C. Chaves, M. M. A. C. Ribeiro, L. M. F. C. Torres, R. A. A. Muñoz, W. T. P. Dos Santos, E. M. Richter, J. Sep. Sci., 38 (2015) 1657.

[67] M. Starek, J. Krzek, Talanta, 77 (2009) 925.

[68] H. Ibrahim, A. Boyer, J. Bouajila, F. Couderc, F. Nepveu, J. Chrom. B, 857 (2007) 59.

[69] K.P. Townsend, D. Praticò, FASEB J. 19 (2005) 1592.

[70] T.-L. Lu, Y.-C. Tsai, Sens, Actuator B 148 (2010) 590.

[71] D. Lawrence, Lancet 360 (2002) 1003.

[72] S. Weggen, M. Rogers, J. Eriksen, Trends Pharmacol. Sci. 28 (2007) 536.

[73] J. Cuzick, F. Otto, J.A. Baron, P.H. Brown, J. Burn, P. Greenwald, J. Jankowski, C.L. Vecchia, F. Meyskens, H.J. Senn, M. Thun, Lancet Oncol. 10 (2009) 501.

[74] A.O. Maree, R.J. Curtin, M. Dooley, R.M. Conroy, P. Crean, D. Cox, D.J. Fitzgerald, J. Am. Coll. Cardiol. 47 (2005) 1258.

[75] T.S. Poulsen, S.R. Kristensen, L. Korsholm, T. Haghfelt, B. Jørgensen, P.B. Licht, H. Mickley, Thromb. Res. 120 (2007).

[76] T. L. Lemke, D.A. Williams, V. F. Roche, S.W. Zito, Principi di Chimica Farmaceutica, VI Ed., Piccin, Padova (2014).

[77] J.R. Vane, R.M. Botting, Thromb res, 110 (2003) 255.

[78] E.H. Awtry, J. Loscalzo, Aspirin, Circulation 101 (2000) 1206.

[79] M. Kurakula, A. B. Mohd, P. Rao, A. Prakash, V. Diwan, Int. J. Chem. Anal. Sci., 2 9 (2011) 1193.

[80] A. D. de Jager, H. Ellis, H. K. L. Hundt, K. J. Swart, A. F. Hund, J. Chrom. B, 729 (1999) 183.

[81] R.N. Brogden, R.C. Heel, T.M. Speight, G.S. Avery, Drugs, 28 (1984) 292.

[82] M. Govindasamy, V. Mani, S.-M. Chen, T. Maiyalaganc, S. Selvarajd, T.-W. Chena, S.-Y. Lee, W.-H. Chang, RSC Advances 7 (2017) 33043.

[83] A. W. Anderson, M. S. Orlando, F. Filho, J. Electroanal. Chem. 799 (2017) 547.

[84] A.K. Singla, M. Chawla, A. Singh, J. Pharma. Pharmacol., 52 (2000) 467.

[85] M. Bevilacqua, E. Magni, Drugs, 46 (1993) 40.

[86] S. Motoca, A. Remesa, A. Popa, F. Manea, J. Schoonman, J. Environ. Sci., 25 4 (2013) 838.

[87] K.D. Rainsford, “Ibuprofen: a critical bibliographic review”, CRC

Press, London (2003).

[88] K.D. Rainsford, Ibuprofen: pharmacology therapeutics and side effects, Springer, UK (2013).

[89] Agenzia Italiana del Farmaco, EMA communication about ibuprofen, 13 April 2015.

[90] J. G. LeBlanc, G. S. De Giori, B group vitamins: Current uses and perspectives, IntechOpen UK (2018).

[91] J. G. LeBlanc, J. E. Laiño, M. J. del Valle, V. Vannini, D. van Sinderen, M.P. Taranto, G. Font de Valdez, G. Savoy de Giori, F. Sesma, J. Appl. Microbiol., 111 (2011) 1297.

[92] C. Campbell, Lancet, 324 (1984) 446.

[93] P. Holtz, D. Palm, Pharmacol. Rev., 16 (1964) 113.

[94] T. Tanaka, T. Tateno, T. Gojobori, Mol. Biol. Evol. 22 2 (2005) 243.

[95] P. Bilski, M.Y. Li, M. Ehrenshaft, M.E. Daub, C.F. Chignell, Photochem. Photobiol., 71 2 (2000) 129.

[96] J. Wang, Analytical Electrochemistry, 3rd Ed., John Wiley & Sons, NW (2006)

[97] F. J. Holler, S. R. Crouch, Foundamentals of analytical chemistry 9th Ed., USA (2014).

[98] D. Briggs, M.P. Seah, "Practical surface analysis by Auger and X-ray photoelectron spectroscopy", Ed. J. Wiley & Sons, NY (1983).

[99] D. A. Skoog, J. J. Leary, "Chimica analitica strumentale", Edises, Napoli (1995).

[100] L. Reimer, "Scanning electron microscopy, physics of image formation and microanalysis" 2nd, Springer, Germany (1998).

[101] G. D. Christian, Analytical Chemistry, 5 Ed., John Wiley & Sons, NW (1994).

[102] Instrument for Electrochemical Research and Voltammetric Analysis, Eco Chemie B. V. 3526 KM Utrecht (2007).

[103] Application Bullettin N° 231/2d, Se. 10 Metrohom.

[104] S.-H. Hyong, W.-I. Cha, Y. Ikada, Polym. Bull., 22 (1989) 119.

[105] C.D. Wagner, Anal. Chem., 51 (1979) 466.

[106] C.D. Wagner, W.M. Riggs, L.E. Davis, J.F. Moulder, G.E. Mouilenberg, Handbook of X-ray photoelectron spectroscopy, Perkin-Elmer Corp., Eden Prairie, MN (1978).

[107] E. Desimoni, I.G. Casella, A. Morone, A.M. Salvi, Surf. Interf. Anal., 15 (1990) 627.

[108] E. Desimoni, I.G. Casella, A.M. Salvi, Carbon, 30 (1992) 521.

[109] M. C. Biesinger, B. P. Payne, A. P. Grosvenor, L. W. M. Lau, A. R. Gerson, R. St. C. Smart, Appl. Surf. Science, 257 (2011) 2717.

[110] A. J. Robell, E.V. Ballou, M. Boudart, J. Phys. Chem., 68 (1964) 2748.

[111] K. J. Vetter, Electrochemical Kinetics: Theoretical and Experimental Aspects, Academic Press, NY (1967).

[112] S. Trasatti, O.A. Petrii, Pure Appl. Chem., 63 (1991) 711.

[113] G.S. Attard, P.N. Bartlett, N.R.B. Coleman, J.M. Elliott, J.R. Owen, J.H. Wang, Science, 278 (1997) 838.

[114] J. Lipkowski, P.N. Ross, Electrocatalysis. Frontiers of Electrochemistry, Eds Wiley-VCH, Weinheim (1998).

[115] O. Haas, E.J. Cairns, Electrochemical Energy Storage. In Annual Reports on the Progress of Chemistry, The Royal Society of Chemistry, London (1999).

[116] A. J. Bard, L.R. Faulkner, Electrochemical Methods: Fundamentals and Applications, John Wiley & Sons, NY (2001).

[117] J. A. Polta, D.C. Johnson, Anal. Chem., 57 (1985) 1373.

[118] I. G. Casella, M. Gatta, J. Agricultural and Food Chem., 50 (2002) 23.

[119] G. P. Jin, X. Q. Lin, Y. F. Ding, J. Solid Electrochem., 10 (2006) 987.

[120] X. Q. Lin, G. P. Jin, Electrochim. Acta, 50 (2005) 3210.

[121] A. Adenier, M. M. Chehimi, I. Gallardo, J. Pinson, N. Vilà, Langmuir, 20 (2004) 8243.

Part B

Development and validation of a
LC-MS/MS method
for the determination of drugs
in wastewater samples
and
two generation toxicity evaluation of
carbamazepine and amoxicillin
on Crustacea Copepoda *Tigriopus fulvus*

1. Introduction

Pharmaceuticals and Personal Care Products (PPCPS) present in the environment are considered “emerging” contaminants [1]. The term “emerging” is used to distinguish these products from conventional pollutants (e.g. metals - such as mercury, lead, etc.) or from those that have been defined as “priority contaminants” (DDT, PCB, PAH, etc ...). The interest from the scientific community on the effects that drugs have on living organisms and the related risks has become particularly relevant in the last decade. The excessive production of drugs and the increasing consumption of the latter have meant that drug pollution turns out to be one of the problems to be solved in the environmental pollution, especially in water pollution [2]. In detail, it is necessary to keep the pollution of the water under control because drugs are released into the sewage systems and transported to domestic waste water treatment plants. Based on their chemical and physical characteristics, some drugs will be degraded while others not [3], and from here these substances have direct access into all environmental compartments. The presence of drugs in water was first identified in 1976 in Missouri (USA) [4] and in the following years hundreds of methods were developed for the detection of these substances in various types of water around the world. Pharmaceutical compounds, analyzed in this work, include three antibiotics, i.e. clarithromycin, erythromycin and amoxicillin, anti-inflammatories, like ibuprofen, naproxen, diclofenac and acetylsalicylic acid, an antiepileptic drug, i.e. carbamazepine, metformin, an active drug against type 2 diabetes, omeprazole, a proton pump inhibitor used for the treatment of gastric ulcer and disease from gastroesophageal reflux and two steroid hormones, i.e. estradiol and ethinyl estradiol, the first used for regulating the menstrual cycle and the second one as a contraceptive.

Most of the drugs chosen in this work are on the priority list of the "World Health Organization" (WHO) [2] and represent compounds pharmacologically active, most found in Italian and/or in global waters [5-18]. Danger and damage that pharmaceutical compounds cause to environment and human beings has been the subject of study in recent years [5,19,20]. In this work, we will evaluate the presence of previously mentioned drugs in the wastewater from purification plant of Basilicata (Italy), before and after the purification treatment.

To date, the reference method for drug analysis is EPA method 1694: "Pharmaceuticals and Personal Care Products in Water, Soil, Sediment, and Biosolids by HPLC-MS/MS" [21]. It is the only one assumed for the determination of 74 pharmaceutical compounds in environmental matrices. EPA method 1694 refers to the determination of pharmaceutical products and for the personal care (PPCPS) in environmental samples (water, soil, sediments and biosolids), by high performance liquid chromatography coupled to tandem mass spectrometry (HPLC-MS/MS) [21]. In this method, the PPCPS target analysis is divided into four groups, which differ in solid phase extraction conditions, mobile phase and ionization mode used.

Moreover, according to the national and community requirements in the context of environmental pollution policies, the Check List (Watch List) [22] of emerging pollutants is updated continuously, both for the analysis methods and for regarding new substances. Substances to include in the checklist are selected from those which, according to the information available, could present a significant risk at European level for the aquatic environment and for which monitoring data is insufficient [22]. Directive 2013/39/EU [22] has inserted into the Watch List the following pharmaceutical products: 17-alpha-ethinyl estradiol, 17-beta-estradiol,

estrone, diclofenac, macrolide antibiotics (erythromycin, clarithromycin and azithromycin). Moreover, in the Watch List, similar to the EPA method l694, the PPCPS target analysis is divided into groups, depending on the chromatographic separation used.

In literature, pharmaceutical compounds in waste waters, after solid phase extraction (SPE) in reverse phase with polymeric sorbent or silicic stationary phase [15,20,23-27], are determined by liquid chromatography coupled with tandem mass spectrometry. Similarly to EPA method l694 and Watch List, also in literature a variety of mobile phases are used depending on the chemical-physical properties of the drugs to be separated, by reversed phase partition mechanism. In general, the methods present in the literature report the use of biphasic system as a mobile phase. However, there are two examples of use of three-phase system for pharmaceuticals applications [28,29]. In all the works, to allow the revelation of drugs at low concentrations, the SRM mode is used for the acquisition of mass spectra.

Evaluation of drug LogP is an important parameter for environmental consideration; it is in fact useful for the understanding of their destiny once they are released into the environment. Generally, compounds characterized by low volatility and moderate hydrophilicity are distributed in the environment through aqueous transport [30]. Furthermore, some PPCPS have been found in sludge samples from wastewater treatment. The sludge is capable of absorbing these drugs and contaminate the soil when it is used as fertilizers. This leads to an absorption of pharmaceutical products by the crops which, following bioaccumulation and biomagnification processes, represents a potential route of exposure human to PPCPS [31]. Drugs concentration in the environment can be reduced by phenomena such as biodegradation,

photodegradation and other abiotic transformation processes, such as hydrolysis [32]. For example, diclofenac is rapidly degraded by direct photolysis with one pseudo first order elimination rate [33]. Similar results are reported for ibuprofen, whose concentration on the surface of the water in summer can decrease by 68% [34,35]. Often, however, drug degradation leads to production of metabolites that are more toxic than the drug itself. An example is carbamazepine, whose main photodegradation product is acridine, a toxic metabolite, mutagenic and carcinogenic [36]. Degradation of drugs in the environment may also occur by microorganisms that can use PPCPS as a carbon source. However, too high concentrations of pharmaceutical products can inhibit the biodegradation process becoming toxic to the microorganism itself [7]. Long-term drug dispersal could lead to chronic and diverse toxicity effects including microbial resistance, endocrine disruption, growth inhibition, destruction of microbial ecosystems, cytotoxicity, mutagenicity, and teratogenicity [37]. To date, no systematic studies have been performed on the possible toxicity to humans, but adverse effects of drugs on fauna and flora have been widely demonstrated [7,37]. Particularly, some PPCPs, found in low quantities in the marine environment (from ng/L to µg/L), together with their metabolites can harm aquatic organisms [7,38,39] through the phenomenon of bioaccumulation, which is expressed in irreversible damage to the organism [37]. Although a vast literature is available about the quantification of pharmaceutical drugs in environmental samples, there is still a long way to go through regarding their toxic impacts, especially concerning chronic exposures, since the majority of works looking at the biological effects of pharmaceuticals have thus far concentrated on acute studies [40]. To generate the informations on the ecological risks on

marine organisms, the chronic effects of the two drugs carbamazepine and amoxicillin, alone and in combination, were evaluated across two generations of the Crustacea Copepoda: *Tigriopus fulvus*

These two molecules have been chosen based on their important pharmacological function, the first is an antiepileptic, while the second one is an antibiotic, which leads them to be among the drugs most consumed by humans, as previously reported. Particularly, carbamazepine was selected for this study, since it is one of the most frequently detected antiepileptic drugs in aquatic environments worldwide [12,41,42]; it is very difficult to remove through the classic wastewater treatments (removal rate below 10%) [43,44] and it is classified as potentially hazardous compound for the aquatic environment due to its chemical proprieties [45]. The amoxicillin is a broad-spectrum antibiotic, largely utilized both in human and in veterinary medicine in many different countries. Although recorded environmental levels are usually low (ng/ L to mg/L in waters), it is considered to be "pseudopersistant" contaminants due to their continued release into the environment and permanent presence [46,47].

The tests were performed on aquatic organisms, particularly important targets, because they are exposed to the toxic molecules, via wastewater residues, over their whole life. In particular, we focus on *Tigriopus fulvus* which, as primary consumers and the most numerous metazoans in the marine ecosystem, play an important role in the transportation not only of energy but also of aquatic pollutants across the marine food chain [48-50]. This copepod is both an omnivore and a filter-feeding organism [50], and it may prove useful as a test organism for estimating the influence of emerging pollutant in the marine environment. To date, no studies have been conducted on the potential toxicity of carbamazepine

and amoxicillin on *T. fulvus*, however from literature chronic effects observed in organisms from different trophic levels (algae, cladocerans, and fish) indicate that carbamazepine presents an action in the reproductive system of these species including modifications in fecundity [45].

1.1 Antibiotics

Erithromycin, clarithromycin and amoxicillin are three antibiotics. Particularly, erythromycin, whose structure is showed in figure1.1, is the prototype of the macrolide class and it is a structurally complex secondary metabolite isolated in 1952 from the culture broth of *Saccharopolyspora erythraea* [51].

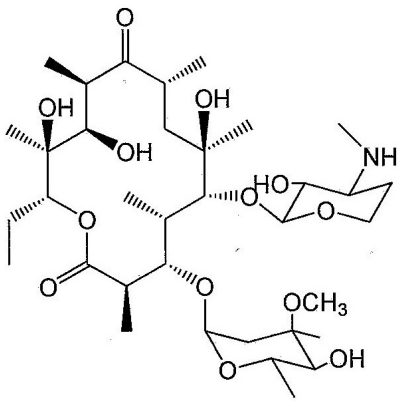

Figure 1.1: Chemical structure of erythromycin, LogP 2.7.

It is used for the treatment of a number of bacterial infections, includes respiratory tract infections, skin infections, chlamydia infections, pelvic inflammatory disease and syphilis.

Clarithromycin, showed in figure 1.2, is an acid-stable orally administered macrolide antimicrobial drug. It has a broad spectrum of

antimicrobial activity and inhibits a range of Gram-positive and Gram-negative organisms, atypical pathogens and some anaerobes [52].

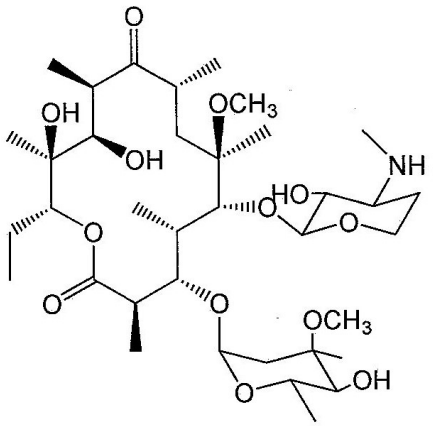

Figure 1.1: Chemical structure of clarithromycin, LogP 3.2.

Macrolides are a class of chemical compounds formed from lactones in whose molecule there is a macrocycle consisting of at least 12 atoms. The macrocycle of clarithromycin is a ring made up of 14 atoms which, in addition to the presence of various methyl branches, has glycosidic bonds with amino sugar desosamine and cladinosio sugar [53].

Amoxicillin, showed in figure 1.3, is an antibiotic belonging to the class penicellin.

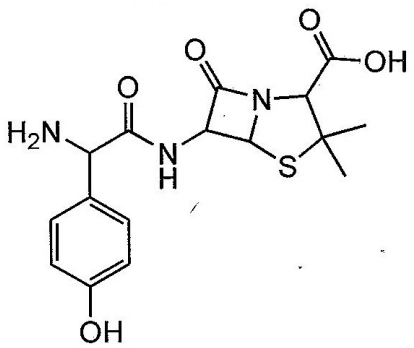

Figure 1.3: Chemical structure of amoxicillin, LogP -2.

This molecule contains a beta lactam ring condensed with a thiazole ring. On the amide carbonyl group of the beta lactam ring there is a 1-[5-hydroxy]-phenylamine substituent [53]. It's used to treat bacterial infections, such as chest infections (including pneumonia), dental abscesses and urinary tract infections (UTIs). It is reported on the World Health Organization's List of Essential Medicines, which lists the most effective and safe medicines needed in a health system [54]. It is one of the most commonly prescribed antibiotics in children [55].

1.2 Antiinflammatories

Acetylsalicylic acid, ibuprofen, diclofenac and naproxen are antiinflammatory drugs. More specifically, acetylsalicylic acid, reported in figure 1.4, is a pharmaceutical product with antiinflammatory, analgesic, and antipyretic qualities.

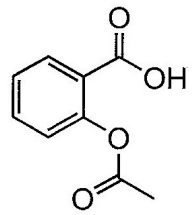

Figure 1.4: Chemical structure of acetylsalicylic acid, LogP 1.2.

This molecule is part of the class of non-steroidal salicylated inflammatory compounds, deriving from the esterification of salicylic acid [53], and is one of the most widely used medications globally, with an estimated 40,000 tonnes consumed each year [56,57]. It is present on the World Health Organization's List of Essential Medicines too as the safest and most effective medicines needed in a health system.

Diclofenac, in figure 1.5, is a diphenylamine compound which presents two chlorine atoms as substituents on one of the aromatic rings and an acetate group on the other one [53].

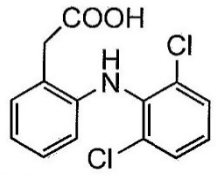

Figure 1.5: Chemical structure of diclofenac, LogP 4.4.

Diclofenac is used to treat arthritis, rheumatoid arthritis, polymyositis, dermatomyositis, osteoarthritis, dental pain, temporomandibular joint.

Ibuprofen, in figure 1.6, consists of a benzene unit replaced with 2-methyl-propane and with 1-methyl-acetate [53].

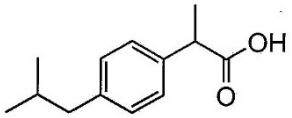

Figure 1.6: Chemical structure of ibuprofen, LogP 3.5.

It is used for treating pain, fever and inflammation and it is reported on the World Health Organization's List of Essential Medicines too [58].

Naproxen, showed in figure 1.7, has a naphthalene ring with a methoxy and propionic acid pendant groups [53].

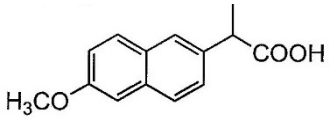

Figure 1.7: Chemical structure of naproxen, LogP 3.3.

It is a nonsteroidal anti-inflammatory drug (NSAID) used to treat pain, menstrual cramps, inflammatory diseases, such as rheumatoid arthritis, and fever and it was the 68th most prescribed medication in the United States, with more than 11 million prescriptions [59].

1.3 Steroidal hormones

Estradiol, whose structure is reported in figure 1.8, and ethinylestradiol, illustrated in figure 1.9, are steroidal hormones and therefore show the basic nucleus of steroids, consisting of an aromatic ring condensed with three saturated rings.

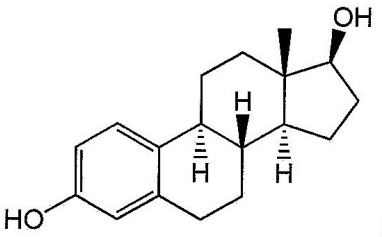

Figure 1.8: Chemical structure of estradiol, LogP 4.0.

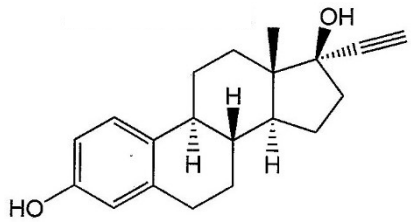

Figure 1.9: Chemical structure of ethinylestradiol, LogP 3.7.

Estradiol is the most known and active member of the class of steroid hormones, commonly known as estrogens. Estradiol controls development and maintenance of female sex characteristics and is often referred to as the "female hormone" [60].

Ethinylestradiol is used widely in birth control pills in combination with progestins and it is occasionally used as a component of menopausal hormone therapy for the treatment of menopausal symptoms too.

1.4 Antiepileptic

Carbamazepine, in figure 1.10, belongs to the class of dibenzazepine and is characterized by the presence of a tricyclic structure 6-7-6 [53].

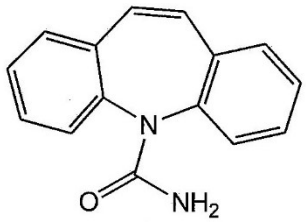

Figure 1.10: Chemical structure of carbamazepine, LogP 2.5.

It is an anticonvulsant medication used primarily in the treatment of epilepsy and neuropathic pain. This compound is on the World Health Organization's List of Essential Medicines too [58].

1.5 Proton pump inhibitor

Omeprazole, in figure 1.11, presents three aromatic cycles, i.e. a pyridine, an imidazole and a benzene, these last two condensed between them [53].

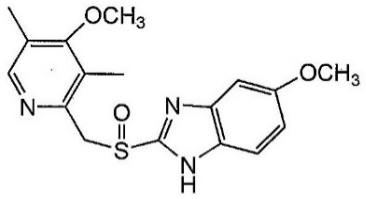

Figure 1.11: Chemical structure of omeprazole, LogP 2.2.

It is a proton pump inhibitor that decreases the amount of acid produced in the stomach. It relieves specific symptoms such as heartburn, difficult swallowing, and persistent cough. This medication helps heal acid damage to the stomach and esophagus, helps prevent ulcers and may help prevent cancer of the esophagus.

1.6 Drug for the treatment of type 2-diabetes

Metformin, in figure 1.12, consists of two guanidine molecules condensed together [53].

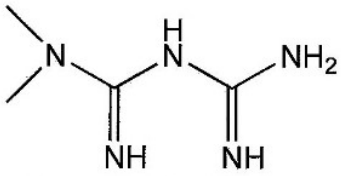

Figure 1.12: Chemical structure of metformin, LogP -1.3.

This molecule has been used extensively in multiple reproductive settings to ameliorate hyperandrogenism and chronic anovulation, to treat infertility, to prevent miscarriage and to prevent later pregnancy complications [61].

1.7 Toxicity of aquatic ecosystem

The aquatic ecosystem is a very complex dynamic system, whose chemical, physical and biological properties vary continuously due to natural or artificial phenomena. In the last decades, an exponential increase in water pollution has been noted, which is defined as alteration of the chemical, physical or biological quality of the water which causes unacceptable depreciation for the purposes of normal use or conservation of the environment. From this definition derives a classification of pollutants in terms of chemical, physical and biological components [62,63]:

- Chemical pollution is generated by organic and inorganic substances released into the water, which can carry out their polluting action both directly and indirectly, through biological processes. The direct action is expressed through the removal of oxygen from the water body caused by the presence of reducing substances (nitrates and/or phosphates), which are decomposed by the bacteria that use dissolved gas for their vital processes. When the numerous populations of decomposer bacteria convert these substances, the level of oxygen in the water can decrease significantly until it is depleted. This leads to the excessive development of algae and other aquatic plants, which exhaust the oxygen reserves of the water, and cause the consequent death of other aquatic organisms, such as fish.
- Physical pollution can be caused by alterations in the colour, odour, taste, density, turbidity and from the decrease or increase in temperature.
- Biological pollution is caused by the presence of bacteria, certain fungi, protozoa, viruses and parasitic worms.

The most common causes of water pollution can be traced to one of the following cases: pollution of the atmosphere, removal of water resources, discharge of waste water into surface waters, discharge of liquid or solid waste on the territory, development of urbanized, industrial or agricultural areas [64].

1.8 Ecotoxicology

Ecotoxicology is the study of the effects of natural and synthetic chemicals (stressors) in the biosphere. The term ecotoxicology was introduced by Truhaut in 1969 and was derived from the words ecology and toxicology [63,65]. The essence of ecotoxicology lies in two main areas: a study of the environment, with origins in the science of ecology, and a study of the interactions of toxic chemicals with individual living organisms – the science of toxicology [66]. Ecotoxicology represents the field of study that integrates the ecological and toxicological effects of chemical pollutants on populations, communities and ecosystems with their destiny in the environment (transport, transformation, and degradation). The major concerns of ecotoxicology are the interactions between living organisms and toxic chemicals in the environment [66]. Ecotoxicology aims to discover the chemicals that pose risks in order to apply preventive measures before any serious damage to natural ecosystems occurs [67]. The main parameter for determining the toxicity of a substance is the dose; indeed, all substances can be toxic in certain doses. Another basic concept is exposure, defined as a function of the concentration of the substance, its shape, the type of administration and the time of interaction with the organism. It is important to know that an adverse effect is defined as an abnormal, undesirable or harmful change in an organism exposed to a potentially toxic substance. A statistically

significant change from the "normal" state does not necessarily constitute an adverse effect; indeed, to become such, the effect must alter an important property and be placed in relation to the overall health of the exposed organism. It is therefore possible to define, more generally, the harmful effect as the cause of functional or anatomical damage, irreversible changes in homeostasis, or as responsible for the increased susceptibility to other substances or to biological stress.

Behavioural response results from the level of the organism, which can be defined as the action, reaction, or activation of a given system. This system is subjected to a set of specific conditions that represent the integration of biochemical and physiological processes [68].

A further important component that characterizes ecotoxicology is the forecasting one, which uses mathematical models able to provide predictions both about the environmental fate of the substances and about their effects on exposed organisms and ecological systems.

1.8.1 Ecotoxicological test

Ecotoxicology is applied through tests that measure the toxicity of substances found in the environment by exposing standard living organisms to them. Ecotoxicological tests allow assessing environmental contamination caused by different pollution sources. These tests have the advantage of covering a wide variety of biological substances available in a sample. They have the inherent ability to detect deleterious effects produced by a toxic agent, or mixture, on living organisms. Thus, these tests allow to identify the dangerousness of these substances. A large number of ecotoxicological trials have been developed, or improved, due to a wide variety of studied species and ecosystems. Aquatic, sedimentary, and terrestrial systems can be used in tests to verify the

degree of contaminations caused by toxic agents and their possible ecological implications [68]. For aquatic organisms, the effects of a given concentration (amount of the substance administered with exposure per unit of volume in water or in the surrounding medium) are generally evaluated rather than the dose (amount of substance supplied with exposure per unit of body mass). An organism can be exposed to a defined quantity of toxic substance without developing any negative effects; however, for each organism there is a threshold dose of that toxic above which detoxification processes start to set in motion. As long as these processes are sufficient to counteract the toxic, no negative effect is observed, however, when the detoxification mechanisms are no longer sufficient to counteract the toxic, one will begin to observe chronic manifestations and even high acute doses.

The most commonly used parameters to quantify the response of ecotoxicological assays are the following [69-71]:

- LD_{50}/LC_{50} (Lethal Dose/Lethal Concentration): dose/concentration of a substance that causes the death of 50% of individuals in acute toxicity tests for effective median exposure; that is the dose/concentration that causes a certain effect on 50% of the population tested.
- ED_{50}/EC_{50} (Effect Dose/Effect Concentration): effective median dose/concentration; that is the dose/concentration that causes a certain effect on 50% of the population tested other than death (immobilization, stunting in acute or chronic tests); must be referred to the exposure time.
- NOED/NOEC (NO Effect Dose/NO Effect Concentration): dose/concentration that does not produce observable effects.

- LOED/LOEC (Lowest Observed Effect Dose/Lowest Observed Effect Concentration): minimum dose/concentration that produces observable effects, or difference from statistically significant control.
- TED/TEC (Threshold Effect Dose/Threshold Effect Concentration): minimum dose/concentration necessary to induce a detectable effect.

1.9 Copepodes in aquatic ecotoxicology

Marine copepods have been selected for use in toxicity tests for their ecological importance as a prey source for many marine consumer species, their widespread occurrence in marine waters, their relative ease of culture in the laboratory and comparatively short life-cycles [72]. In particular, harpacticoid copepods can be useful test-organisms owing to their wide distribution and key-position within the food web, and because they are easier to rear than pelagic copepods; thus, they have been indicated to be suitable for toxicity trials. The Mediterranean harpacticoid *T. fulvus*, especially, can be considered a target-species in ecotoxicology [73]. This species has been extensively studied from the biological, biochemical and ecological point of view [74,75]. *T. fulvus* has already been used for toxicity test and represents a standardised species, for ecotoxicological studies, for the Italian legislation [76,77], for example in Veneto region [78] and Tuscany [79,80], moreover, so much is the interest for this new subject that a new standardized procedure for breeding in the laboratory and for testing have been published by UNICHIM in method 2396: 2014 [81]. To date, no toxicity studies have been carried out on the drugs carbamazepine and amoxicillin with this species, however acute and chronic toxicity studies have been reported in the literature with other different pollutants such as heavy metals (Cu, Cd, Cr, Zn and Hg) [74, 77]

1.9.1 *Tigriopus fulvus*

Copepods are aquatic animals, mainly marine, although they also occur in vast numbers in fresh water environment. The Copepode forms the subclass of the phylum Crustacea. There are ten orders of copepods containing different number of families, genera and species [82]. The ten orders are: Platycopioida, Calanoida, Mormonilloida, Poecilostomatoida, Siphonostomatoida, Misophrioida, Cyclopoida, Monstrilloida, Harpacticoida and Gelyelloida. In this study we focus on Harpacticoida that comprises 463 genera and about 3,000 species; its members are benthic copepods found throughout the world in the marine environment (most families) and in fresh water (essentially the Ameiridae, Parastenocarididae and the Canthocamptidae). A few of them are planktonic or live in association with other organisms. One of generus of Harpacticoida order is *Tigriopus*, which includes four families:

- *Tigriopus brevicornis*,
- *Tigriopus californicus*,
- *Tigriopus fulvus*,
- *Tigriopus japonicus*.

Tigriopus fulvus, showed in figure 1.13, is an autochthonous, meiobenthic, euryhaline and eurythermal harpacticoid copepod widely distributed in the Mediterranean Sea.

Figure 1.13: Nauplio and adult of *Tigriopus fulvus*.

The biology of *T. fulvus* is well known [82-84]. The species has been found very suitable for laboratory rearing and does not present any particular difficulties for maintenance. It also showed a good sensitivity to different toxicants and the test with the species is easy-to-use and low-cost [85,86]. *T. fulvus* has small dimensions (length 0.7 - 0.8 mm), separated sexes, sexual dimorphism and it is characterized by a short life cycle. It undergoes anamorphic development with 12 distinctive post-embryonic developmental stages, 6 naupliar stages, 5 copepodid stages and an adult stage [82], as showed in figure 1.14.

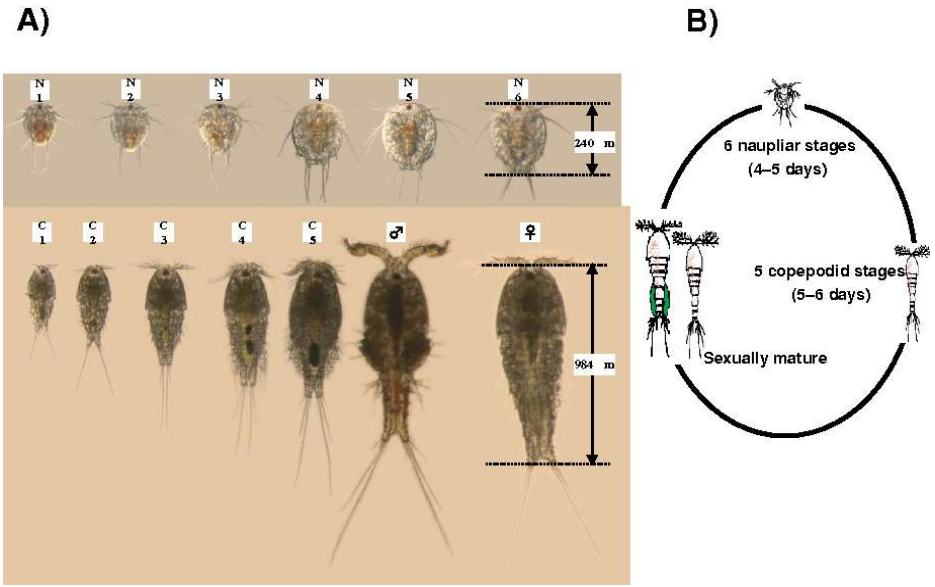

Figure 1.14: A) 12 distinctive post-embryonic developmental stages of *Tigriopus*, B) link between time and stage of development.

The sexual dimorphism is evident in the adult state: the males are distinguished from the females, because the firsts are slightly smaller than the second one and they have a very evident secondary sexual character, indeed, the males have the front antennas conformed with large ampoules that serve as suckers for prehension and fixation of the female during coupling. In figure 1.15, it is showed an ovigera female and eggs with naupliare eye.

Figure 1.15: Ovigera female and eggs with naupliare eye of *T. fulvus*

The females are highly fertile and mate only once, generating more broods of 30 to 50 nauplii. The mature eggs are recognizable thanks to a colour variation, that will occur from green to red, and because of the evidence of the naupliare eye of the embryo.

2. Principles of Analytical techniques

2.1 Solid phase extraction (SPE)

Solid phase extraction is a very popular technique, currently available for rapid and selective sample preparation [87,88]. Briefly, we can identify three ways in which SPE can help us [88]:

- pass a large volume of sample through the smallest bed of sorbent that will completely retain all of our compound of interest;
- elute compounds of interest in the smallest volume of solvent possible;
- elute compounds of interest in a solvent that permits easy concentration.

The principle of SPE is similar to that of liquid-liquid extraction (LLE), involving a partitioning of solutes between two phases. However, instead of two immiscible liquid phases, as in LLE, SPE involves partitioning between a liquid (sample matrix or solvent with analytes) and a solid (sorbent) phase [88]. The general steps involved in performing SPE are:

- pre-treat the sample (e.g. dilution, adjustment of pH);
- conditioning of the cartridge (run water or solvent through it);
- load the sample;
- elute the fractions.

The entire process of the SPE is represented in figure 2.1.

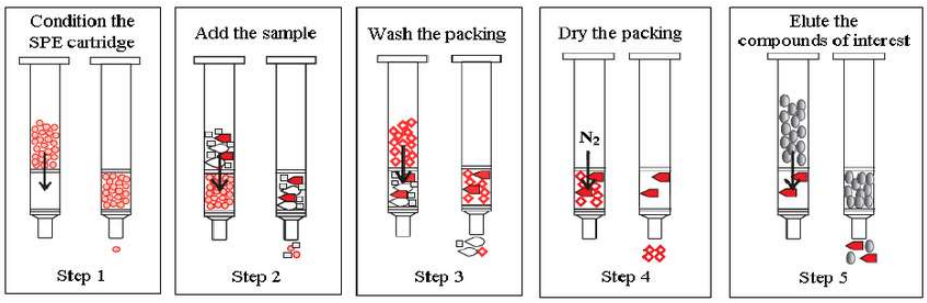

Figure 2.1: The steps of a solid phase extraction.

SPE methods start with a conditioning step (Step 1 of figure 2.1). This consists of rinsing the SPE cartridge with a solvent similar to the matrix of the sample you want to load. Once the cartridge has been conditioned, the sample is then loaded on the cartridge (Step 2 figure 2.1). The amount of sample loaded will vary depending on the purchased cartridge. The cartridges can be loaded on a vacuum manifold to apply a vacuum or centrifuged to speed up the separation process. This separation can be done using gravity too, but this would make this step very time consuming. Once the sample has been collected on the adsorbent, the cartridge can be rinsed with 100% of washing eluent to remove unretained compounds (Step 3 in figure 2.1). Then, the packing has to be dried (Step 4 in figure 2.1) and finally the cartridge can be rinsed with an eluent to obtain the compound of interest (Step 5 in figure 2.1).

Depending on the analyte (non-polar, polar or ionic), different eluents and packing materials can be used. The latter can be divided into several categories:

- Adsorption Reversed phase SPE techniques are optimal for analytes with moderate to low polarity, and separate analytes based on hydrophobicity with the most polar compounds eluting first. Because many analyses involve analytes dissolved in an aqueous sample (e.g. surface waters, wastewater, urine or plasma), SPE using reversed phase sorbents are commonly employed.
- Adsorption Normal phase SPE techniques are commonly used when the analyte of interest has low to high polarity or it is neutral. The cartridge contains a polar adsorbent, such as silica. This separation will be based on polarity, with the less polar components eluting first. The sample is usually solubilized in a non-aqueous matrix.

- Ion exchange SPE separate compounds based on charge. There are two types of ion exchange SPE, that is to say cation and anion exchange.
- Mixed-mode SPE combines the capabilities of ion-exchange and reversed-phase SPE for an enhanced separation. Examples of mixed-mode SPE include: reversed-phase/strong cation-exchange, reversed-phase/strong anion-exchange, reversed-phase/weak cation-exchange and reversed-phase/weak anion-exchange. The ion-exchange component of the cartridge allows the appropriately charged compounds to be retained for further extraction. Once the appropriately charged compounds are retained, the SPE can be rinsed to remove any impurities. Then, the pH of the eluent can be adjusted to reduce the charge on the analyte molecules, which will release them from the ion-exchange component of the cartridge causing them to elute. Mixed-mode is commonly used in the separation of basic, acidic, and neutral compounds in a mixture. This is widely used in the concentration, purification, and analysis of pharmaceutical compounds and antibacterial agents found in wastewater.

Fundamental parameters that characterize solid phase extraction are:

- selectivity: capacity of the adsorbent to distinguish between substances to be isolated and interferents to be removed. The selectivity will be maximum when the adsorbent interacts only with the functional groups of the analyte, without having any interaction with other molecules.
- capacity of the adsorbent: amount of analyte retained by a certain amount of adsorbent under optimal conditions.

2.2 Chromatography

Chromatography is an analytical technique that is used both for identification and for the quantification of analytes present in a given sample.

There are two types of chromatography: column and planar chromatography. Focusing on column chromatography, it exploits the elution of a mobile phase, inside a column containing a stationary phase. Depending on the used stationary phase, we will have a specific chromatographic method [89]. Table 2.1 shows a summary of the classification of chromatographic methods on column.

General classification	Specific method	Stazionary phase	Equilibrium type
Gas chromatografy (GC)	Gas-liquid	Liquid absorbed or bound on a solid surface	Distribution between gas and liquid
Liquid chromatography (LC)	Gas-solid	Solid	Adsorption
	Liquid-liquid	Liquid absorbed or bound on a solid surface	Distribution between immiscible liquids
	Liquid-solid	Solid	Adsorption
	Ionic exchange	Ion exchange resin	Ionic exchange
	Size exclusion	Liquid in the interstices of a polymeric solid	Distribution/ sieving
	Affinity	Liquid with specific groups bound on a solid surface	Distribution between the surface liquid film and the liquid of the mobile phase
Supercritical fluid chromatography (SFC)		Organic species linked to a solid surface	Distribution between supercritical fluid and bound surface

Table 2.1: Classification of chromatographic methods on column.

The stationary phase is linked to the column by a finely divided inert solid. The different affinity of the analytes for the stationary and the mobile phases, respectively, determines the separation and the order of their elution. The choice of the phases to be used must be made to balance the intermolecular forces that are established between the analytes, the mobile and the stationary phase. Intermolecular forces that are too strong with the stationary phase would leave the analytes in the column, so there would be no sample elution. On the other hand, intermolecular forces that are too weak would lead to a non-retention of the analytes that would simultaneously elute without having any separation.

For a sample X what will happen once entered the column will be the establishment of an equilibrium:

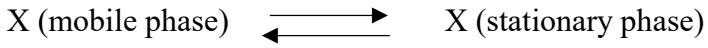

therefore, we can define the constant of this equilibrium as a distribution constant, which will be given by:

$$K_c = \frac{(a_X)_S}{(a_X)_M} \tag{2.1}$$

where

$(a_X)_S$ = activity of compound X in the stationary phase

$(a_X)_M$ = activity of compound X in the mobile phase

It can be deduced that substances with high Kc values will be strongly retained by the stationary phase, therefore they will have longer retention times; on the other hand, low Kc values indicate a substance that will have greater affinity for the mobile phase.

By passing a sufficient amount of eluent through the column it will be possible to get all the bands that have formed out of the column.
Using appropriate detectors, it will be possible to obtain a graph in which the intensity of the bands will be reported as a function of time. This graph is called a chromatogram, see figure 2.2.

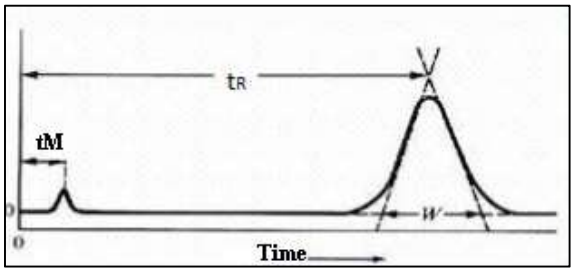

Figure 2.2: Example of chromatogram.

The elution time, also defined as retention time in the column can be defined as:

$$t_R = t_M + t_S \qquad (2.2)$$

in which
t_S = time that the analyte passes into the stationary phase
t_M = dead time, or the time that uses a non-retained species, i.e. the eluent, to escape from the column.

In the ideal case the analytes will elute with their net retention time t_R, and the peaks observed in the chromatogram will be Gaussian peaks. In the real case, instead, there will be diffusion processes and irregularities in the equilibrium between the mobile phase and the stationary phase, so that the analytes will elute with retention times greater or less than their

net retention time. The longer the time in the column is, the higher is the probability related to diffusion motions that would contribute to the broadening of the band.

The deviation from the ideal situation can be described by means of the asymmetry factor T:

$$T = \frac{B}{A} \tag{2.3}$$

where A and B are the distances between the central axis of the peak and the sides of the distribution at 10% of their height.

At this point it will be possible to determine the following parameters [90]:

- Elution rate:

$$v = \frac{L}{t_R} \tag{2.4}$$

where

L = column length

t_R = retention time

- Capacity factor

$$K' = \frac{t_R - t_M}{t_M} \tag{2.5}$$

if $t_M = 0$ then K '= ∞ and we are in presence of a substance that has no affinity for the stationary phase;

if $t_M = \infty$ then K '= 0 and we are in the presence of a substance that is

strongly retained by the stationary phase and therefore will not elute from the column.

Optimal values of K ' lie between 1 and 5.

- Selectivity coefficient

The selectivity of a column is defined as its ability to separate two analytes and it is indicated as:

$$\alpha = \frac{t_{R1} - t_M}{t_{R2} - t_M} = \frac{t_{R1}}{t_{R2}} = \frac{K_1}{K_2} \qquad (2.6)$$

in which

K_1 = distribution constant of the most strongly retained analyte, the one which elutes after;

K_2 = constant of distribution of the analyte less strongly retained, that which elutes before.

If α is equal to 1 then there would be a simultaneous elution of the two substances without the separation taking place; on the contrary, too large values of α would lead to a better separation, but also to an increase in the elution time. The most desirable value for α is around 1.5.

The efficiency of a chromatographic column can be assessed by the number of theoretical plates. A theoretical plate is defined as a portion of the column in which an equilibrium of the analyte is established between the mobile phase and the stationary phase. The number of theoretical plates can be defined as follows:

$$N = \frac{L}{H} \qquad (2.7)$$

with N = number of theoretical plates

H = height of the theoretical plate

L = length of the column

considering that

$$H = \frac{\sigma^2}{L} \tag{2.8}$$

with σ = variance

As can be seen from the above equations, the number of theoretical plates is inversely proportional to the variance. More appropriately we can define the number of theoretical plates as follows:

$$N = 5.545 \left(\frac{t_R}{W_{0.5}}\right)^2 \tag{2.9}$$

or, taking into account the asymmetry factor, with the relation of Foley and Dorsey:

$$N = \frac{47.1 \left(\frac{t_R}{W_{0.1}}\right)^2}{T + 1.25} \tag{2.10}$$

The height of the theoretical plate, H, is generally indicated with:

$$H = \frac{B}{u} + C_s u + C_M u \tag{2.11}$$

where:

u = mobile phase rate

B = longitudinal diffusion coefficient; it takes into account the diffusion motions that are created when there is a medium in which different concentrations are present. It is known that a fluid moves spontaneously from more concentrated areas to less concentrated areas. The diffusion motions are inversely proportional to the flow velocity, since when this rate increases the solute will have less time to spread. Since a gas diffuses approximately 1000 times faster than a liquid, this contribution will be more marked in gas chromatography than in liquid chromatography.

C_S = mass transfer coefficient for the stationary phase. In the case of a solid stationary phase, this coefficient is directly proportional to the time required for a species to be adsorbed or desorbed on the surface of the solid.

C_M = mass transfer coefficient for the mobile or turbulent diffusion phase, which is inversely proportional to the coefficient of diffusion of the analyte in the mobile phase. For packed columns it is proportional to the square of the particle diameter of the packing material. For capillary columns it is proportional to the square of the column diameter and it is a function of the flow velocity. In a packed column the molecules of the same analyte can follow different paths, which have different lengths, or they will suffer the effect of the presence of multiple paths. This implies that molecules of the same analyte can have slightly different elution times which lead to a widening of the chromatographic peak. For low velocities of the mobile phase the molecules are not significantly dispersed by the effect of multiple paths of packing.

Only in the case of C_S there will be a linear dependence on the flow velocity, in the case of B/u there will be a more hyperbolic dependence, while in the case of C_M there will be a more parabolic one. The optimal

value of the flow will occur when the height of the plate has a minimum value, and when there will be a maximum value of separation efficiency. For sufficiently high rates, the turbulent diffusion coefficient becomes independent from the flow velocity; this means that for packed columns with high flow rates, the height of the theoretical plates can be defined by the van Deemter equation:

$$H = A + \frac{B}{u} + C_s u \tag{2.12}$$

A = turbulent diffusion coefficient, due to multiple paths that are created inside the column because column packing is made up of non-homogeneous material. Therefore, it is possible that the same molecules follow different paths to cross the column; such paths, for the same column length, may require slightly different times for crossing, which will lead to a greater widening of the chromatographic peaks.

Another parameter to be considered in chromatography is the resolution, which provides a quantitative measure of the column ability to separate two analytes. Assuming that a sample consists of two analytes A and B, the resolution is defined as follows:

$$R_s = \frac{\Delta Z}{\frac{W_A}{2} + \frac{W_B}{2}} = 2\frac{\Delta Z}{W_A + W_B} = 2\frac{(t_{RA} - t_{RB})}{W_A + W_B} \tag{2.13}$$

where

ΔZ = distance between the peaks A and B

W_A = peak width of A, calculated at the base of the peak

W_B = peak width of B, calculated at the base of the peak

Values of Rs = 0.5 can be considered good, even if for qualitative analysis we try to have a value of Rs = 1, while for quantitative analysis Rs = between 1.2 and 1.5.

By expressing the resolution in the following way, instead, we can appreciate the relationships between resolution, selectivity and retention factor:

$$R_s = \frac{\sqrt{N}}{4}\left(\frac{\alpha - 1}{\alpha}\right)\left(\frac{K_B}{K_B + 1}\right) \tag{2.14}$$

taking into account the equation (2.13) we can rewrite the number of theoretical plates as follows:

$$N = 16R_s^2\left(\frac{\alpha - 1}{\alpha}\right)^2\left(\frac{1 + K_B}{K_B}\right)^2 \tag{2.15}$$

To express the link between resolution and elution time of a given species we will have the following equation:

$$t_{RB} = 16\frac{R_s^2 H}{u}\left(\frac{\alpha}{\alpha - 1}\right)\frac{(1 + K_B)^3}{K_B^2} \tag{2.16}$$

Considering all the formulas described above, we can deduce the following:

- Change in the height of the plate: from equation (2.14) we note that the resolution is proportional to the square root of the number of theoretical plates N, so the higher N is, the better the resolution will be. If the increase of N is made through an increase in the length of the column, there will be lengthening of the analysis times; on the

contrary, if the length of the column is kept constant and the height of the single plate is reduced, this undesired effect does not occur.

- Change of the retention factor: an increase in the retention factor generally leads to an increase in the resolution; however, once again the separation times are increased, as indicated in equation (2.16).
- Change of the selectivity factor: if the value of α is close to one, it would be insufficient to vary only N and K_B, so it would be more useful to vary α. The available possibilities are: to vary the mobile phase, even if it involves a change of the whole method of analysis; change column temperature, which appears to be the most widely used method in ionic chromatography; variation of the stationary phase, which would entail a change in the column itself, but laboratories cannot always afford the purchase of multiple columns.

2.2.1 High-Performance Liquid Chromatography (HPLC)

High-performance liquid chromatography (HPLC), formerly called high-pressure liquid chromatography, was developed from classical column liquid chromatography. The introduction of smaller particles into the packing materials in the 1970s generated higher backpressure, which also required high-pressure mobile phase delivery units [91]. In liquid chromatography there are five different separation techniques: partition, ion exchange, adsorption and dimensional exclusion.

Adsorption chromatography is constituted by normal phase and reversing phase based on the material of stationary phase. The most common type of stationary phase employed for reverse phase HPLC (RPLC) consists of monolayer, hydrophobic organic species attached by siloxane (or silyl ether) bonds to the surface of a silica support. The stationary phases are prepared by reacting organochlorosilanes with

reactive silanol groups on the surface of the silica [92], as shown figure 2.3.

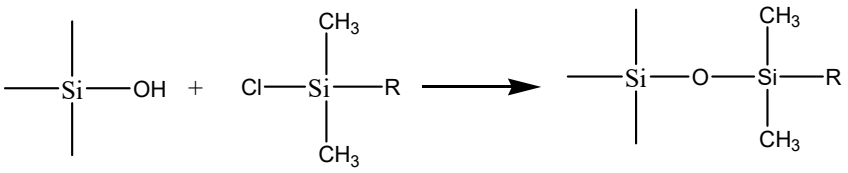

Figure 2.3: Reaction between organochlorosilanes with reactive silanol groups.

The silica inorganic network is the most commonly used support material, because of its many beneficial properties. Small, spherical particles of silica are available in a wide variety of particle diameters and pore size of narrow distribution. The mechanical strength of silica allows porous particles with very large surface areas to be used at high mobile-phase pressures, which yields fast mass-transfer conditions during chromatographic separation [92].

2.3 Mass Spectrometry (MS)

The basic principle of mass spectrometry (MS) is to generate ions from either inorganic or organic compounds by any suitable method, to separate these ions by their mass-to-charge ratio (m/z) and to detect them qualitatively and quantitatively by their respective m/z and abundance. Ionization of a sample can be affected not only by electrons, but also by (atomic) ions or photons, energetic neutral atoms, electronically excited atoms, massive cluster ions, and even electrostatically charged microdroplets. A mass spectrometer consists of an ion source, a mass analyzer, and a detector which are operated under high vacuum conditions. A closer look at the front end of such a device might separate

the steps of sample introduction, evaporation, and successive ionization or desorption/ionization, respectively.

The combination of liquid chromatography and mass spectrometry represents an ideal fusion between separation and revelation. Since HPLC works in liquid phase, while mass spectrometry works in gas phase, it is necessary to use an interface. The possible interfaces are of two types:

- interfaces that merely evaporate and transfer the sample from the HPLC system to the mass spectrometer;
- interfaces that play an active role in ionization.

Currently, electrospray ionization is the preferred source of ionization and interface. Electrospray ionization (ESI) is the most prominent technique among the group of atmospheric pressure ionization (API) methods and the leading method of choice for liquid chromatography-mass spectrometry coupling. ESI is a soft ionization technique that accomplishes the transfer of ions from solution to the gas phase. In ESI the solution is composed of a volatile solvent containing the ionic analyte at very low concentration, typically $10^{-6} \div 10^{-4}$ M. In addition, the transfer of ions from the condensed phase into the state of isolated gas-phase ions starts at atmospheric pressure and incrementally proceeds into the high vacuum of the mass analyzer. The dilute sample solution is supplied by a syringe pump through a hypodermic needle – the spray capillary – at a rate of 5 – 20 µl/min. The spray capillary is kept at a potential of 3 – 4 kV relative to a surrounding cylindrical electrode. Then, the electrosprayed aerosol expands into a countercurrent stream of hot nitrogen gas serving as a heat supply for vaporization of the solvent. A small portion of the sprayed material enters into a short capillary (0.2 mm inner diameter, 60 mm length) connecting the atmospheric pressure

spray zone to the first pumping stage (≈ 102 Pa) that is accessed by the gas in a free jet expansion. A minor portion passes through the orifice of a skimmer (a cone-shaped electrode with a small aperture at its apex) into the high vacuum behind ($\approx 10^{-3} \div 10^{-4}$ Pa). At this stage, desolvation of the ions is completed, while the ions are focused into the mass analyzer. Suitable potentials applied to capillary, skimmer, and lenses behind provide an effective transfer of ions through the interface, while the neutral gas is not affected and exits via the vacuum system [93]. In figure 2.4 was represented a schematization schematic representation of the ESI source is showed.

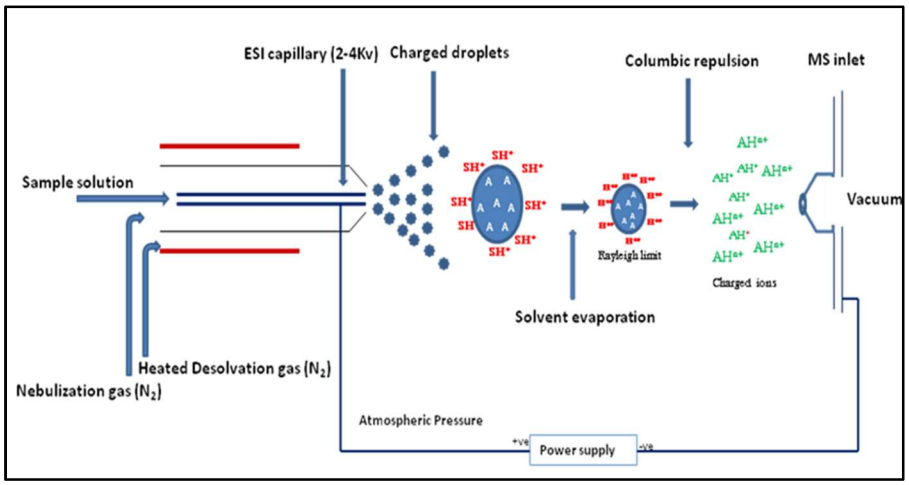

Figure 2.4 Schematization of ESI source.

The analyzers are devices able to separate ions based on their m/z ratio. The quadrupolar ion trap analyzer, showed in figure 2.5, consists of a set of quadrupolar electrodes to confine the ions radially and an electrostatic potential on the terminal electrodes to trap the ions axially, from two cap electrodes and a central ring electrode arranged in a geometry sandwich.

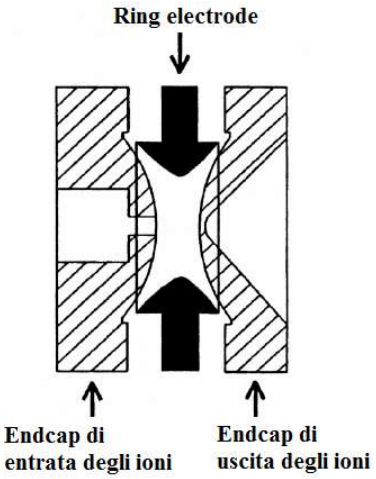

Figure 2.5: Schematization of a linear ion trap.

Together, these electrodes form a cavity in which it is possible to trap and analyse the ions; both dome-shaped electrodes have a small hole through which ions can enter and exit the trap. In this kind of traps, in the space between the electrodes, only ions having a given range of ratios m/z, determined by the applied potentials, can persist in a stable motion. Indeed, a constant frequency (RF) potential and variable amplitude are applied to the ring electrode in such a way as to create a three-dimensional quadrupolar field inside the trap. In this way, the ions will begin to move along oscillating trajectories confined within the cavity of the analyzer. The nature of the trajectory will depend both on the potential applied to the ring electrode, but also on the m/z ratio of the ions. By varying the potential applied to the electrodes it is possible to destabilize the trajectories of the ions present in the cavity, causing their expulsion from the ion trap [94]. The mass spectrum is produced by varying the potential so as to eject the ions sequentially, in increasing order of m/z.

At now there are new ionic traps whose working principle is the one described above, but they have a different geometry of the electrodes that allows to reach higher scanning speeds and greater numbers of trapped ions. With the ion trap, it is possible to carry out experiments up to MS^{12}, which has made it a sensitive and versatile analytical system.

2.3.1 Tandem Mass Spectrometry (MS/MS)

Tandem mass spectrometry comprises the acquisition and study of the spectra of ionic products or precursors of m/z-selected ions, or of precursor ions of a selected neutral mass loss. There are two basic instrumental concepts for MS/MS. The first is known as "tandem mass spectrometry in space" (or tandem-in-space MS). In order to perform two consecutive mass-analysing steps, two mass analyzers may be mounted in tandem. Thus, tandem-in-space refers to MS/MS instrumentation where product ion spectra are recorded using spatially separated m/z analyzers. Specific m/z separation is performed so that in one section of the instrument ions are selected, then dissociated in an intermediate region, and the products are finally transmitted to a second analyzer for mass analysis. The second approach, known as "tandem mass spectrometry in time" (or tandem-in-time MS), employs a single m/z analyzer that may be operated by executing the discrete steps of ion selection, activation, and product ion analysis in the very same place but sequentially in time.

The success of any tandem mass spectrometric experiment depends on the occurrence of some kind of reaction between the consecutive steps of precursor ion selection and product ion analysis. This requires that ions entering the zone and/or period for reaction either possess or receive sufficient internal energy for doing so; alternatively, a partner for

reaction may be presented. Even though collisions of ions with neutral gas atoms or molecules appear contradictory to the conditions of high vacuum, most mass spectrometers are equipped (or can be upgraded) to allow for their study. Consequently, fundamental and analytical studies make use of activating or reactive collisions within the mass spectrometer. The most prominent collision technique is collision-induced dissociation (CID) [93]. CID allows fragmentation of gaseous ions that were otherwise perfectly stable. Thus, CID is especially useful for elucidating the structure of ions of low internal energy as for those created by soft ionization methods.

3. Experimental section

3.1 LC-MS/MS experiments

3.1.1 Reagents and materials

All analytical standards used within this study, carbamazepine, clarithromycin, erythromycin, metformin, omeprazole and amoxicillin, were purchased from Sigma-Aldrich (Milan, Italy). HPLC gradient grade methanol and acetonitrile for pharmaceutical extraction, separation and detection were obtained from Sigma-Aldrich (Milan, Italy). Formic acid (98%), used as additive of aqueous mobile phase, was purchased from Carlo Erba Srl (Milan, Italy). Deionized water was prepared with a Milli-Q (Millipore, Darmstadt, Germany) water purification system. OASIS HLB solid phase extraction (SPE) cartridges (200 mg/6 ml) were obtained from Waters Corporation (Milford, MA, USA). Stock solutions with approximately 1000 mg/l concentration were prepared by dissolving 10 mg of standard in methanol. The stock solutions were stored at -20°C. The working standard solutions within the concentration range of 0.001-200 μg/l were prepared by diluting the appropriate volume of stock solution in methanol. The working standard solutions were stored at −20°C.

3.1.2 Samples of wastewater

The wastewater samples analyzed in this work come from the main wastewater treatment plant of Basilicata, located in Potenza, C/da Tiera di Vaglio, shown in figure 3.1.

Figure 3.1. Wastewater treatment plant from which the water samples come.

Wastewater treatment plant is located in an area characterized by low density of population of Southern Italy and serves a population of 160,00 equivalent inhabitants, with a wastewater flow of about 3750 m^3d^{-1}. Influent waters were sampled before the grilling phase and the effluent waters after the unit of disinfection in October 2018. Once delivered to the laboratory, the samples were extracted within 24 h. Sample extracts were stored at -20°C and analyzed within 40 days of extraction.

3.1.3 Solid phase extraction (SPE)

For solid phase extraction, SPE OASIS HLB cartridges (Waters, Milford, MA, USA), 6 cc, 0.2 g, were used. Oasis HLB cartridges contain the Oasis HLB sorbent, which is a universal polymeric reversed-phase sorbent that was developed for the extraction of a wide range of acidic, basic, and neutral compounds from various matrices using a simple, generic protocol. More specifically, sorbent phase consists of a specific ratio of two monomers, the hydrophilic compound N-vinyl pyrrolidone and the high lipophilic divinylbenzene. Particles diameter is 30μm and pore size 80Å. This type of sorbent phase allows excellent retention of analytes, with a wide range of polarity, including the drugs

studied in this work. Cartridges were conditioned with 6 ml of methanol and 5 ml of deionized water. The samples (20 ml) were loaded on the SPE cartridge, and then washed with 5 ml of deionized water, followed by elution with 5 ml (×2 times) of methanol. Finally, the elutes were filtered through 0.2 μm PTFE membrane (Whatman, Maidstone, UK) before LC-MS/MS analysis.

3.1.4 LC-MS/MS analysis

Instrument used in this work for drug analysis is a Reversed-Phase Liquid Chromatography coupled to ESI Linear Ion Trap Mass Spectrometry system (RPLC-ESI-LTQ MS, Thermo Fisher Scientific, Bremen, Germany) consisting of an HPLC pump Surveyor, an autosampler, an electrospray source (ESI), a photodiode array detector (DAD), a solvent degasser and a linear ion trap mass spectrometer (LTQ). Samples analysis were carried out by injecting in the column 25 μl of the sample, using an autosampler. LC separation was performed at room temperature on a Accucore-150-C18 column (150 x 4.6 mm id., particle size 2.6 μm), equipped with Accucore-150-C18 pre-column (10 x 4.6 mm id, particle size 2.6 μm, Thermo Scientific, USA). The technical characteristics of the column used are shown in table 3.1.

Particles form/diameters (µm)	Silica with solid nucleus, spherical, 2.6
Pores size (Å)	150
Nominal superficial area (m^2/g)	80
pH range	1 - 11
Active groups	Octadecylsilane, endcapped
Carbon load (%)	7

Table 3.1: Technical specifications of the Accucore-150-C18 column (150 x 4.6mm).

Obtained data from this LC-MS analysis were processed using the Xcalibur software version 2.0 and displayed in XIC (extracted ion chromatogram) mode. Finally, results were imported and processed with the Systat software Inc SigmaPlot version 11.0 (London, UK).

Full-scan MS and MS/MS experiments have been performed, the latter in SRM mode (selected reaction monitoring). To obtain tandem mass spectra, the precursor ion was isolated and fragmented in the linear ion trap by collision-induced dissociation (CID), with a collisional energy between 14% and 40%, expressed in arbitrary units (100 u.a. correspond to 35 eV). Two different LC-MS/MS methods have been optimized to analyze the 12 drugs, object of study. Drugs amoxicillin, metformin, omeprazole, carbamazepine, erythromycin and clarithromycin were ionized by electrospray in positive mode (ESI +), after chromatographic separation in acidic conditions. Acetylsalicylic acid, diclofenac, naproxen, ibuprofen, estradiol and ethinyl estradiol, on the other hand, were separated by means of a neutral gradient and ionized by electrospray in negative mode (ESI-).

3.1.4.1 LC-MS/MS (ESI+) analysis

For chromatographic separation of drugs amoxicillin, erythromycin, clarithromycin, carbamazepine, metformin and omeprazole, the flow rate was set at 0.6 ml/min and a 4:1 splitting system has been inserted after the column, in order to send in the ESI source 150 µl/min. The solvents used for the mobile phase are water (solvent A), water acidified with 0.1% formic acid (solvent B) and acetonitrile (solvent C). The gradient elution program is shown in the table 3.2.

Time (min.)	**%A**	**%B**	**%C**
0	70	0	30
6	60	0	40
7	0	60	40
15	0	25	75
17	0	0	100
20	70	0	30
25	70	0	30

Table 3.2: Gradient elution program of drugs analyzed by ESI+.

Electrospray ionization in positive mode (ESI+), was conducted as summarized in table 3.3.

Source and polarity	ESI+
Potential (kV)	+4,50
Capillary voltage (V)	+47,0
Capillary temperature (°C)	350
Nebulization gas flow (a.u.)	50
MS range	125-1000

Table 3.3: MS condition.

Full-scan MS and MS/MS experiments have been performed, the latter in SRM mode (selected reaction monitoring) in a range of 125-1000 m/z. In table 3.4, SRM transitions, monitored for the analysis of drugs amoxicillin, clarithromycin, erythromycin, metformin, omeprazole and carbamazepine and collisional energy (in eV) necessary for their fragmentation in the linear trap, are reported.

Drugs	**[M+H$^+$]**	**CID energy (eV)**	**SRM**
Amoxicillin	398.0	8.1	398.0 > 381.0
Carbamazepine	237.0	5.2	237.0 > 194.0
Clarithromycin	748.4	5.2	748.4 > 590.4
Erythromycin	734.4	4.9	734.4 > 576.4
Metformin	130.0	11.2	130.0 > 60.0
Omeprazole	346.1	5.2	346.1 > 198.0

Table 3.4: SRM transition used for drugs analyzed by LC-MS/MS (ESI+).

3.1.4.2 LC-MS/MS (ESI-) analysis

For chromatographic separation of drugs acetylsalicylic acid, ibuprofen, diclofenac, naproxen, estradiol and ethinylestradiol, the flow rate was set at 0.8 ml/min, and a 4:1 splitting system has been inserted after the column, in order to send in the source ESI 200 µl/min. The solvents used for the mobile phase are water (solvent A), and acetonitrile (solvent B). The gradient elution program is shown in the table 3.5.

Time (min.)	%A	%B
0	80	20
14	25	75
16	5	95
20	80	20
30	80	20

Table 3.5: Gradient elution program of drugs analyzed by ESI-.

Electrospray ionization in negative mode (ESI-), was conducted as summarized in table 3.6.

Source and polarity	ESI-
Potential (kV)	-4,50
Capillary voltage (V)	-24,0
Capillary temperature (°C)	350
Nebulization gas flow (a.u.)	50
MS range	50 - 450

Table 3.6: MS condition.

In mass spectrometer MS and MS/MS experiments have been performed, in SRM mode (selected reaction monitoring) in a range of 50-450 m/z. In table 3.7, SRM transitions, monitored for the analysis of drugs acetylsalicylic acid, ibuprofen, diclofenac, naproxen, estradiol and ethinylestradiol and collisional energy (in eV) necessary for their fragmentation in the linear trap, are reported.

Drugs	**[M-H]$^-$**	**CID energy (eV)**	**SRM**
Acetylsalicylic acid	179.0	6.3	179.0 > 137.0
Diclofenac	294.1	8.8	294.1 > 250.0
Estradiol	271.1	14.0	271.1 > 253.0
Ethinylestradiol	295.1	14.0	295.1 > 267.0
Ibuprofen	205.0	8.8	205.0 > 161.0
Naproxen	229.0	7.0	229.0 > 185.0

Table 3.4: SRM transition used for drugs analyzed by LC-MS/MS (ESI-).

3.1.5 Statistical analysis

Before chromatographic analysis, the LogP values of the various drugs were compared to evaluate the significant difference between their hydrophobicity using a statistical test t. The test performed is a paired t test. Since the LogP used derive from a computational calculation for which only a single standard deviation value is defined [95], there is no significant difference between the variances of the measurement sets; therefore, the value of t was calculated by the following relation [89]:

$$t_{calc} = \frac{|x_1 - x_2|}{S} \sqrt{\frac{N_1 N_2}{N_1 + N_2}}$$

where

X_1 = mean value of the first set of measures

N_1 = number of replicas

X_2 = mean value of the second set of measurements

N_2 = number of replicas

S = standard deviation for both set of measures.

The t_{calc} value was compared with the tabulated value for a number of degrees of freedom equal to ($N_1 + N_2 – 2$) and a confidence level of 95%. If the t_{calc} value is greater than the one tabulated then there is a significant difference between the data.

3.1.6 Validation study

In order to validate the method for the determination of pharmacologically active compounds using LC-MS/MS, the following parameters were evaluated: linearity, accuracy, limit of detection (LOD), limit of quantification (LOQ), recovery and uncertainty of the method. Particularly, according to the EURACHEM guidelines [96], ten different calibration standard solutions of drugs in methanol were analyzed at a concentration range between 0.001-200 µg/L for amoxicillin, erythromycin, clarithromycin, metformin, omeprazole and carbamazepine and, in a concentration range of 5-5000 µg/L, for acetylsalicylic acid, ibuprofen, diclofenac, estradiol, naproxen and ethinylestradiol, using the optimal chromatographic separation conditions, in order to study their linearity.

After evaluating the work range for each analyte, the calibration curves were obtained by analyzing six different standard calibration solutions (k = 6) of the drugs in triplicate (n = 3) within the linear range of each compound. The linearity of calibration curve was confirmed by

statistical tests, that is the t-test for the correlation coefficient [97] and the Fisher test [98]. To verify the significance of the correlation coefficient, t_{calc} was compared with t_{tab} value, at the significance level desired, using (n - 2) degrees of freedom. As for the Fisher test, if the value of F_{calc} is less than or equal to F_{tab} then the experimental data set describes an authentic linear correlation, while if $F_{calc} > F_{tab}$ the work range must be reduced as much as possible to obtain a linear calibration function. Detection (LOD) and quantification (LOQ) limit have been calculated, according to the guidelines EURACHEM: LOD is expressed as the concentration at a specified ratio signal/noise, generally 3:1 [99]; while a signal/noise ratio of 10:1 is used for determine the LOQ [99]. LOD and LOQ value were calculated considering the level of lowest concentration for each calibration line. According to the EURACHEM guidelines [96], the accuracy of the method was evaluated as "repeatability" and "intermediate repeatability" by measuring the standard deviation of analyzed samples in conditions of "repeatability" and "intermediate repeatability" for three levels of concentration for each drug. Concentration levels were chosen taking into account, for each drug, the smallest, the highest and an intermediate point of calibration line. Standard deviation for six replicates analyzed in the same day was referred to as "repeatability", while standard deviation calculated on several days for ten replicates was referred to as "intermediate precision". From the various standard deviation, repeatability and intermediate precision limits were calculated at 95% confidence level as follows:

$$r = \sqrt{2} t_{tab} S$$

To better compare the precision results obtained with other data, it was useful to calculate the relative standard deviation percentage (% RSD) as follows:

$$\%\mathrm{RSD} = \frac{S}{C_M}$$

where

S = repeatability and intermediate precision standard deviation

C_M = mean value of the concentrations under repeatability and intermediate precision conditions.

Recovery was assessed by taking 10 aliquot measurements of the actual massive sample individually fortified with the analyte concentration, C_{spk}, and using the following equation:

$$R_m = \frac{C_{obs} - C_{nat}}{C_{spk}}$$

where

C_{obs} = observed concentration

C_{nat} = concentration of drug already presents in the analyzed sample

C_{spk} = added concentration for recovery assessment.

For erythromycin, amoxicillin, clarithromycin, metformin, omeprazole, carbamazepine, acetylsalicylic acid, naproxen, diclofenac, ibuprofen, estradiol and ethinylestradiol, the fortified concentrations were equal to 5 µg/L, 10 µg/L 20 µg/L. On the other hand, for clarithromycin, omeprazole and carbamazepine, recovery was also evaluated at concentrations of 0.5 µg/L and l µg/L. The uncertainty of recovery was calculated as follows:

$$u(R_m) = R_m \sqrt{\left(\frac{S_{obs}^2}{NC_{Mobs}^2}\right) + \left(\frac{u(C_{spk})}{C_{spk}}\right)^2}$$

with

N = number of replicas (n = 10).

Statistical test was used to verify the existence of a significant difference from 1.0 (100%) by comparison with t_{calc}, calculated as follows:

$$t = \frac{|R_m - 1|}{u(R_m)}$$

and t_{tab} for (n - 1) degrees of freedom at 95% of confidence (where n is the number of results used for the estimation of Rm) [100]. If Rm is not significantly different from l ($t_{calc} < t_{tab}$) no corrections will be made on the recovery values.

According to the EURACHEM guide [101], the uncertainty inherent the experimental data has been estimated on the basis of all the sources of uncertainty involved in the analytical process, as shown in following equation:

$$\frac{u_0}{C_0} = \sqrt{\left(\frac{u_{preparative}}{C_0}\right)^2 + \left(\frac{u_{calibration}}{C_0}\right)^2 + \left(\frac{u_{Rm}}{R_m}\right)^2 + \left(\frac{u_{LOD}}{LOD}\right)^2}$$

where

$u_{preparative}$ = uncertainty associated to sample preparation

$u_{calibration}$ = uncertainty associated to calibration curve

u_{Rm} = uncertainty associated to recovery

u_{LOD} = uncertainty associated to limit of detection

C_0 = concentration in µg/L

Values of uncertainty were expressed in terms of extended uncertainty (U), which was determined by multiplying the combined standard uncertainty u_0 with a coverage factor k = 2; for normal distribution, this provides a level of reliability of approximately 95% [102].

3.2 Ecotoxicological experiments

3.2.1 Culture conditions

T. fulvus, specimens used for this study, were originally collected from Mar Mediterraneo (location Calafuria, Livorno) and maintened in the laboratory of ecotoxicology of CNR – IRSA (Centro Nazionale Ricerche – Istituto Ricerca sulle Acque) in Taranto for several generations. The copepods were cultured inside 0.5 L polystyrene culture flasks with filter screw cap in filtered natural sea water (0.45µm) figure 3.2, in climatized chamber under the following conditions (UNICHIM 2396: 2014, 2014):

- salinity 38‰ ± 2 PSU,
- temperature 20 ± 2°C,
- photoperiod 16L/8D,
- luminosity 500 – 1200 lux, cool light,

– weekly feeding ad libitum with aquarium feed Tetramarin ® and a mix of phytoplanktonic algae *Tetraselmis suecica* and *Isochrysis galbana*.

Figure 3.2: Culture flasks with ventilated cap.

The enrichment of the diet with Tetramarin ® feed favours the maintenance of cultures for long periods [103,104].

3.2.2 Algal cultures: *Tetraselmis suecica* and *Isochrysis galbana*

The algal strains of *Tetraselmis suecica* and *Isochrysis galbana*, figure 3.3 A and B, coming from the microalgae collection of CNR IRSA in Taranto, were cultured in complete f/2 medium (Guillard, 1975) using 0.22μm filtered and sterilized seawater at 38 ‰ PSU.

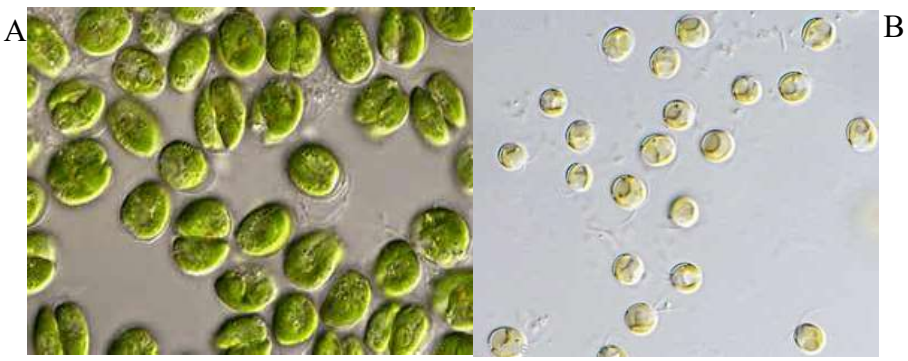

Figure 3.3: A) *Tetraselmis suecica* and B) *Isochrysis galbana*.

The compounds used for the preparation of the medium were all of analytical grade. The cultures were kept in 500 mL flasks closed with sterile gauze pad and hydrophobic cotton, in thermostatic cells at 20 ± 2°C, with cool-white 24h light exposure (7000-8000 lux) and with continuous aeration.

3.2.3 Test organisms

Toxicity tests were carried out on newborn offspring (nauplii) of homogeneous age (i.e. < 24h old) in order to employ the same developmental stage. To obtain the synchronized nauplii, about 200 females with egg sacs were collected from the stock culture and transferred to a 105 μm mesh plankton net fixed on a Plexiglas tube

placed in a petri dish, in order to allow the passage of the nauplii hatched, figure 3.4. *T. suecica* and *I. galbana* were added at a density of approximately 1.5×10^5 and 3.0×10^5 cells/ml, respectively.

Figure 3.4: A) Massive culture of ovigerous females of *T. fulvus*,

The massive culture of ovigerous females was kept in a thermostatically controlled environment under the same conditions as the breeding. After 24 hours newly healty nauplii (i.e. could swim actively) were randomly selected with a Pasteur pipette under a stereomicroscope, washed by gently pipetting in clean water and transferred from the Petri dish to the test wells of 6-well culture plates (Nest Biotech Co., Ltd).

3.2.4 Preparation of test solution

Concentrations of carbamazepine and amoxicillin used in the experiments (5 µg/L and 2 µg/L respectively) were equivalent to those measured in waste waters coming from waste water treatment plant of the Potenza village (Basilicata, Southern Italy). The toxicity tests were carried out with analytical reagent-grade chemicals both purchased from Sigma-Aldrich. Stock solutions (1000 mg/L) were prepared dissolving

each compound in methanol (Sigma Aldrich) and then stored at 4°C in darkness to avoid photodegradation.

Artificial sea water (ASW) Instant Ocean® (pH 8.0 ± 0.1, Salinity, 38 ± 2 PSU) filtered through a GF/C Wathman (0.22 μm) was used as negative control and dilution water to prepare testing solutions at designed nominal concentrations.

Before adding ASW to appropriate volumes of stock solution to obtain final concentrations, methanol, used as carrier solvent, was evaporated under a stream of N_2 gas. Chronic toxicity tests were conducted with carbamazepine and amoxicillin alone and in binary mixtures simultaneously at the same conditions described for the copepod cultures. The dilutions of each drug and their corresponding mixture were freshly prepared before each experiment.

3.2.5 Exposure

To start the first generational life – cycle test, ten newly hatched-nauplii (i.e. < 24 h old) per trial were transferred to 6-well culture plates containing 5 mL of test solution; each sample was organized in six replicates, so 60 nauplii for treatment were used, figure 3.5.

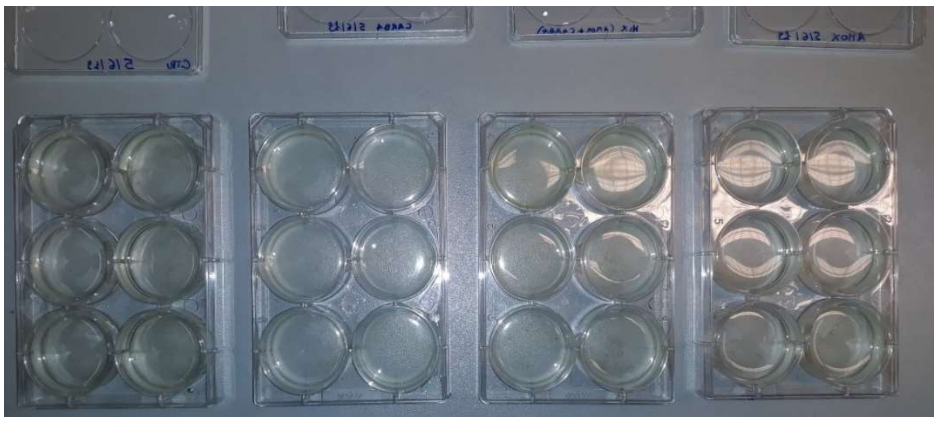

Figure 3.5: Test set up.

To maintain the tested concentrations, test solutions (90% of the working volume) were renewed every two days and *T. suecica* was added at a density of approximately 105 cells/ml. Plates were checked daily under a stereomicroscope to record mortality and developmental stages (time of development from nauplii to copepodite and from nauplii to adults with egg sacs). Time of sexual maturation was determinated when males are easily distinguishable from females by their enlarged geniculate antennae and for the appearance of ovisacs in the females. Survival (%) were determined after the maturation of all copepods. When all copepods reached maturity, males were eliminated from the experiment, which continued only with the remaining females. To measure the fecundity (offspring production), 12 adult females bearing an egg sac per each treatment were individually transferred to new 12-well (2 ml working volume) and were cultured at the same experimental conditions as above. Every day females were inspected and every 48h were transferred to a new culture plate with fresh solutions. The resulting nauplii and unhatched clutches (aborted sacs) were counted and removed under the stereomicroscope; if nauplii belonged to different broods (case presented during the weekend), they were distinguished according to their size. The fecondity (offspring production) was estimated as the total number of nauplii per female; the number of broods produced per female and the number of nauplii per brood were also recorded. The period from females bearing the egg sac to nauplii produced was considered as the hatching time.

For the experiment with the second generation (F1), nauplii (F1) produced by each female (F0) with the fifth or the sixth brood from each treatment were transferred to new 6-well culture plates. The experiment

and exposure conditions were the same as those used for the F0 generational test.

The experimental conditions are summarized in table 3.5.

Parameters	Chronic test
Test organism	Nauplii < 24 h old
Duration	28 days
Light intensity	500 – 1200 lux, cold light
Photoperiod (light / dark)	16h : 8h
Diluition water	Artificial sea water (ASW) Instant Ocean® (0,22 µm)
Salinity ‰ PSU	38 ± 2
Temperature °C	20 ± 2
Test plates	6-well culture plates
Incubation volume	5 mL
N° organisms/reply	10/1
N° replies	6
Concentration	carbamazepine: 5 µg/L amoxicillin: 2 µg/L Mixture: 5 µg/L carbamazepine +2 µg/L amoxicilline
Solution renewal	Every 48h
Feeding	*Tetraselmis suecica* (1 x 10^5 cell/mL)
Endpoint	Survival, developmental stages, N° nauplii/ female, N° broods/ female, N°nauplii/brood, hatching time, etc

Table 3.5: Experimental conditions of the chronic test.

3.2.6 Data processing and statistical analysis

The Microsoft Excel ® program was used to record data and graphic reactions. The assumptions of normality and homogeneity of variances were assessed by the Kolmogorov-Smirnov test and the Levene test, respectively.

One-way ANOVA analyses were used to determine statistical significance of the differences among treatments and the control for all the endpoints ($p < 0.05$). If significant differences were found by the ANOVA, Tukey multiple comparison test was used to discriminate between the means.

Statistical processing was performed with Statgraphics ® Version 5 Plus software (Statistical Graphic Corporation Manugistics TM Inc, Rockville, MD, USA).

4. Results and discussions

In this work it has been developed and validated, according to the guidelines EURACHEM, a method for the analysis of drugs in wastewater samples. Drugs, object of study, include different therapeutic classes: three antibiotics, amoxicillin, clarithromycin and erythromycin; an antiepileptic, carbamazepine; an active drug against the type 2 diabetes, metformin; one drug used to treat gastric problems, omeprazole; two hormones, estradiol and ethinylestradiol and anti-inflammatory ibuprofen, acetylsalicylic acid, diclofenac and naproxen. Most of these drugs are in the priority list of the World Organization of Health (WHO) [6] and represent the most pharmacologically active compounds found in Italian and/or world wastewaters [1,7-9]. Method developed is based on the use of reverse phase liquid chromatography (RPLC), coupled with a quadrupolar ion trap mass spectrometer (LTQ) with electrospray ionization (ESI). Mass detector was used in product ion detection mode (SRM selected reaction monitoring). SRM is a type of double-stage mass experiment in which one or more set of reactions are monitored, precursor ion > fragment ion. Through SRM it is possible a rapid analysis of trace components in complex mixtures. Ion trap was used to carry out MS/MS experiments using the technique of collision induced dissociation (Collision Induced Dissociation, CID), optimizing collisional energy (4.9-14 eV) depending on the precursor ion.

Then, chronic toxicity, with two of the drugs found in the waste water samples (carbamazepine and amoxicillin), was assessed on the model species *Tigriopus fulvus* during a two-generation cycles exposure test.

4.1 ESI-MS/MS analysis of drugs

The first step was to optimize acquisition mass parameters by tandem mass analysis of drugs. Optimization of mass parameters (ionization mode, capillary voltage, capillary temperature, atomization gas flow and collisional energy), were carried out by individually direct injection of 1 mg/L standard solutions of the twelve drugs, in the electrospray ion source (ESI) at a flow rate of 20 µL/min. After ionization, the fragmentation of molecular ions, isolated in the quadrupole ion trap (LTQ), has been optimized by appropriately varying the collision energy (CID), between 4.9 eV and 14 eV. Determination of collisional energy, indeed, is fundamental for the analysis because the spectra acquisition was done by using SRM scanning mode, selecting the transition corresponding to the most intense fragment ion.

Next, from figures 4.1 to 4.24, the fragmentation spectra and the respective peak assignments of the drugs object of study are reported.

- **Amoxicillin**

Amoxicillin is an antibiotic often used for the treatment of a number of bacterial infections and compare in the list of the 20 most prescribed drugs in Italy [17].

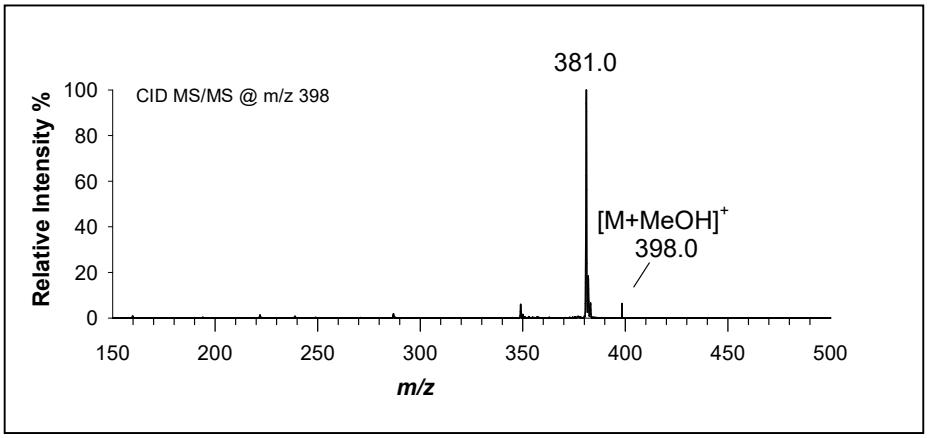

Figure 4.1: Fragmentation spectrum of ion m/z 398.0, isolation window ± 3 m/z, CID at collisional energy 23% (a.u.), i.e. 8.1 eV.

Tandem mass spectrum of this molecule, figure 4.1, was obtained as a methanol adduct [18], in ESI + mode by applying a collisional energy of 8.1 eV (23% a.u.). Signal at m/z 398.0 describes the molecular ion as a methanol adduct, while the peak at m/z 381.0 corresponds to the loss of NH_3 [7], as shown in the figure 4.2.

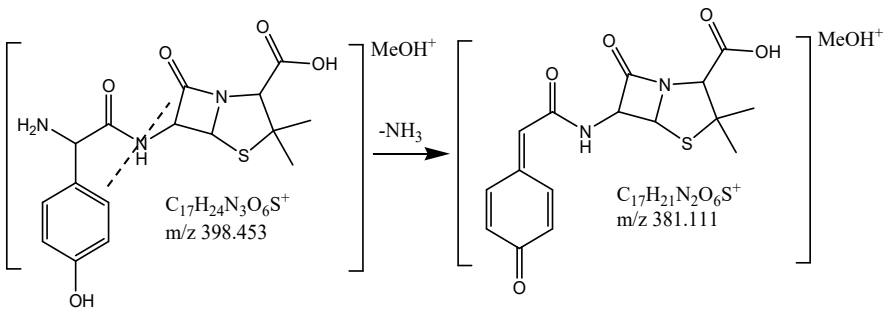

Figure 4.2 Proposed fragment ions at m/z 398.4 and 381.0.

As can be seen from figure 4.2, the methanolic adduct of amoxicillin, following the fragmentation, loses the group NH_3 bound to C in para to the phenolic group.

- **Carbamazepine**

Carbamazepine is an anti-epileptic whose presence in wastewater has been found throughout the world [1].

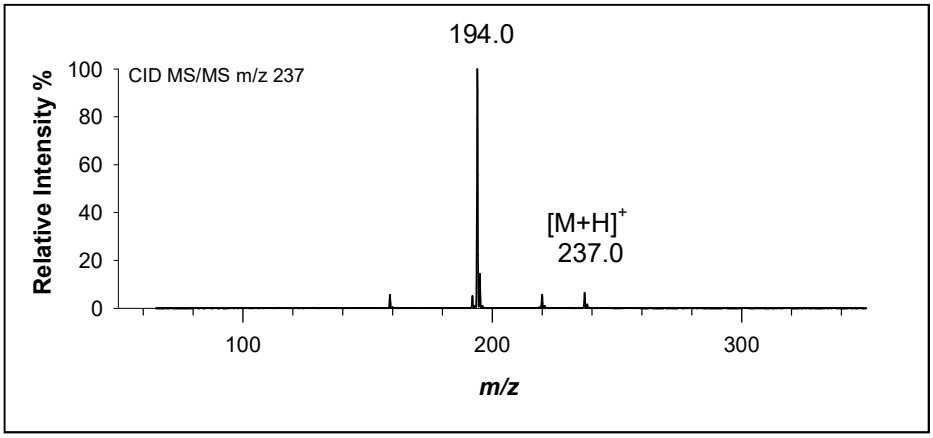

Figure 4.3: Fragmentation spectrum of ion m/z 237.0, isolation window ± 3 m/z, CID at collisional energy 15% (5.2 eV).

Tandem mass spectrum of this molecule, figure 4.3, was obtained in ESI + mode by applying a collisional energy of 5.2 eV (15% a.u.). Signal at m/z 237.0 describes the molecular ion, while the peak at m/z 194.0 corresponds to the loss of NHCO [12], as shown in the figure 4.4.

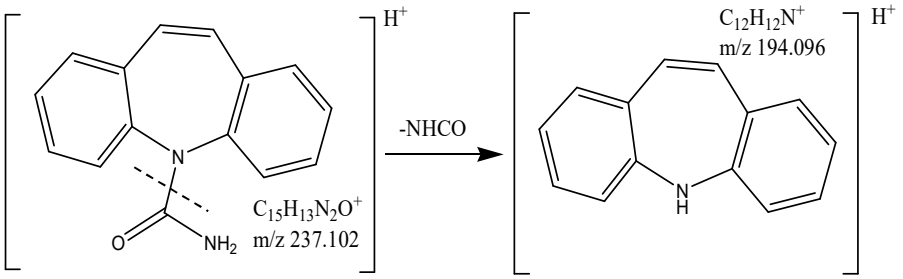

Figure 4.4: Proposed fragment ion at m/z 237.1 and 194.0.

As can be seen from figure 4.4, the molecular ion of carbamazepine, following the fragmentation, records the rupture of one and the N-C bonds of the diamidic group.

- **Clarithromycin**

Clarithromycin is a broad-spectrum antibiotic, classified as an emerging contaminant [1].

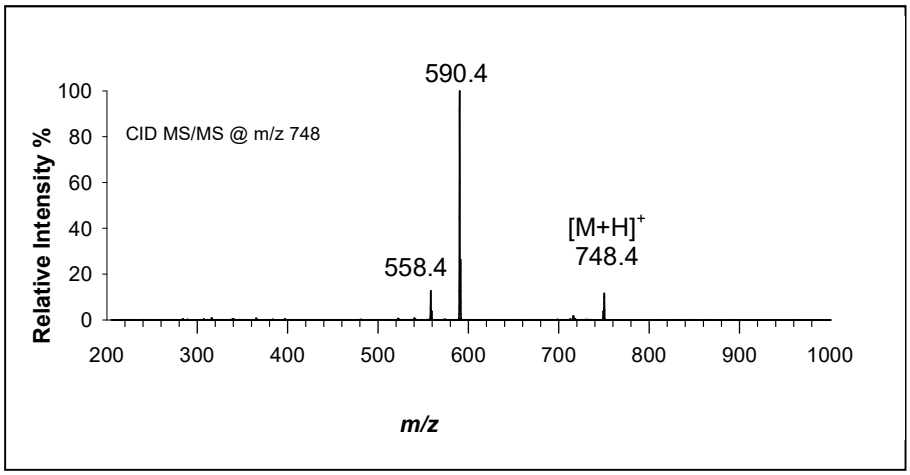

Figure 4.5: Fragmentation spectrum of ion m/z 748.4, isolation window ± 3 m/z, CID at collisional energy 15% (5.2 eV).

Tandem mass spectrum of this molecule, figure 4.5, was obtained in ESI + mode by applying a collisional energy of 5.2 eV (15% a.u.). Signal at m/z 748.4 describes the molecular ion, while the peaks at m/z 590.4 and m/z 558.4 correspond to the loss of $C_8H_{14}O_3$ [14] and $C_9H_{18}O_4$ [15] respectively, as shown in the figure 4.6.

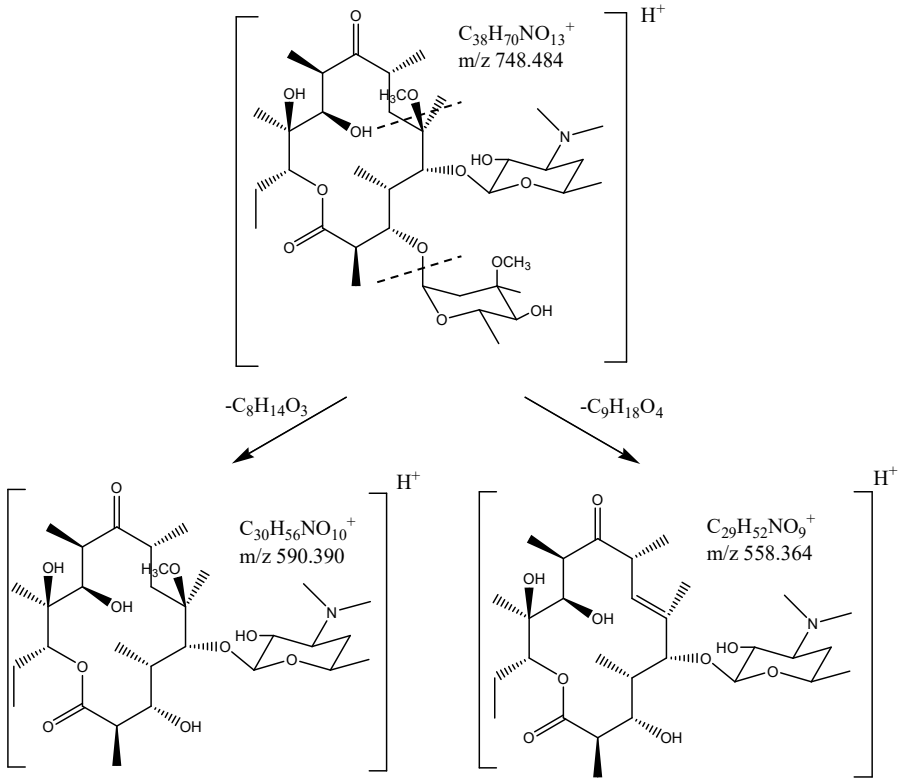

Figure 4.6: Proposed fragment ion at m/z 748.4, 590.4 and 558.4.

- **Erythromycin**

Erythromycin is commonly used in the treatment of infectious processes affecting the upper and lower airways, skin and soft tissues, and it has also been classified as an emerging contaminant [1].

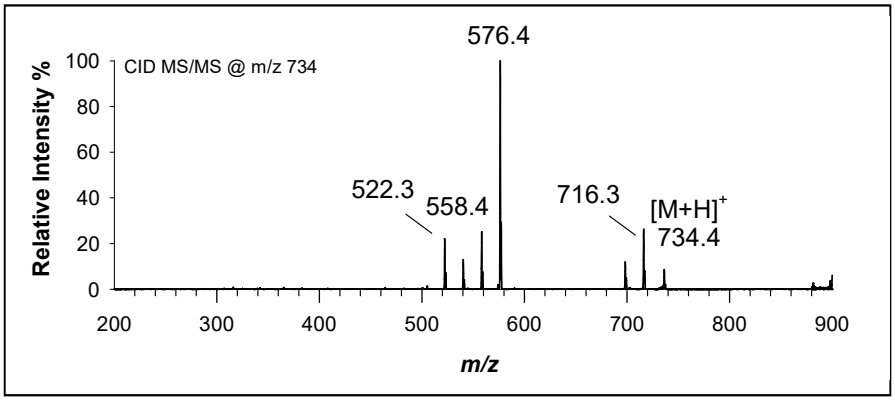

Figure 4.7: Fragmentation spectrum of ion m/z 734.4, isolation window ± 3 m/z, CID at collisional energy14% (4.9 eV).

Tandem mass spectrum of this molecule, figure 4.7, was obtained in ESI + mode by applying a collisional energy of 4.9 eV (14% a.u.). Signal at m/z 734.4 describes the molecular ion, while the peaks at m/z 716.3, m/z 576.4, m/z 558.4 and m/z 522.3 correspond to the loss of H_2O [15], $C_8H_{12}O_3$ [16], $C_8H_{14}O_4$ [15] and $C_8H_{20}O_6$ [15] respectively, as shown in the figure 4.8.

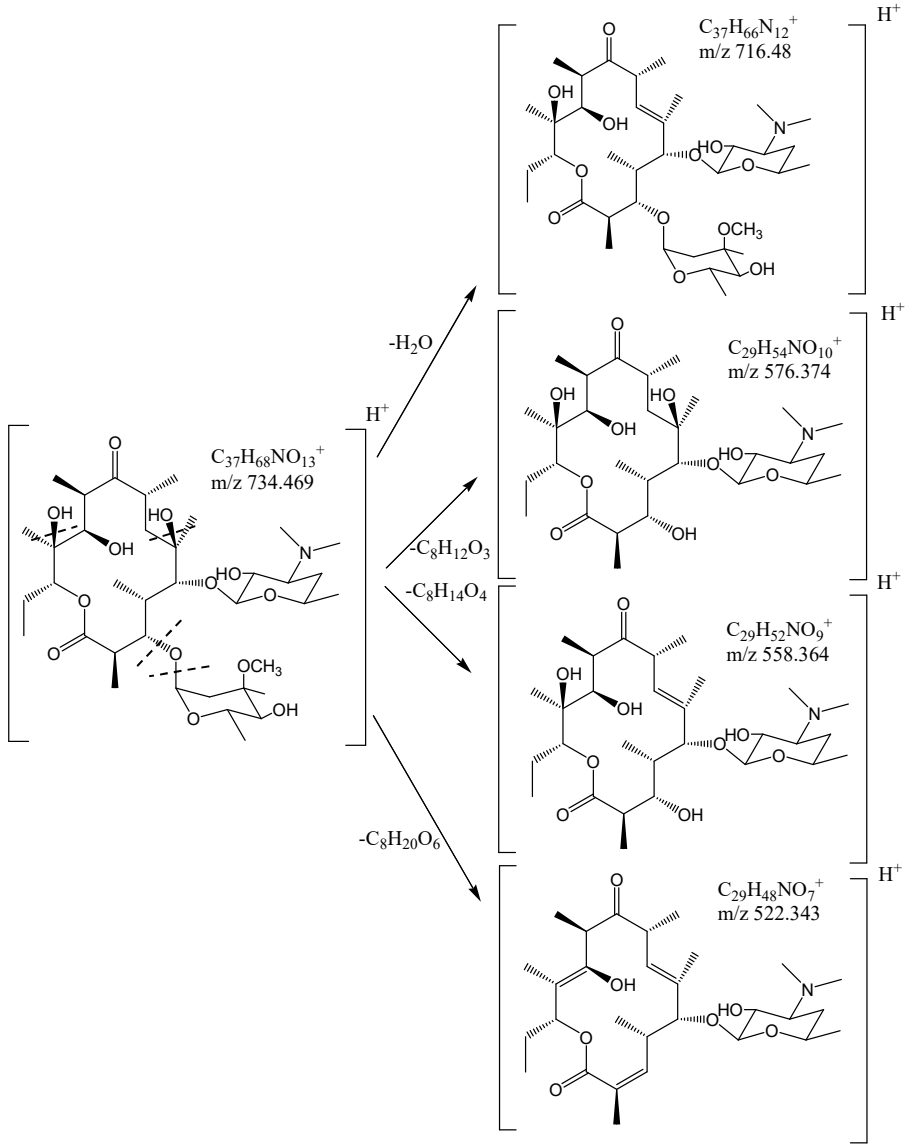

Figure 4.8: Proposed fragment ion at m/z 716.3, m/z 576.4, m/z 558.4 and m/z 522.3.

- **Metformin**

Metformin is the first-line medication for the treatment of type 2 diabetes, particularly in people who are overweight.

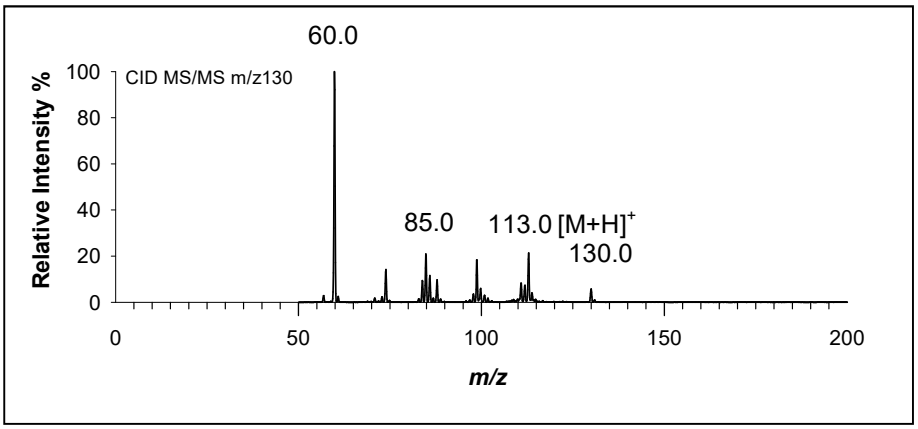

Figure 4.9: Fragmentation spectrum of ion m/z 130.0, isolation window ± 3 m/z, CID at collisional energy 32% (11.2 eV).

Tandem mass spectrum of this molecule, figure 4.9, was obtained in ESI + mode by applying a collisional energy of 11.2 eV (32% a.u.). Signal at m/z 130.0 describes the molecular ion, while the peaks at m/z 113.0, m/z 85.0 and m/z 60.0 has been hypothesized to be attributable to losses of NH_3, C_7H_7N and $C_3H_6N_2$ [13] respectively, as shown in the figure 4.10.

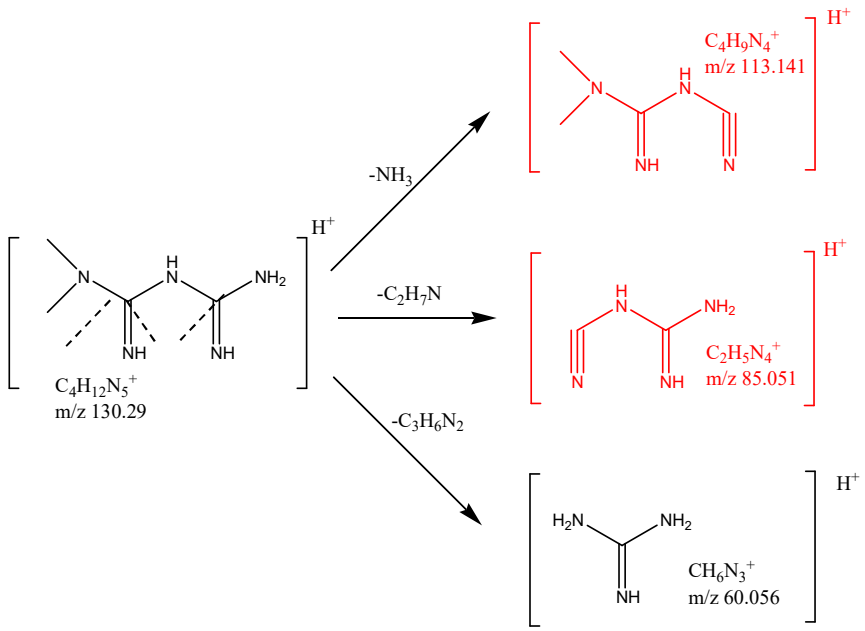

Figure 4.10: Proposed fragment ion at m/z 130.0, m/z 113.0, m/z 85.0 and m/z 60.0.

- **Omeprazole**

Omeprazole is a proton-pump inhibitor used in the treatment of gastroesophageal reflux disease, peptic ulcer disease.

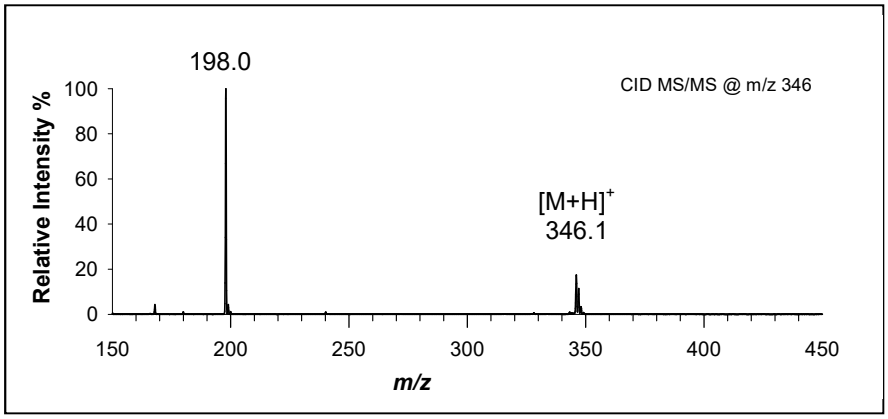

Figure 4.11: Fragmentation spectrum of ion m/z 346.1, isolation window ± 3 m/z, CID at collisional energy 15% (5.2 eV).

Tandem mass spectrum of this molecule, figure 4.11, was obtained in ESI + mode by applying a collisional energy of 5.2 eV (15% a.u.). Signal at m/z 346.1 describes the molecular ion, while the peaks at m/z 198.0 correspond to a loss of $C_8H_8N_2O$ [11] as shown in the figure 4.12.

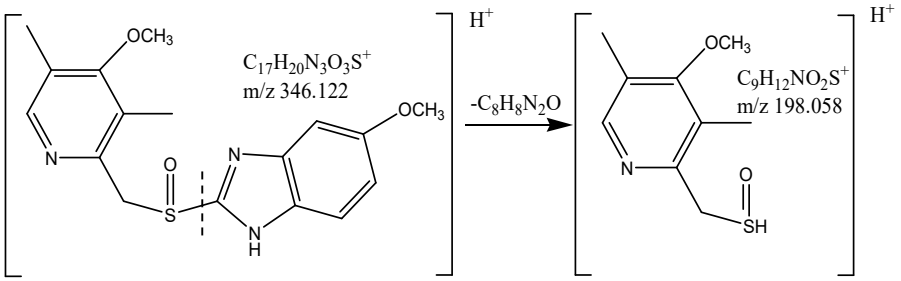

Figure 4.12: Proposed fragment ion at m/z 346.1 and m/z 198.0.

- **Acetylsalicylic acid**

Aspirin is one of the most widely used medications globally, with an estimated 40,000 tonnes (50 to 120 billion pills) consumed each year [56,57]. It is on the World Health Organization's List of Essential Medicines, the safest and most effective medicines needed in a health system [6].

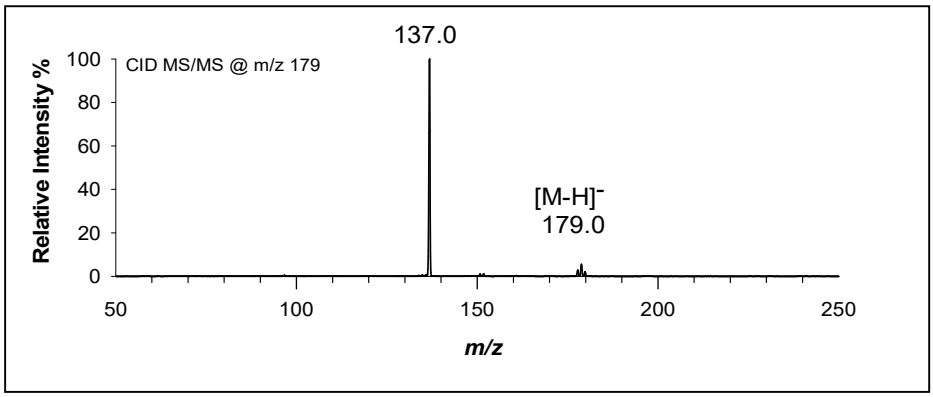

Figure 4.13: Fragmentation spectrum of ion m/z 179.0, isolation window ± 3 m/z, CID at collisional energy 18% (6.3 eV).

Tandem mass spectrum of this molecule, figure 4.13, was obtained in ESI - mode by applying a collisional energy of 6.3 eV (18% a.u.). Signal at m/z 179.0 describes the molecular ion, while the peaks at m/z 137.0 correspond to a loss of C_2H_2O [105] as shown in the figure 4.14.

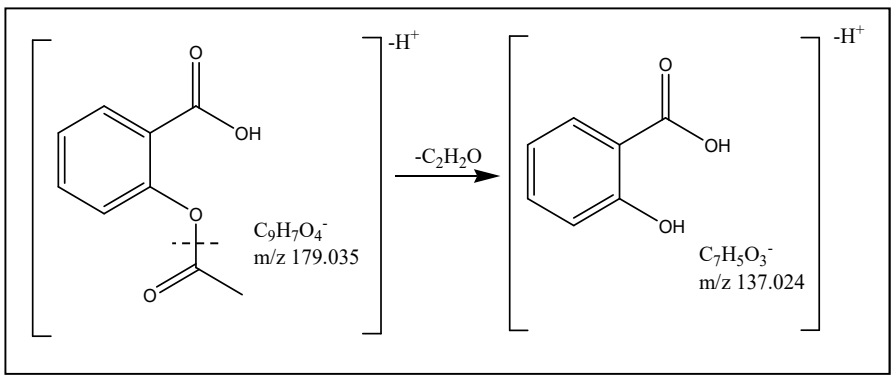

Figure 4.14: Proposed fragment ion at m/z 179.0 and m/z 137.0.

- **Diclofenac**

Diclofenac is a nonsteroidal antiinflammatory drug and at now it was the 78th most prescribed medication in the United States with more than 9 million prescriptions [59], and it has been classified as an emerging contaminant [1].

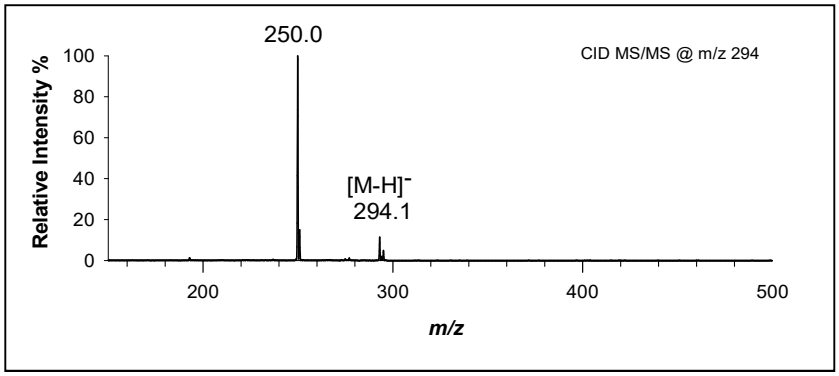

Figure 4.15: Fragmentation spectrum of ion m/z 294.1, isolation window ± 3 m/z, CID at collisional energy 25% (8.8 eV).

Tandem mass spectrum of this molecule, figure 4.15, was obtained in ESI - mode by applying a collisional energy of 8.8 eV (25% a.u.). Signal at m/z 294.1 describes the molecular ion, while the peaks at m/z 250.0 correspond to a loss of CO_2 [20] as shown in the figure 4.16.

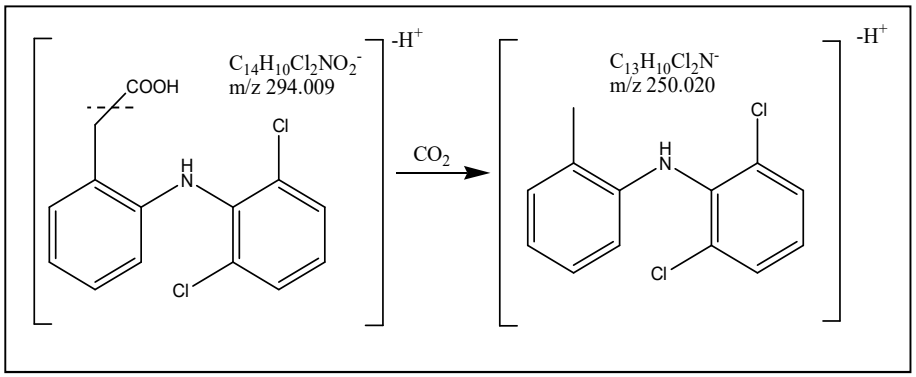

Figure 4.16: Proposed fragment ion at m/z 294.0 and m/z 250.0.

- **Estradiol**

Estradiol is used as a medication, primarily in hormone therapy for menopausal symptoms as well as transgender hormone replacement therapy [106] and represents 3.2% of most consumed drugs in Italy [11].

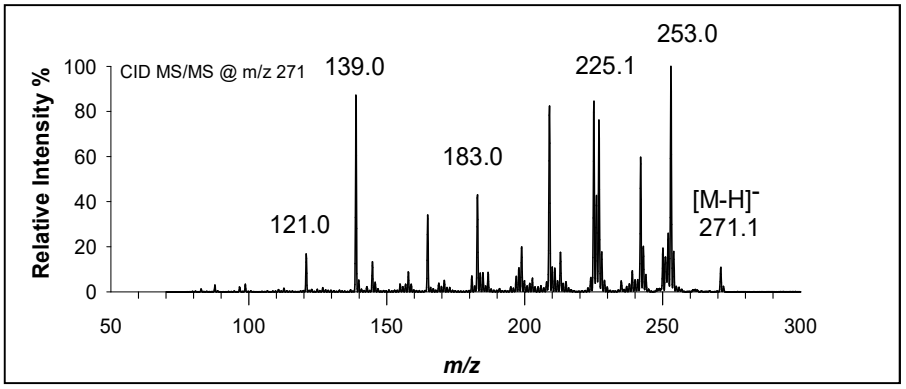

Figure 4.17: Fragmentation spectrum of ion m/z 271.1, isolation window ± 3 m/z, CID at collisional energy 40% (14.0 eV).

Tandem mass spectrum of this molecule, figure 4.17, was obtained in ESI - mode by applying a collisional energy of 14.0 eV (40% a.u.). Signal at m/z 271.1 describes the molecular ion, while the peaks at m/z 253.0, m/z 225.1, m/z 183.0, m/z 139.0 and m/z 121.0 have been hypothesized to be losses of H_2O, CH_2O_2, $C_4H_8O_2$, C_9H_8O and $C_9H_{10}O_2$ respectively, as shown in figure 4.18.

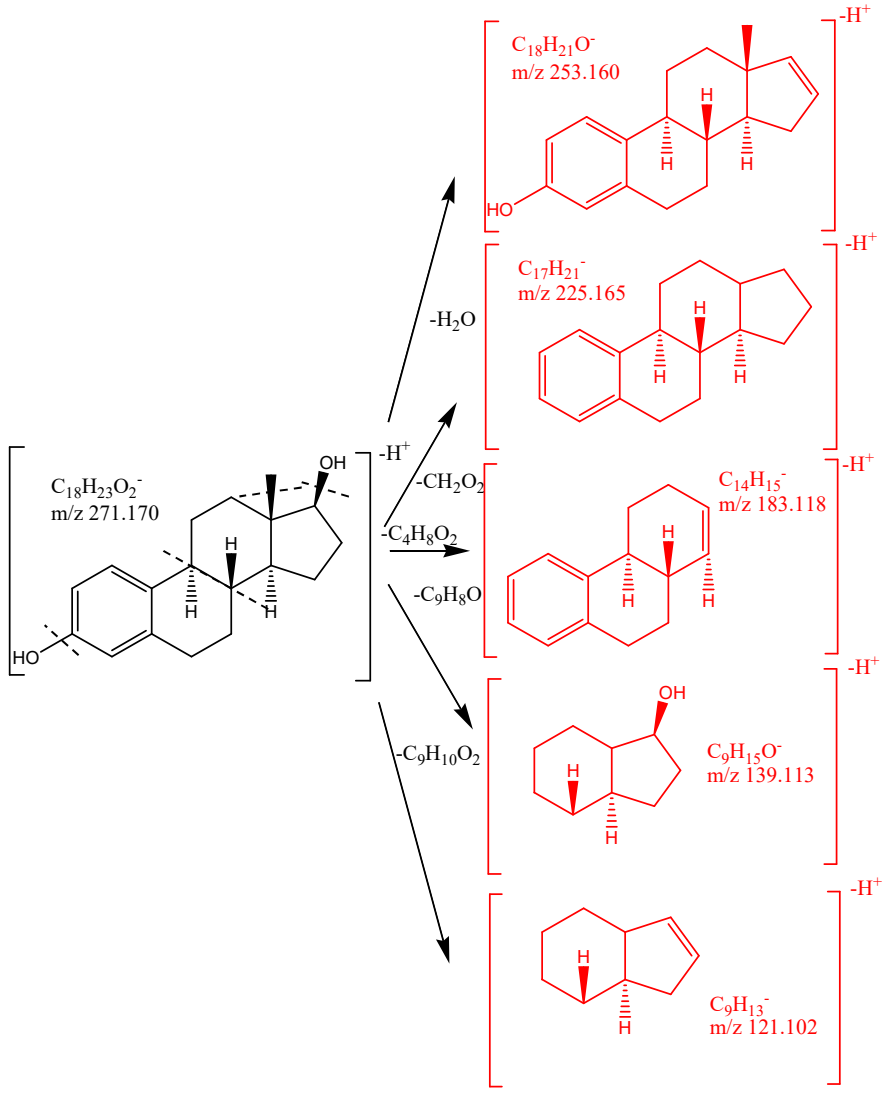

Figure 4.18: Proposed fragment ion at m/z 271.1, m/z 253.0, m/z 225.1, m/z,183.0, m/z 139.0 and m/z 121.0.

- **Ethinylestradiol**

Ethinylestradiol is an estrogen medication which is used widely in birth control pills in combination with progestins [106,107]. Today it is found in almost all combined forms of birth control pills and is nearly the exclusive estrogen used for this purpose, making it one of the most widely used estrogens [108,109].

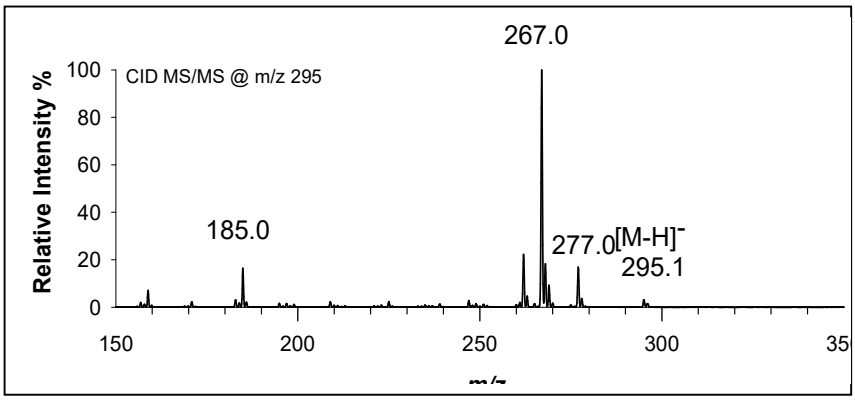

Figure 4.19: Fragmentation spectrum of ion m/z 295.1, isolation window ± 3 m/z, CID at collisional energy 40% (14.0 eV).

Tandem mass spectrum of this molecule, figure 4.19, was obtained in ESI - mode by applying a collisional energy of 14.0 eV (40% a.u.). Signal at m/z 295.1 describes the molecular ion, while the peaks at m/z 277.0, m/z 267.0, m/z 185.0 have been hypothesized to be losses of H_2O, CO and $C_6H_5O_2$ respectively, as reported in figure 4.20.

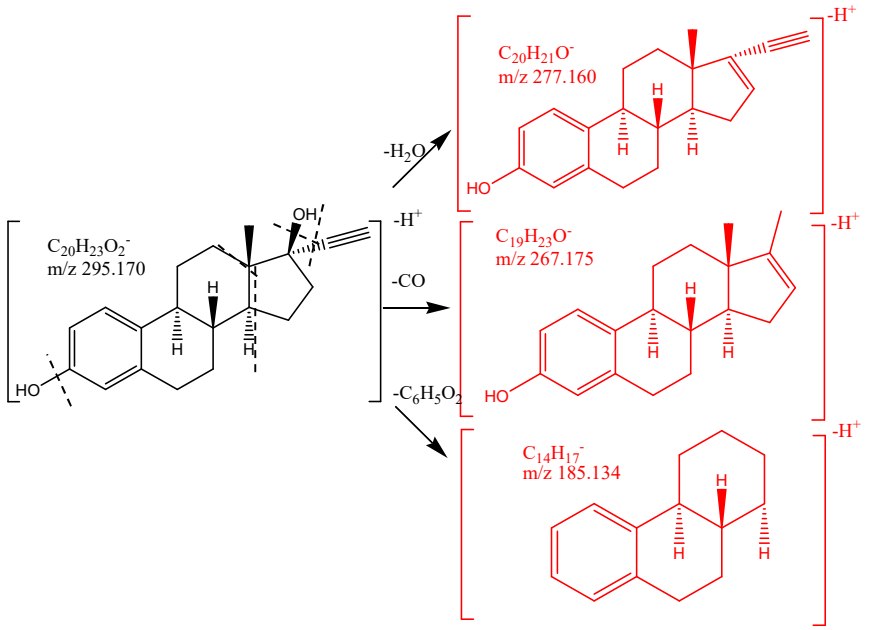

Figure 4.20: Proposed fragment ion at m/z 295.1, m/z 277.0, m/z 267.0 and m/z 185.0.

- **Ibuprofen**

Ibuprofen is a medication in the nonsteroidal anti-inflammatory drug class that is used for treating pain, fever, and inflammation. At now, it was the 35th-most prescribed medication in the United States, with more than 21 million prescriptions [59] and it has been classified as an emerging contaminant [1].

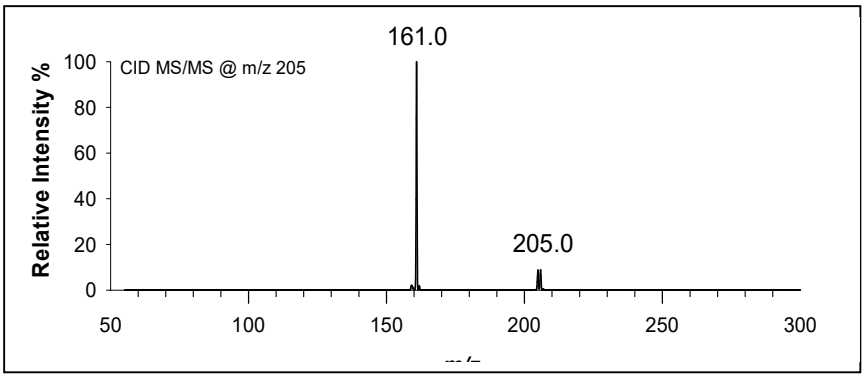

Figure 4.21: Fragmentation spectrum of ion m/z 205.0, isolation window ± 3 m/z, CID at collisional energy 25% (8.8 eV).

Tandem mass spectrum of this molecule, figure 4.21, was obtained in ESI - mode by applying a collisional energy of 8.8 eV (25% a.u.). Signal at m/z 205.0 describes the molecular ion, while the peak at m/z 161.0 is due to the loss of CO_2 [19], as reported in figure 4.22.

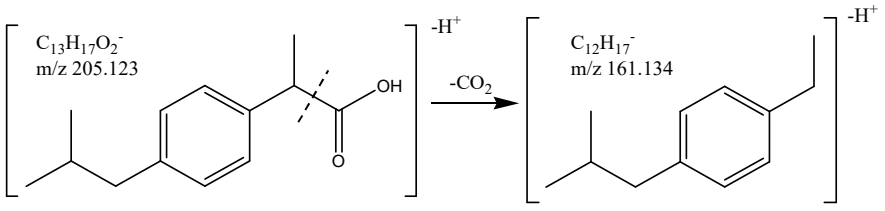

Figure 4.22: Proposed fragment ion at m/z 205.1 and m/z 161.0.

- **Naproxen**

Naproxen is a nonsteroidal anti-inflammatory drug, and at now it was the 68th most prescribed medication in the United States, with more than 11 million prescriptions [59].

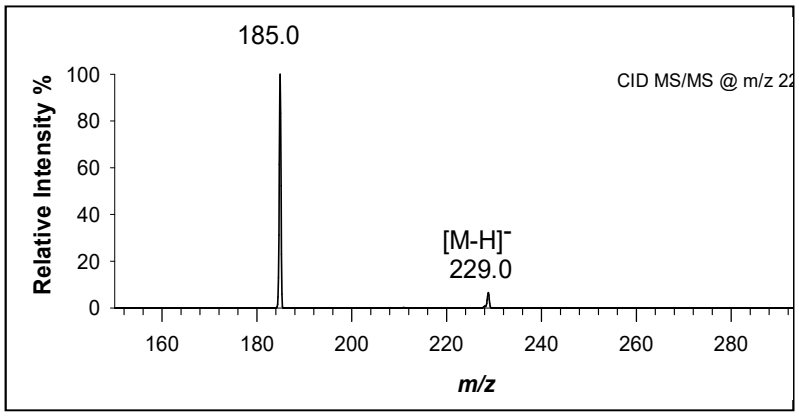

Figure 4.23: Fragmentation spectrum of ion m/z 229.0, isolation window ± 3 m/z, CID at collisional energy 20% (7.0 eV).

Tandem mass spectrum of this molecule, figure 4.23, was obtained in ESI - mode by applying a collisional energy of 7.0 eV (20% a.u.). Signal at m/z 229.0 describes the molecular ion, while the peak at m/z 185.0 is due to the loss of CO_2 [110], as reported in figure 4.24.

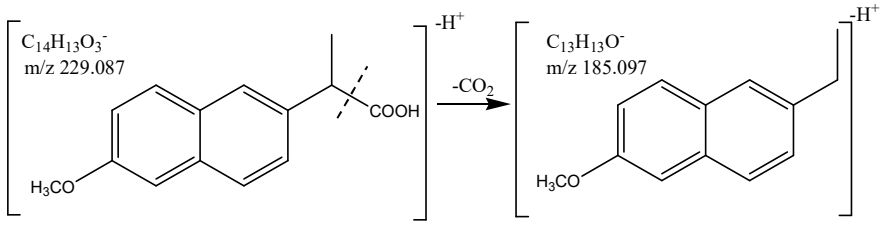

Figure 4.24: Proposed fragment ion at m/z 229.0 and m/z 185.0.

4.2 Selection of transitions for SRM experiments

Results of tandem mass experiments carried out for drugs have been used for selecting the ions to be monitored in the Selected Reaction Monitoring (SRM) experiments.

It is possible to see from the analysis of tandem mass spectra on the drugs, that these can be divided into two categories. First category is that of drugs whose analysis was performed by electrospray ionization in positive mode (ESI +), among these we find: amoxicillin, metformin, omeprazole, carbamazepine, clarithromycin and erythromycin. The second one is that of the drugs whose analysis was performed using electrospray ionization in negative mode (ESI-), these are: acetylsalicylic acid, naproxen, diclofenac, ibuprofen, estradiol and ethinyl estradiol. In table 4.1 was reported for each drug, the ionization mode, the mass-charge ratio of the precursor ion, the selected fragment ion, monitored during the SRM scan, and the collision energy used to promote fragmentation in the quadruple ion trap.

Drugs	Ionization mode	Preursor ion*	Energy CID (eV)	SRM
Amoxicillin	ESI+	398	8.1	398 > 381
Carbamazepine	ESI+	237	5.2	237 > 194
Clarithromycin	ESI+	748	5.2	748 > 590
Erythromycin	ESI+	734	4.9	734 > 576
Metformin	ESI+	130	11.2	130 > 60
Omeprazole	ESI+	346	5.2	346 > 198
Acetylsalicylic acid	ESI-	179	6.3	179 > 137
Diclofenac	ESI-	294	8.8	294 > 250
Estradiol	ESI-	271	14.0	271 > 253
Ethinylestradiol	ESI-	295	14.0	295 > 267
Ibuprofen	ESI-	205	8.8	205 > 161
Naproxen	ESI-	229	7.0	229 > 185

* $[M+H]^+$ for drugs with ESI+ ionization mode; $[M-H]^-$ for drugs with ESI - ionization mode.
Table 4.1: Optimised mass parameters for each drug.

4.3 Optimization of RPLC conditions

Chromatographic separation of drugs was carried out using a reverse phase stationary phase (Accucore-150-C18-150 X 4.6 mm i.d., 2.6 um). Mass detector (LTQ) has been used in full-scan mode in the ion range with m/z from 125 to 1000 m/z for amoxicillin, erythromycin, clarithromycin, omeprazole, carbamazepine and metformin, and 100 to 450 m/z for acetylsalicylic acid, naproxen, ibuprofen, estradiol, ethinyl estradiol and diclofenac. Chromatograms of total ionic current (TIC) were acquired and, starting from these, chromatograms of the extracted ions (XIC) were built. XIC chromatograms report only the intensities of

the ions that fall in a narrow m/z window. This last mode of representation is useful when there is the possibility that some analytes have the same retention time.

For the analysis of amoxicillin, metformin, omeprazole, carbamazepine, clarithromycin and erythromycin a triphasic gradient was used figure 4.25.

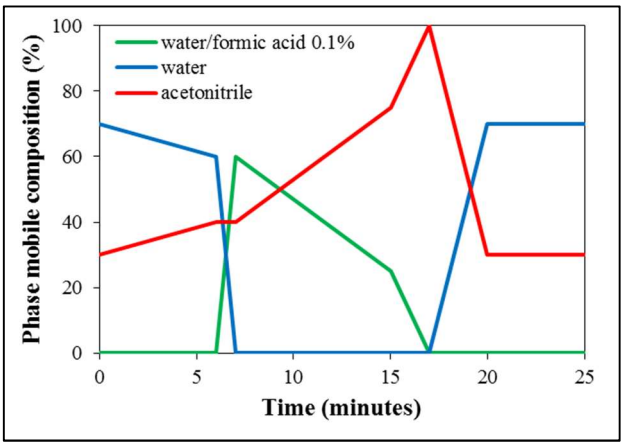

Figure 4.25: Triphasic gradient used for separation of drugs detected in positive mode (ESI+).

Using three-phase gradient conditions all the ions are well separated, figure 4.26, which allowed a correct quantification of the pharmaceutical compounds analyzed, using the SRM acquisition method.

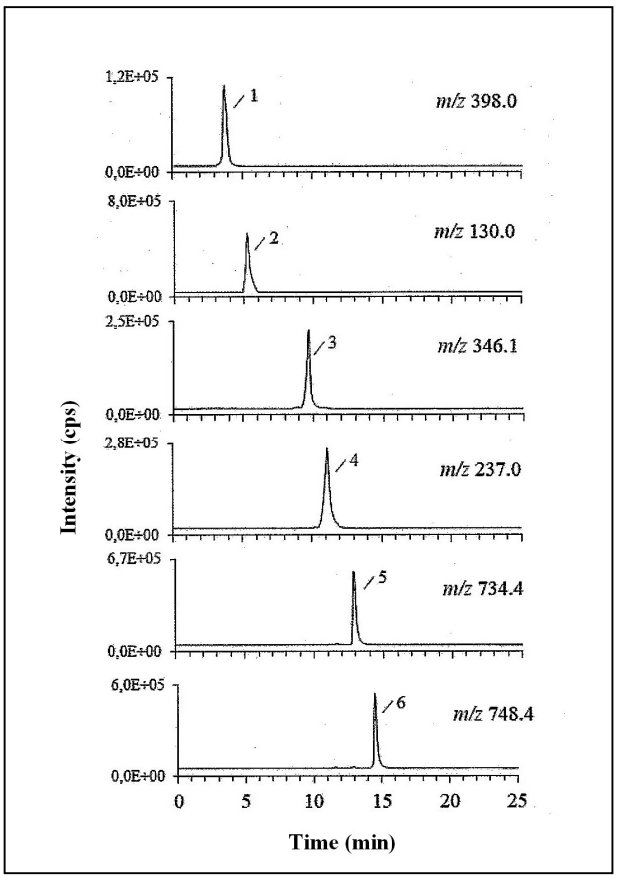

Figure 4.26: Chromatograms of the extracted ions (XICS) of a standard mixture of 1 mg/L of (1) methanolic adoption of amoxicillin, (2) metformin, (3) omeprazole, (4) carbamazepine, (5) erythromycin and (6) clarithromycin acquired by RPLC-ESI-(+)-LTQ MS/MS. Three phase gradient used is shown in figure 4.25.

From the chromatographic profile, shown in figure 4.26, we deduce the following elution times: amoxicillin 3.7 min., metformin 5.2 min., omeprazole 9.7 min., carbamazepine 11.1 min., erythromycin 13.1 min. and clarithromycin 14.5 min.

Chromatographic separation of acetylsalicylic acid, ibuprofen, naproxen, diclofenac, estradiol and ethinyl estradiol, analyzed by negative

ionization (ESI-), was made using water and acetonitrile as a mobile phase, figure 4.27.

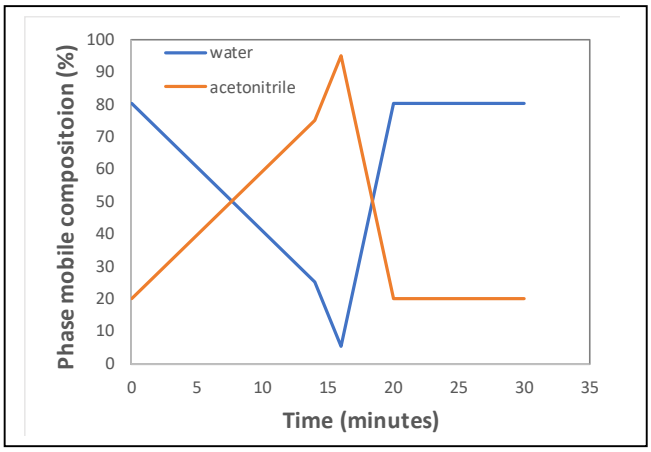

Figure 4.27: Biphasic gradient used for separation of drugs detected in negative mode (ESI-).

In figure 4.28 it is reported XIC chromatogram of drugs detected in negative mode (ESI-).

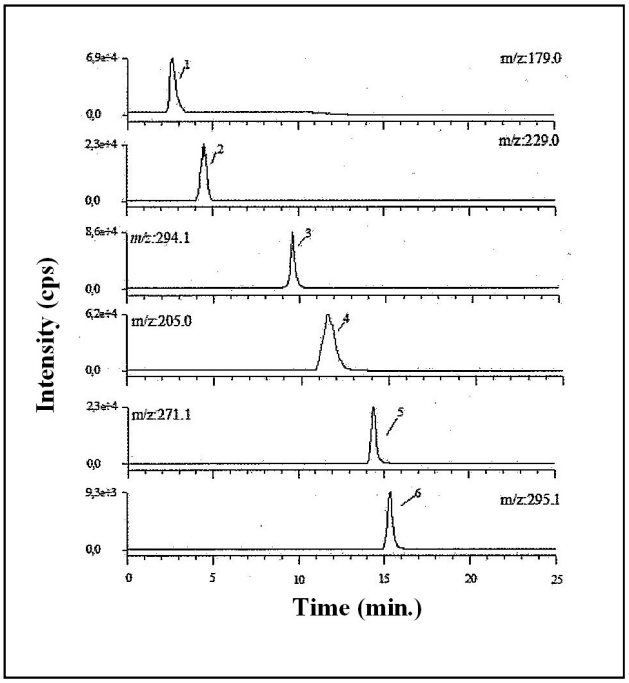

Figure 4.28. B) Chromatograms of the extracted ions (XICs) of a standard mixture of l mg/L of (1) acetylsalicylic acid, (2) naproxen, (3) diclofenac, (4) ibuprofen, (5) estradiol and (6) ethinyl estradiol.1 acquired by LC-ESI-LTQ-MS in negative mode. Biphasic gradient used
is shown in figure 4.27.

From the chromatographic profile shown in figure 4.28 we deduce the following elution times: acetylsalicylic acid 2.6 min., naproxen 4.5 min., diclofenac 9.6 min., ibuprofen 11.5 min., estradiol 14.4 min. and ethinyl estradiol 15.3 min.

In summary, the LC and MS conditions, optimized for 12 drugs, were reported in table 4.2.

	LC conditions	MS conditions			
Drugs	**Retention time (min.)**	**SRM range (min.)**	**Precursor ion**	**CID esergy (eV)**	**SRM**
Amoxicillin	3.7	0 - 4	398.0	8.1	398.0>381.0
Metformin	5.2	4 – 8	130.0	11.2	130.0>60.0
Omeprazole	9.7	8 – 10.2	346.1	5.2	346.1>198.0
Carbamazepine	11.1	10.2 – 12.5	237.0	5.2	237.0>194.0
Erythromycin	13.1	12.5 – 14	734.4	4.9	734.4>576.4
Clarithromycin	14.4	14 – 25	748.4	5.2	748.4>590.4
Acetylsalicylic acid	2.6	0 – 2.8	179.0	6.3	179.0>137.0
Naproxen	4.5	2.8 – 6	229.0	7.0	229.0>185.0
Diclofenac	9.6	6 – 9.8	294.1	8.8	294.1>250.0
Ibuprofen	11.5	9.8 – 12	205.0	8.8	205.0>161.0
Estradiol	14.4	12 – 15	271.1	14.0	271.1>253.0
Ethinylestradiol	15.3	15 – 30	295.1	14.0	295.1>267.0

Table 4.2: Chromatographic and mass conditions for the analysis of selected drugs.

4.4 RPLC-ESI-MS/MS method validation

Importance of validating analysis methods is explicated in the UNI CEI EN ISO/IEC standard 17025. According to this, the validation is the confirmation through examination and the objective evidence that the particular requirements for the intended use are met [108]. Validation of a method is necessary when:

- new analytical method must be developed for particular purposes;
- analytical method in use must be updated, improved or extended to a new one analytical problem;
- quality control shows changes in the performance of the method in use over time;
- analytical method in use must be used in a different laboratory, by different operator, with different instrumentation;
- it is necessary to demonstrate the equivalence of the analytical method in question with a standard method.

Validation of the LC-ESI-LTQ MS/MS method for the analysis of drugs in wastewater samples was carried out following the EURACHEM guidelines (European Analytical Chemistry) [111]. According to this guide, the parameters commonly evaluated during the validation of method are: linear range, precision (repeatability, intermediate repeatability and reproducibility), limit of detection (LOD) and limit of quantification (LOQ), recovery, and measurement uncertainty [111]. Performances of the LC-ESI-LTQ MS/MS method, validated in this work, were compared with the EPA method 1694: “Pharmaceutical and Personal Care Products in Water, Soil, Sediments and Biosolids by HPLC/MS/MS” [21] for clarithromycin erythromycin, carbamazepine, metformin, ibuprofen and naproxen. For drugs estradiol, ethinyl estradiol and diclofenac, classified as priority substances in the field of water

policy [22], the comparison made use of the ISPRA 260/2017 report "First monitoring of substances of the watch list (Watch list) which contains information about the analytical instrumentation and to the minimum sensitivity of the method of analysis defined with respect to the potential effect in surface water" [112]. Finally, further comparisons were made with the data reported in literature for the drugs acetylsalicylic acid, omeprazole and amoxicillin, which are not mentioned nor in the EPA method 1694 or in the Watch list.

4.4.1 Linear range

Work range is defined as the concentration range of the analyte, in which the method is applicable [113]. According to the EURACHEM guide, it was evaluated by analysing ten different calibration standard solutions of drug in methanol in the range of concentration of 0.001-200 µg/L for amoxicillin, metformin, omeprazole carbamazepine, erythromycin and clarithromycin and in the range of 5-5000 µg/L for acetylsalicylic acid, naproxen, diclofenac, ibuprofen, estradiol and ethinylestradiol. The relationship between the response of the instrument and the concentration should preferably be linear to be acceptable. Linearity is confirmed by statistical tests, or the t-test for the correlation coefficient [97] and the Fisher test [98] since it is known that R^2 coefficient is not an exhaustive parameter to indicate the linearity of the calibration line [114]. After evaluating the work range for each analyte, the calibration curves were built analyzing six different standard calibration solutions ($k = 6$) of drugs in triplicate ($n = 3$) in the linear range of each compound and using the linear least squares regression method. Each point of the calibration curve is given by the value of the area below the chromatographic peak.

Linearity parameters, obtained by analyzing six concentration levels in linear intervals 2 - 200 µg/L for amoxicillin (m/z 398.0 > 381.0); 5 - 200 µg/L for metformin (m/z l30.0 > 60.0); 0.001 - 20 µg/L for omeprazole (m/z 346.l > l98.0); 0.005 - 200 µg/L for carbamazepine (m/z 237.0 > l94.0); 0.005 - 200 µg/L for the erythromycin (m/z 734.4 > 576.4); 0.005 - 50 µg/L for the clarithromycin (m/z 748.4 > 590.4), are shown in table 4.3 together with the parameters of regression and the values of test F.

Drug	Range (µg/L)	R^2	Equation of the calibration line	t_{calc}	F_{calc}
Amoxicillin	2-2000	0.999	$(9.59\pm0.04)*10^2+(11.69\pm0.45)*10^3$	235.7	0.001
Metformin	5-200	0.993	$(14.97\pm0.63)*10^3+(24.34\pm7.06)*10^4$	23.76	3.257
Omeprazole	0.001-20	0.999	$(10.72\pm0.09)*10^3+(0.62\pm0.76)*10^3$	119.23	0.017
Carbamazepine	0.005-200	0.998	$(19.20\pm0.3)*10^2+(11.40\pm4.17)*10^5$	51.51	0.979
Erythromycin	0.005-20	0.999	$(30.14\pm0.49)*10^2+(11.97\pm0.42)*10^2$	61.26	0.061
Clarithromycin	0.005-50	0.999	$(42.13\pm0.61)*10^2+(73.93\pm13.55)*10^2$	68.67	2.856

Table 4.3: Linear range, regression parameters and value of test F for drugs analyzed by positive ionization mode

Analyzing the values of the t test and the F test for each drug and comparing them with the values of reference, for the test t, $t_{0.05,2} = 2.78$, k = 6; while for the test F, $F_{0.05,4,12} = 3.259$, I = 6, J = 3, is possible to confirm a linear correlation. As shown in table 4.4, the values of the linear range were compared with those reported in the EPA method [21], in the Watch List [112] and in literature [24,115]

Drug	**Range (µg/L)**	**EPA range (µg/L)**	**Watch List range (µg/L)**	**Literature range (µg/L)**
Amoxicillin	0.001-20	-	-	0.001-300 [57,58]
Metformin	0.005-200	1.25-250 [27]	-	-
Omeprazole	5-200	25-500 [27]	-	-
Carbamazepine	0.005-50	1.25-250 [27]	0.01-1 [29]	-
Erythromycin	0.005-20	0.25-50 [27]	0.01-1 [29]	-
Clarithromycin	2-200	-	-	0.010-200[55,56]

Table 4.4: Comparison between linear range with EPA range, Watch List range and literature.

It can be seen how the linear range of omeprazole, carbamazepine, erythromycin and clarithromycin were more extensive than those taken as a reference. This allow us to evaluate different levels of contamination with the same calibration curve. It is also possible to see that the first calibration point is less than or equal to the reference one, causing that

the method developed can be used for trace measurements. For the amoxicillin, instead, the RPLC-ESI method - (+) - SRM does not allow the determination of trace concentrations. Finally, for metformin, the range is narrower than that defined in the method EPA, but allows the evaluation of lower concentrations.

Linearity parameters, obtained by analyzing six concentration levels in linear range: 5 - 5000 µg/L for acetylsalicylic acid (m/z l79.0 > l37.0); 5 - 5000 µg/L for naproxen (m/z 229.0 > l85.0); 5 - 5000 µg/L for diclofenac (m/z 294.l > 250.0); 5 - 1000 µg/L for ibuprofen (m/z 205.0 > 16l.0); 5 - 5000 µg/L for estradiol (m/z 27l.l > 253.0); 20 - 5000 µg/L for ethinylestradiol (m/z 295.1 > 267.0), are shown in table 4.5 together with the parameters of regression and the values of the t test and the F test.

Drug	Range (µg/L)	R^2	Equation of the calibration line	t_{calc}	F_{calc}
Acetylsalicylic acid	5-5000	0.999	$(2.38\pm0.02)*10^2+(17.96\pm5.25)*10^3$	95.02	0.165
Naproxen	5-5000	0.999	$(0.40\pm0.03)*10^1+(6.89\pm0.69)*10^3$	125.08	2.226
Diclofenac	5-5000	0.999	$(11.20\pm0.05)*10^1-(0.79\pm1.04)*10^3$	224.31	0.261
Ibuprofen	5-1000	0.999	$(2.27\pm0.01)*10^2+(3.99\pm0.68)*10^3$	138.31	1.325
Estradiol	5-5000	0.999	$(1.26\pm0.02)*10^1+(0.89\pm0.33)*10^3$	79.62	2.410
Ethinylestradiol	20-5000	0.999	$(1.71\pm0.02)*10^1+(5.40\pm3.25)*10^2$	109.61	0.249

Table 4.5: Linear range, regression parameters and value of test F for drugs analyzed by negative ionization mode.

Analyzing the values of the t test and the F test for each drug and comparing them with the reference values, for the t test, $t_{0.05,2} = 2.78$, k = 6; while for the test F, $F_{0.05,4,12} = 3.259$, I = 6, J = 3, it is possible to observe that there is a linear correlation in the intervals explored.

Also in this case, values of the linear range were compared with those indicated in EPA method [21], with the data reported in the Watch List [112] and in the literature [22], table 4.6.

Drug	**Range (µg/L)**	**EPA range (µg/L)**	**Watch List range (µg/L)**	**Literature range (µg/L)**
Acetylsalicylic acid	5-5000	-	-	0.1-2 [56]
Naproxen	5-5000	2.5-500[27]	-	-
Diclofenac	5-5000	-	0.0005-5 [29]	-
Ibuprofen	5-1000	12.5-2500 [27]	-	-
Estradiol	5-5000	-	0.00007-0.00224 [29]	-
Ethinylestradiol	20-5000	-	0.00003-0.00112 [29]	-

Table 4.6: Comparison between linear range with EPA range, Watch List range and literature.

From table 4.6, it can be seen how the linear range determined for acetylsalicylic acid, naproxen, diclofenac, estradiol and ethinylestradiol cover higher concentrations than those defined by reference values, which indicates the inadequacy of the method in being able to determine the drugs in trace concentrations. As for ibuprofen, the determined range

of work allows to measure lower concentration levels than those defined by the EPA reference method.

4.4.2 Precision

Accuracy is the goodness of the agreement between the results of subsequent measurements of the same measuring, or the measure of the mutual proximity of the measures within a set of measurements on the same sample [113]. We deal with repeatability when the measurements replicates are conducted by a single analyst on the same material and using the same method in a very short period of time. We speak of intermediate repeatability when the repeated measurements are carried out in the same laboratory but under varying conditions. Repeatability and intermediate repeatability were expressed as a relative standard deviation percentage, RDS%, a parameter easily comparable with literature values [116].

Table 4.7 shows the accuracy values for drugs amoxicillin, erythromycin, clarithromycin, metformin, omeprazole and carbamazepine at three different concentration levels within the corresponding linear range.

Drugs	Concentration (µg/L)	Repeatability (%RSD)[a]-r	Intermediate repeatability (%RSD)[b]-r
Omeprazole	0.001	7.19-0.006	10.23-0.007
	2	2.29-0.009	9.89-0.17
	20	10.57-2.84	14.56-6.77
Carbamazepine	0.005	9.58-0.14	14.47-0.32
	100	1.53-3.80	4.22-4.53
	200	3.26-3.91	5.39-7.60
Metformin	5	2.05-0.87	10.68-2.67
	100	1.92-8.63	4.81-19.36
	200	0.98-7.21	2.66-13.01
Clarithromycin	0.005	6.99-0.12	15.66-0.26
	20	2.57-2.14	11.46-5.50
	50	3.38-6.23	10.63-15.27
Erythromycin	0.005	0.99-0.008	5.86-0.043
	2	2.66-0.07	5.27-0.15
	20	6.80-4.96	11.10-5.38
Amoxicillin	2	11.91-2.23	14.85-3.65
	100	10.39-3.40	13.22-3.96
	200	5.69-12.44	14.79-15.63

[a] n = 6; $t_{0.05,5} = 2.57$

[b] n = 10; $t_{0.05,9} = 2.26$

Table 4.7: Repeatability, intermediate repeatability, repeatability limit and intermediate repeatability for three concentration levels chosen for each calibration line.

It is possible to observe, from table 4.7, how relative percentages of standard deviations are all less than 30% which represents the reference value [21].

Table 4.8 shows the accuracy values for the drugs acetylsalicylic acid, ibuprofen, diclofenac, estradiol, ethinyl estradiol and naproxen at three different concentration levels within the corresponding linear range.

Drugs	Concentration (µg/L)	Repeatability (%RSD)[a]-r	Intermediate repeatability (%RSD)[b]-r
Acetylsalicylic acid	5 1000 5000	7.71-4.50 6.26-92.20 6.93-352.79	10.86-7.65 7.96-137.17 9.15-944.48
Naproxen	5 500 5000	9.58-1.10 1.53-75.04 3.26-9.24	14.47-2.63 4.22-86.38 5.39-358.01
Diclofenac	5 1000 5000	4.65-1.17 1.91-23.09 1.60-102.47	10.35-2.46 6.73-62.04 4.78-204.85
Ibuprofen	5 100 1000	4.75-0.95 3.86-7.66 1.88-69.77	10.24-1.02 7.08-12.87 3.33-84.67
Estradiol	5 1000 5000	2.93-2.24 2.01-83.85 4.39-546.59	11.17-2.68 7.51-133.80 9.17-593.61
Ethinylestradiol	20 1000 5000	2.38-3.01 1.97-7.39 1.85-22.77	5.07-3.18 11.40-61.29 11.31-249.93

[a] n = 6; $t_{0.05,5} = 2.57$

[b] n = 10; $t_{0.05,9} = 2.26$

Table 4.8: Repeatability, intermediate repeatability, repeatability limit and intermediate repeatability for three concentration levels chosen for each calibration line.

4.4.3 Limit of quantification (LOQ) and limit of detection (LOD)

Limit of detection (LOD) is defined as the minimum concentration detectable by the method, at a specified trust level, which produces a significantly different signal from the white. This is expressed as the concentration corresponding to a specified ratio signal/noise, typically 3: 1 [99]. The limit of quantification (LOQ) instead, is defined as the lower level of analyte that can be determined with acceptable performance. Often a signal-to-noise ratio of 10: 1 is used to determine LOQ [99].

LOD and LOQ values calculated for the drugs amoxicillin, erythromycin, clarithromycin, metformin, omeprazole and

carbamazepine, are included in the ranges 0.0001-0.5114 µg/L and 0.0004-1.6955 µg/L, respectively, table 4.9, and are compared to the reference values reported in the EPA method [21], in the Watch List [112] and in the literature [23-25,115,117].

			EPA method	**Watch list**	**Literature**
Drugs	**LOD (µg/L)**	**LOQ (µg/L)**	**LOD (µg/L)**	**LOD (µg/L)**	**LOD (µg/L)**
Omeprazole	0.0001	0.0004	-	-	0.001-0.002 [58,61]
Carbamazepine	0.0006	0.0019	0.005 [27]	-	-
Metformin	0.5114	1.6955	0.0001 [27]	-	-
Clarithromycin	0.0026	0.0089	0.005 [27]	0.090 [29]	-
Erythromycin	0.0007	0.0024	0.001 [27]	0.090 [29]	-
Amoxicillin	0.3526	1.1960	-	-	0.009-0.063 [55-57]

Table 4.9: LOD and LOQ obtained with the RPLC-ESI - (+) - SRM method, validated in this work, for the determination of omeprazole, carbamazepine, metformin, clarithromycin, erythromycin and amoxicillin and LoD values reported in the EPA method, in the Watch List and in literature.

LOD values of carbamazepine, clarithromycin and erythromycin are lower than those reported in the EPA method; this allows the detection of extremely low analyte concentrations. The same can be said for

omeprazole, whose comparison was made with literature data. Metformin LOD, on the other hand, is greater than that present in the EPA method, as well as the LOD value of amoxicillin compared to the data reported in the literature.

LOD and LOQ values calculated for the drugs acetylsalicylic acid, naproxen, diclofenac, ibuprofen, estradiol and ethinyl estradiol, are shown in table 4.10 and are compared to reference values reported in the EPA method [21], in the Watch List [112] and in literature [28].

			EPA method	**Watch list**	**Literature**
Drugs	**LOD (µg/L)**	**LOQ (µg/L)**	**LOD (µg/L)**	**LOD (µg/L)**	**LOD (µg/L)**
Acetylsalicylic acid	0.7211	2.4038	-	-	0.05 [56]
Naproxen,	0.6293	2.0978	0.0039 [27]	-	-
Diclofenac	0.1249	0.4164	-	0.01 [29]	-
Ibuprofen	0.3115	1.0383	0.006 [27]	-	-
Estradiol	0.2231	0.7438	-	0.0004 [29]	-
Ethinylestradiol	0.0751	0.2502	-	0.000035 [29]	-

Table 4.10: LOD and LOQ obtained with the RPLC-ESI - (+) - SRM method, validated in this work, for the determination of acetylsalicylic acid, naproxen, diclofenac, ibuprofen, estradiol and ethinyl estradiol and LoD values reported in the EPA method, in the Watch List and in literature.

From table 4.10, It can be seen that the detection limit values for all drugs are always higher with respect to the reference values, preventing the detection of trace concentration levels.

4.4.4 Recovery

To evaluate the recovery of drugs amoxicillin, erythromycin, omeprazole, clarithromycin, metformin and carbamazepine, the real samples were fortified at three different levels of concentration of the linear range: 5 µg/L, 10 µg/L and 20 µg/L. Furthermore, for omeprazole, erythromycin, carbamazepine and clarithromycin, two levels of concentration were evaluated additional: of 0.5 µg/L and 1 µg/L. The average recovery values obtained and the corresponding standard deviations, are shown in table 4.11, where it is also possible to observe the reference values of the EPA method [21], of the Watch List [112] and of literature [23,24,28,115,117].

Drugs	Spiked (µg/L)	$R_m \pm u(R_m)$ *t_{calc} *compare to $t_{tab0.5,9}$=2.26	R_m EPA method	R_m Watch list	R_m literature
Omeprazole	0.5 1 5 10 20	1.18±0.07 (t =1.36) 0.86±0.02 (t =1.63) 1.03±0.04 (t =0.37) 1.01±0.01 (t =1.37) 1.06±0.02 (t =0.33)	-	-	0.49-0.95 [58,61]
Carbamazepine	0.5 1 5 10 20	1.04±0.01 (t =0.60) 1.00±0.01 (t =0.04) 1.02±0.05 (t =0.65) 0.99±0.05 (t =0.03) 0.99±0.05 (t =0.39)	0.23-1.23 [27]	-	-
Metformin	5 10 20	1.01±0.09 (t =0.17) 0.89±0.01 (t =0.43) 0.96±0.01 (t =0.50)	0.55-1.34 [27]	-	-
Clarithromycin	0.5 1 5 10 20	1.16±0.01 (t =1.73) 0.45±0.27 (t =63.55) 1.10±0.02 (t =0.80) 1.29±0.15 (t =3.02) 1.12±0.04 (t =0.73)	0.08-1.39 [27]	-	-
Erythromycin	0.5 1 5 10 20	0.77±0.11 (t =2.63) 0.70±0.04 (t =1.25) 0.99±0.01 (t =0.03) 1.00±0.02 (t =0.04) 1.04±0.03 (t =0.29)	0.05-1.42 [27]	-	-
Amoxicillin	5 10 20	1.06±0.02 (t =1.38) 1.10±0.03 (t =0.90) 0.96±0.03 (t =1.07)	-	-	0.35-1.27 [55-57]

Table 4.11: Values of recovery, associated uncertainty and t_{calc} for amoxicillin drugs erythromycin, clarithromycin, carbamazepine, omeprazole and metformin and recovery values reported in EPA method, in the Watch List and in the literature.

Except for omeprazole, for which higher recovery values were calculated, the results obtained agree with the recovery values reported in the EPA method [21], in the Watch List [112] and in the literature [23,24,28,115,117].
The matrix effect was also evaluated with the following equation:

$$\%\ \text{effetto matrice} = \frac{m_{matrix}}{m_{MeOH}} 100$$

where m_{MeOH} is the slope of the calibration line obtained by analyzing the standard samples of the drugs in methanol, while m_{matrix} is the slope of the calibration line obtained by analyzing the same concentrations of the drugs in the real matrix. A value of 100%, when the straight lines obtained are parallel and overlapping, indicates the absence of matrix effect; while a value greater than 100% indicates an increase in the signal and a value less than 100% indicates a signal suppression.
Regarding the matrix effect for drugs amoxicillin, erythromycin, omeprazole, clarithromycin, metformin and carbamazepine values between 83% and 98% indicate a non-significant decrease in the signal.

To evaluate the recovery of drugs acetylsalicylic acid, ibuprofen, naproxen, diclofenac, estradiol and ethinyl estradiol, real samples of wastewater were fortified at three different levels of concentration within the linear range: 5 µg/L, 10 µg/L and 20 µg/L. The results obtained are reported in table 4.12 and compared with the reference values of the EPA method [21], of the Watch List [112] and literature [28].

Drugs	Spiked (µg/L)	$R_m \pm u(R_m)*t_{calc}$ *compare to $t_{tab0.5,9}=2.26$	R_m EPA method	R_m Watch list	R_m literature
Acetylsalicylic acid	5 10 20	1.05±0.05 (t =0.04) 1.12±0.02 (t =1.32) 0.96±0.09 (t =0.43)	-	-	0.66-0.95 [56]
Naproxen	5 10 20	1.03±0.02 (t =0.82) 0.97±0.01 (t =0.40) 1.01±0.06 (t =0.20)	0.55-1.08 [27]	-	-
Diclofenc	5 10 20	1.03±0.02 (t =0.64) 1.08±0.04 (t =3.41) 0.99±0.04 (t =4.93)	-	0.84 [29]	-
Ibuprofen	5 10 20	0.95±0.03 (t =0.72) 0.95±0.02 (t =0.06) 0.96±0.02 (t =1.92)	0.55-1.08 [27]	-	-
Estradiol	5 10 20	1.06±0.02 (t =0.27) 1.01±0.08 (t =0.29) 1.02±0.02 (t =1.19)	-	1.01 [29]	-
Ethinylestradiol	20	1.03±0.05 (t =0.63)	-	0.97 [29]	-

Table 4.12: Values of recovery, of the associated uncertainty and t_{calc} for the acetylsalicylic acid, ibuprofen, naproxen, diclofenac, estradiol and ethinylestradiol and recovery values reported in EPA method, in the Watch List and in literature.

From table 4.12, we can observe that recovery values of naproxen and ibuprofen are in line with the values reported in the EPA method [21]. The average recovery values obtained for acetylsalicylic acid, the diclofenac and ethinylestradiol, on the other hand, were superior to those reported in literature [28], which implies a better accuracy. As for estradiol, the values appear to be similar to the value reported in the Watch list [112]. Regarding the matrix effect, the calculated values are between 17% and 28%, indicative of significant signal decrease.

4.4.5 Measurement uncertainty

ISO 25 (International Organization for Standardization) [118] defines the measurement uncertainty as a parameter associated with the result of a measurement, which characterizes the dispersion of values that can reasonably be attributed to the measurand if all the error sources have been considered. An unfinished measure of his uncertainty cannot be compared either with other measures or with reference values or with legal or compositional limits. When estimating the uncertainty, all sources of significant uncertainty in a given situation must be taken into account, using appropriate analysis methods [101]. The sources that contribute to the measurement uncertainty include, in non-exhaustive way, reference samples and reference materials used, methods and equipment used, environmental conditions, condition of the objects to be tested or calibration and operator [101]. The method used to estimate uncertainty is the metrological approach (bottom-up) based on the evaluation of partial uncertainties related to all steps of an analytical procedure. This approach turns out to be the most rigorous, indeed, because it takes into account all possible sources of uncertainty [102]. According to the metrological approach the estimate of the uncertainty can be divided into the following passages [102]:

- identification of the measurement model;
- identification of the sources of uncertainty;
- evaluation and expression of the same as standard deviations, also called standard uncertainties, classified in category A (when they can be estimated as standard deviations of experimental results) and in category B (if they derive from information relating to the instruments or reference materials);

- calculation of the compound uncertainty (u_0) which is an estimated standard deviation as the positive square root of the total variance obtained by combining all the sources of uncertainty;
- calculation of the extended uncertainty (U), which provides an internal range where there is the true value of the measurement and it is obtained by multiplying the composed uncertainty for a coverage factor k whose choice depends on the level of trust considered.

Before proceeding to estimate the measurement uncertainty by metrological approach, we have to consider the entire analytical process, in order to identify all the possible sources of uncertainty.

Therefore, the main contributions are:

- the preparatory phase;
- calibration;
- limit of detection;
- recovery;

- Calculation of uncertainty due to sample preparation

Standard solution 1000 mg/L was prepared for each drug. From this the other solutions were obtained by dilution. The uncertainty due to the preparation of sample, therefore, must take into account the error made on the parent solution, which includes errors on weighing and volume and the error due to subsequent dilutions. The error on class A glassware used must be divided by $\sqrt{6}$ because we assume a triangular distribution [113]. Therefore, considering all the contributions, the uncertainty was calculated as follows:

$$\frac{u_{preparation}}{C_0} = \sqrt{(u_{rel})^2_{weight} + \sum (u_{rel})^2_{volume} + \sum (u_{rel})^2_{pipette}}$$

The uncertainty due to the sample preparation, at three different concentration levels with each linear range is shown in table 4.13 for amoxicillin drugs, erythromycin, clarithromycin, metformin, omeprazole, and carbamazepine, and in table 4.14 for drugs acetylsalicylic acid, naproxen, diclofenac, ibuprofen, estradiol and ethinyl estradiol.

Drugs	C_0 (µg/L)	u (preparative)
Omeprazole	0.001	0.00003
	2	0.04554
	20	0.43932
Carbamazepine	0.005	0.00014
	100	2.21705
	200	28.0196
Metformin	5	0.11002
	100	2.20046
	200	28.0144
Clarithromycin	0.005	0.00016
	20	0.43932
	50	1.09829
Erythromycin	0.005	0.00016
	2	0.44254
	20	0.04585
Amoxicillin	2	0.04577
	100	2.20853
	200	28.0169

Table 4.13: Values of uncertainties related to the preparation of standard solutions at the three levels of concentration.

Drugs	C_0 (µg/L)	u (preparative)
Acetylsalicylic acid	5	0.08358
	1000	0.01801
	5000	0.16609
Naproxen	5	0.08359
	500	0.01989
	5000	0.16072
Diclofenac	5	0.08350
	1000	0.01778
	5000	0.16067
Ibuprofen	5	0.08357
	100	0.08260
	1000	0.01810
Estradiol	5	0.08358
	1000	0.01815
	5000	0.16071
Ethinylestradiol	20	0.02281
	1000	0.01801
	5000	0.16070

Table 4.14: Values of uncertainties related to the preparation of standard solutions at the three levels of concentration.

- Calculation of the uncertainty due to calibration

The uncertainty associated with the calibration line is considered taking into account the associated uncertainties of the use of the linear least squares regression method; this method assumes that uncertainties of the abscissa values are considerably smaller than the uncertainties on the ordinate values, therefore uncertainties does not depend on the uncertainties of the calibration materials, neither from successive dilutions of the same starting solution because these contributions result be negligible. The relationship necessary to calculate the uncertainty on the calibration line is the following:

$$u(\text{calibration}) = \frac{Sy/_x}{m}\sqrt{\frac{1}{M}+\frac{1}{N}+\frac{\left(\overline{y_{C_0}}-\bar{y}\right)^2}{m^2\sum(x_i-\bar{x})^2}}$$

Where M is the number of replicas, 3 in our case; N is the number of calibration points, therefore 6; m is the slope of the calibration line; y_{c0} is the mean value of the M measurements for the standard at the chosen concentration level; y is the mean value of y values of the N points of calibration while $s_{y/x}$ is given by the following relation:

$$s_{y/x} = \sqrt{\frac{\sum_{i=1}^{n}(y_i - \hat{y}_i)^2}{n-2}}$$

where y_i is the value of y found experimentally and $\hat{y}_i$ is the value of y calculated from the line of calibration.

The values of the uncertainty due to calibration, at three different levels of concentration, are reported in table 4.15 for the drugs amoxicillin, erythromycin, clarithromycin, metformin, omeprazole, and carbamazepine, and in table 4.16 for the drugs acetylsalicylic acid, naproxen, diclofenac, ibuprofen, estradiol and ethinyl estradiol.

Drugs	C_0 (µg/L)	u (calibration)
Omeprazole	0.001	0.00111
	2	0.01063
	20	0.01661
Carbamazepine	0.005	0.02991
	100	0.25265
	200	0.34227
Metformin	5	0.64145
	100	0.51627
	200	0.68601
Clarithromycin	0.005	0.00494
	20	0.04200
	50	0.06349
Erythromycin	0.005	0.00215
	2	0.02055
	20	0.03239
Amoxicillin	2	0.06442
	100	0.05423
	200	0.07280

Table 4.15: Values of uncertainties related to calibration at the three levels of concentration for omeprazole, carbamazepine, metformin, clarithromycin, erythromycin, amoxicillin.

Drugs	C_0 (µg/L)	u (calibration)
Acetylsalicylic acid	5	0.34288
	1000	0.32416
	5000	0.52339
Naproxen	5	0.26393
	500	0.25410
	5000	0.04103
Diclofenac	5	0.14728
	1000	0.14040
	5000	0.22670
Ibuprofen	5	0.04729
	100	0.04576
	1000	0.07352
Estradiol	5	0.41470
	1000	0.38905
	5000	0.62546
Ethinylestradiol	20	0.29785
	1000	0.28006
	5000	0.45104

Table 4.16: Values of uncertainties related to calibration at the three levels of concentration for acetylsalicylic acid, naproxen, diclofenac, ibuprofen, estradiol and ethinyl estradiol.

- Calculation of uncertainty due to recovery

The calculation of the uncertainty associated with the recovery was discussed in section 4.4.4, tables 4.11 and 4.12.

- Calculation of the uncertainty due to the limit of detection

The uncertainty associated with the LOD was calculated for each drug as the ratio of the standard deviation and the square root of the number of replicates. In table 4.17 and table 4.18 are reported the values of the uncertainty due to the limit of detection for all drugs, object of study.

Drugs	LOD (µg/L)	u(LOD) (µg/L)
Omeprazole	0.00012	0.00002
Carbamazepine	0.00058	0.00006
Metformin	0.51144	0.06393
Clarithromycin	0.00267	0.00001
Erythromycin	0.00072	0.00005
Amoxicillin	0.35261	0.02012

Table 4.17: Uncertainty values (in µg/L) due to the detection limit for amoxicillin drugs, erythromycin, clarithromycin, metformin, omeprazole, and carbamazepine.

Drugs	LOD (µg/L)	u(LOD) (µg/L)
Acetylsalicylic acid	0.72115	0.02509
Naproxen	0.62934	0.05030
Diclofenac	0.12491	0.01030
Ibuprofen	0.31148	0.05030
Estradiol	0.22314	0.05030
Ethinylestradiol	0.07507	0.00201

Table 4.18: Uncertainty values (in µg/L) due to the detection limit for acetylsalicylic acid, naproxen, diclofenac, ibuprofen, estradiol and ethinyl estradiol.

- Calculation of compound uncertainty

The compound type uncertainty was estimated as the positive square root of the total variance, obtained by combining all the components of the uncertainty, in accordance with the following equation:

$$\frac{u_0}{C_0} = \sqrt{\left(\frac{u_{preparative}}{C_0}\right)^2 + \left(\frac{u_{calibration}}{C_0}\right)^2 + \left(\frac{u_{Rm}}{R_m}\right)^2 + \left(\frac{u_{LOD}}{LOD}\right)^2}$$

Values of compound uncertainty are shown in table 4.19 for amoxicillin drugs, erythromycin, clarithromycin, metformin, omeprazole, and carbamazepine, and in table 4.20 for drugs acetylsalicylic acid, naproxen, diclofenac, ibuprofen, estradiol and ethinyl estradiol.

Drugs	C_0 (µg/L)	u (preparative) (µg/L)	u (calibration) (µg/L)	u (recovery) (µg/L)*	U (LOD) (µg/L)	u_0 (µg/L)
Omeprazole	0.001	0.00003	0.00111	0.07263	0.00002	0.001
	2	0.04554	0.01063	0.01787	0.00002	0.338
	20	0.43932	0.01661	0.00232	0.00002	3.401
Carbamazepine	0.005	0.00014	0.02991	0.00963	0.00006	0.003
	100	2.21705	0.25265	0.00005	0.00006	10.582
	200	28.0196	0.34227	0.00005	0.00006	34.831
Metformin	5	0.11002	0.64145	0.00096	0.06393	0.931
	100	2.20046	0.51627	0.00017	0.06393	12.828
	200	28.0144	0.68601	0.00017	0.06393	37.553
Clarithromycin	0.005	0.00016	0.00494	0.01482	0.00001	0.004
	20	0.43932	0.04200	0.00048	0.00001	0.447
	50	1.09829	0.06349	0.00048	0.00001	1.116
Erythromycin	0.005	0.00016	0.00215	0.11608	0.00005	0.002
	2	0.44254	0.02055	0.04377	0.00005	0.193
	20	0.04585	0.03239	0.00037	0.00005	1.458
Amoxicillin	2	0.04577	0.06442	0.00208	0.02012	0.139
	100	2.20853	0.05423	0.00034	0.02012	6.315
	200	28.0169	0.07280	0.00034	0.02012	30.251

*u(recovery) value for 0.001 µg/L e 0.005 µg/L are referred to spike 0.5 µg/L; for 2 µg/L are referred to spike 1 µg/L; for 100 µg/L and 200 are referred to spike 20 µg/L.

Table 4.19: Values of compound uncertainty for amoxicillin, erythromycin, clarithromycin, metformin, omeprazole, and carbamazepine.

Drugs	C_0 (µg/L)	u (preparative) (µg/L)	u (calibration) (µg/L)	u (recovery) (µg/L)*	U (LOD) (µg/L)	u_0 (µg/L)
Acetylsalicylic acid	5	0.08358	0.34288	0.00564	0.02509	1.056
	1000	0.01801	0.32416	0.00090	0.02509	42.190
	5000	0.16609	0.52339	0.00090	0.02509	434.763
Naproxen	5	0.08359	0.26393	0.00214	0.05030	0.635
	500	0.01989	0.25410	0.00060	0.05030	41.919
	5000	0.16072	0.04103	0.00060	0.05030	470.514
Diclofenac	5	0.08350	0.14728	0.00232	0.01030	0.605
	1000	0.01778	0.14040	0.00391	0.01030	85.795
	5000	0.16067	0.22670	0.00391	0.01030	903.188
Ibuprofen	5	0.08357	0.04729	0.00308	0.05030	0.910
	100	0.08260	0.04576	0.00026	0.05030	18.206
	1000	0.01810	0.07352	0.00026	0.05030	162.499
Estradiol	5	0.08358	0.41470	0.01194	0.05030	1.687
	1000	0.01815	0.38905	0.00085	0.05030	44.997
	5000	0.16071	0.62546	0.00085	0.05030	234.568
Ethinylestradiol	20	0.02281	0.29785	0.00053	0.00201	1.780
	1000	0.01801	0.28006	0.00053	0.00201	35.866
	5000	0.16070	0.45104	0.00053	0.00201	841.195

*u(recovery) value for 100 µg/L, 500 µg/L, 1000 µg/L and 5000 µg/L are referred to spike 20 µg/L.

Table 4.20: Values of compound uncertainty for acetylsalicylic acid, naproxen, diclofenac, ibuprofen, estradiol and ethinyl estradiol.

- Calculation of the extended uncertainty

The definition of UNI ENV 13005 shows that extended uncertainty is a quantity that defines, around the result of a measurement, a range that contain a significant fraction of the distribution of values reasonably attributable to the measurand. In practical terms, to increase the statistical significance of the range defined by the compound uncertainty, the latter is multiplied by a factor, called coverage factor [120]. The coverage factor k is 1.98 for a 95% confidence level.

$$U = k * u_0$$

Below are the tables 4.21 and 4.22 with all the values of the extended uncertainty for drugs studied in this work.

Drugs	C_0 (µg/L)	u_0(µg/L)	k	U(µg/L)
Omeprazole	0.001	0.001	1.98	0.0022
	2	0.338	1.98	0.67
	20	3.401	1.98	6.7
Carbamazepine	0.005	0.003	1.98	0.0060
	100	10.582	1.98	20
	200	34.831	1.98	69
Metformin	5	0.931	1.98	1.8
	100	12.828	1.98	24
	200	37.553	1.98	74
Clarithromycin	0.005	0.004	1.98	0.0097
	20	0.447	1.98	0.89
	50	1.116	1.98	2.2
Erythromycin	0.005	0.002	1.98	0.0045
	2	0.193	1.98	0.38
	20	1.458	1.98	2.9
Amoxicillin	2	0.139	1.98	0.27
	100	6.315	1.98	13
	200	30.251	1.98	60

Table 4.21: Values of extended uncertainty for amoxicillin, erythromycin, clarithromycin, metformin, omeprazole, and carbamazepine.

Drugs	C_0 (µg/L)	u_0 (µg/L)	k	U(µg/L)
Acetylsalicylic acid	5	1.056	1.98	1.1
	1000	42.190	1.98	83
	5000	434.763	1.98	$86 \cdot 10^1$
Naproxen	5	0.635	1.98	1.2
	500	41.919	1.98	83
	5000	470.514	1.98	$93 \cdot 10^1$
Diclofenac	5	0.605	1.98	1.2
	1000	85.795	1.98	$17 \cdot 10^1$
	5000	903.188	1.98	$18 \cdot 10^2$
Ibuprofen	5	0.910	1.98	1.8
	100	18.206	1.98	36
	1000	162.499	1.98	$32 \cdot 10^1$
Estradiol	5	1.687	1.98	3.3
	1000	44.997	1.98	82
	5000	234.568	1.98	$46 \cdot 10^1$
Ethinylestradiol	20	1.780	1.98	3.5
	1000	35.866	1.98	7.1
	5000	841.195	1.98	$16 \cdot 10^2$

Table 4.22: Values of extended uncertainty for acetylsalicylic acid, naproxen, diclofenac, ibuprofen, estradiol and ethinyl estradiol.

4.5 Application to wastewater samples

After validation, the RPLC-ESI-LTQ-MS/MS method for the determination of 12 drugs was used for their determination in samples of wastewaters. Water samples analyzed come from the main purification plant in Basilicata, located in Potenza village. Sampling was performed by taking a sample of water before the grilling process and a sample of water at the end of the purification treatment.

Table 4.23 shows the results obtained from the RPLC-ESI-LTQ MS/MS analysis of water samples, before and after purification treatment, analyzed in triplicate.

Drugs	Before treatment C ± U (µg/L)	After treatment C ± U (µg/L)
Amoxicillin	2.1 ± 0.3	1.5 ± 0.3
Metformin	< LOD	< LOD
Omeprazole	0.008 ± 0.002	0.002 ± 0.002
Carbamazepine	4.986 ± 0.006	4.420 ± 0.006
Erythromycin	< LOD	< LOD
Clarithromycin	0.009 ± 0.009	0.009 ± 0.009
Acetylsalicylic acid	< LOD	< LOD
Naproxen	< LOD	< LOD
Diclofenac	7 ± 1	7 ± 1
Ibuprofen	< LOD	< LOD
Estradiol	< LOD	< LOD
Ethinylestradiol	< LOD	< LOD

Table 4.23: Drugs concentration in wastewater analyzed.

For wastewater before purification treatment the drugs analyzed were found in concentrations included in the range: 0.008-7.160 µg/L. The compound found in larger quantities are diclofenac (7 ± 1 µg/L), followed by carbamazepine (4.986 ± 0.006 µg/L), amoxicillin (2.1 ± 0.3 µg/L), clarithromycin (0.009 ± 0.009 µg/L), omeprazole (0.008 ± 0.002 µg/L); the rest of the drugs have lower concentration levels than LOD (< LOD). Drug concentration, after purification treatment was not practically different from their concentration before purification treatment. Again, diclofenac was found to be the compound present in greater quantity (7 ± 1 µg/L) followed by carbamazepine (4.986 ± 0.006 µg/L), amoxicillin (2.1 ± 0.3 µg/L) clarithromycin (0.009 ± 0.009 µg/L), omeprazole (0.008 ± 0.002 µg/L) and all others at concentration levels <

LOD. Although several studies have examined the levels of pharmaceutical products in wastewaters [16,28,120,121], it is known that such contaminants actually depend on several factors, including size system, operating conditions and daily water flow, as well as the number of habitants served and local consumption of drugs; therefore, a comparison with the literature results difficult. However, the results of this study are consistent with those of many works present in the literature, in which low concentrations of products were found in municipal waste waters [28,120,121]. Furthermore, the results obtained show how the concentration of various drugs before and after purification treatment is similar; this indicates, as already supported by other scientific values, that the traditional water treatment processes are ineffective in completely removing these compounds [121]. As a result, wastewater is a way of access of drugs in aquatic environment, thus contributing to environmental pollution by drugs, with a real risk to human health and to all plant and animal organisms.

4.6 Ecotoxicological test: first generation

After 28 days exposure survival of *T. fulvus* exposed to farmaceuticals compounds and their mixture in F0 generation was always above 95% in all treatments with not significant differences compared with the control. The developmental time from nauplii to copepodite was around 5 days in the control and in all treatments (ANOVA, $p>0.05$).

The mean time for adult female to became ovigerous did not differ among carbamazepine, amoxicillin and control (around 10d), whereas differed among mixture, where about one day delay was observed, in all treatments ($p <0.05$). Data obtained and statistical analysis were reported in table 4.24, table 4.25 and figure 4.29.

Sample	Maturity (days)
CTR	10.1 ± 0.5
AMOX	10 ± 1
CBZ	9.8 ± 0.7
MIX	11.7 ± 0.7

Table 4.24: Appearance day of ovigerous females.

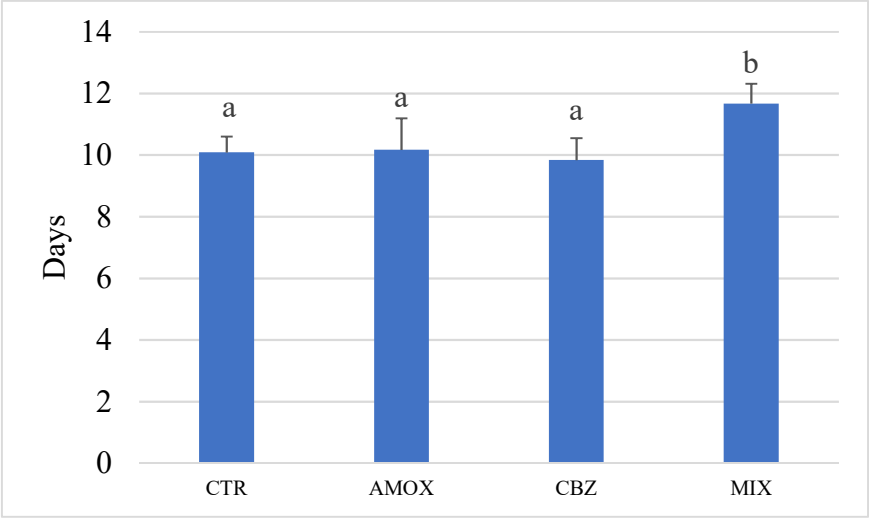

Figure 4.29: Appearance day of ovigerous females in treatment groups. Same letter indicate that the means are not statistically different (p>0.05).

Variation origin	SQ	gdl	MQ	F	p-value	F crit
Inter groups	24.89583	3	8.298611	14.6544	9.35091E-07	2.816466
Intra groups	24.91667	44	0.566288			
Total	49.8125	47				

Table 4.25: Statistical analysis and p-value obtained on appearance day of ovigerous female.

The cumulative sum of total nauplii produced by all tested females (n=12) at the end of experiment was lower in the samples containing the drugs compared with the control, as figure 4.30 clearly shows, ranging from 1413 in the control to 985 in the binary mixture.

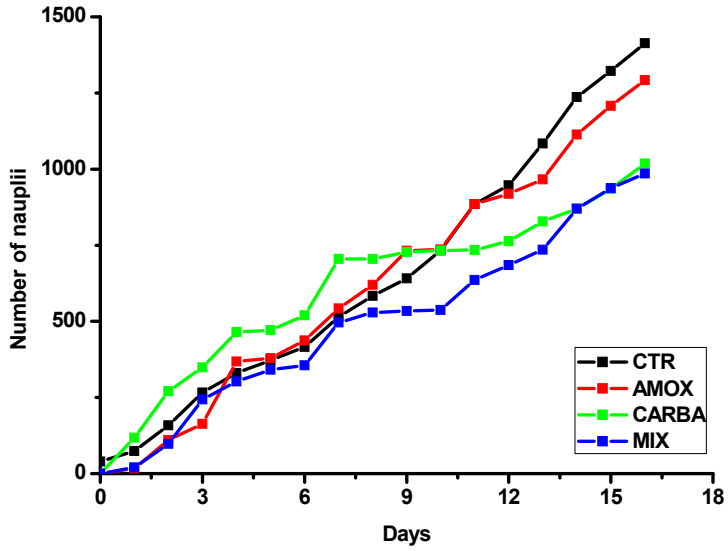

Figure 4.30: Cumulative sum of nauplii produced by females (n=12).

Although fecundity (mean total number of nauplii per female) on day 28, was reduced in all treatments, table 4.26 and figure 4.31, from the statistical analysis reported in table 4.27 it is observed that the differences were not significant ($p > 0.05$).

Sample	Mean total number of nauplii/female
CTR	144 ± 27
AMOX	114 ± 32
CBZ	92 ± 28
MIX	102 ± 25

Table 4.26: Mean total number of nauplii per female during 28 days.

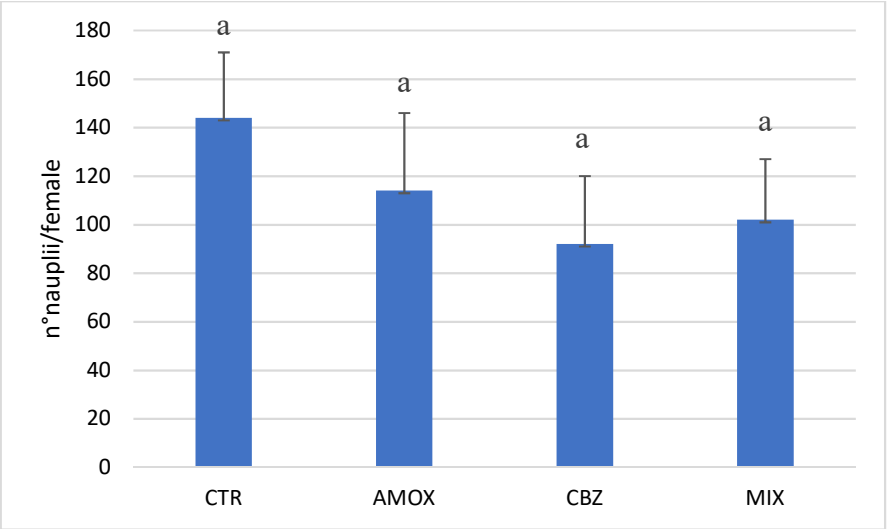

Figure 4.31: Mean total number of nauplii per female on day 28.
Same letter indicate that the means are not statistically different (p>0.05).

Variation origin	SQ	gdl	MQ	F	p-Value	F crit
Inter groups	10922.17	3	3640.722	1.909284	0.141995172	2.816466
Intra groups	83901.5	44	1906.852			
Total	94823.67	47				

Table 4.27: Statistical analysis and p-value obtained on mean total number of nauplii for female.

Data regarding the mean number of nauplii per brood obtained for each group are shown in table 4.28 and represented graphically in figure 4.32. No significant effect of drugs ($p > 0.05$) was observed, table 4.29.

Sample	Mean number of nauplii/brood
CTR	20 ± 3
AMOX	17 ± 4
CBZ	18 ± 6
MIX	18 ± 5

Table 4.28: Mean number of nauplii per brood in each treatment.

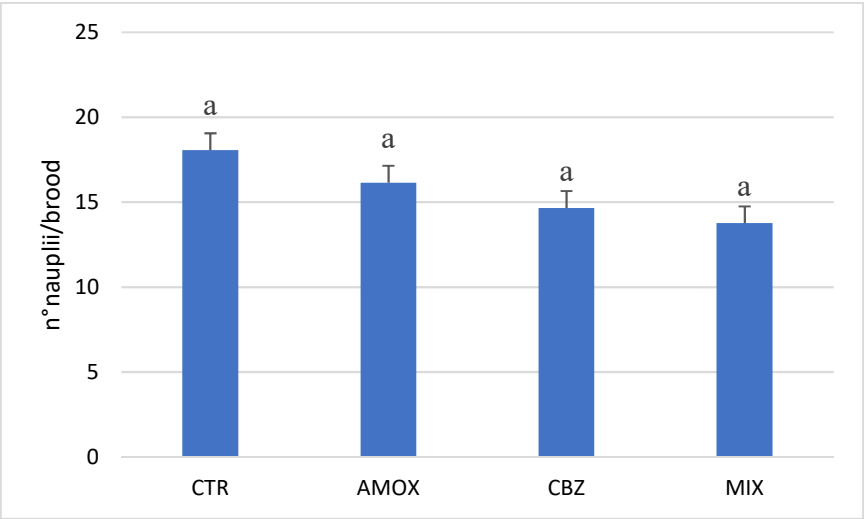

Figure 4.32: Mean number of nauplii produced per brood.
Same letter indicate that the means are not statistically different ($p > 0.05$).

Variation origin	SQ	gdl	MQ	F	p-Value	F crit
Inter groups	127.062	3	42.35401	0.982306	0.409799652	2.816466
Intra groups	1897.144	44	43.11692			
Total	2024.206	47				

Table 4.29: Statistical analysis and p-value obtained on mean number of nauplii per brood.

The mean number of brood per female obtained for each group are shown in table 4.30 and represented graphically in figure 4.33.

Carbamazepine showed significant few broods than the control and the amoxicillin treatment ($p<0.05$) while no significant differences were observed between carbamazepine and binary mixture treatment ($p>0.05$), table 4.31.

Sample	N° broods per female
CTR	6.4 ± 0.7
AMOX	6.7 ± 0.7
CARBA	5.8 ± 0.6
MIX	6.0 ± 0.9

Table 4.30: Number of broods for female.

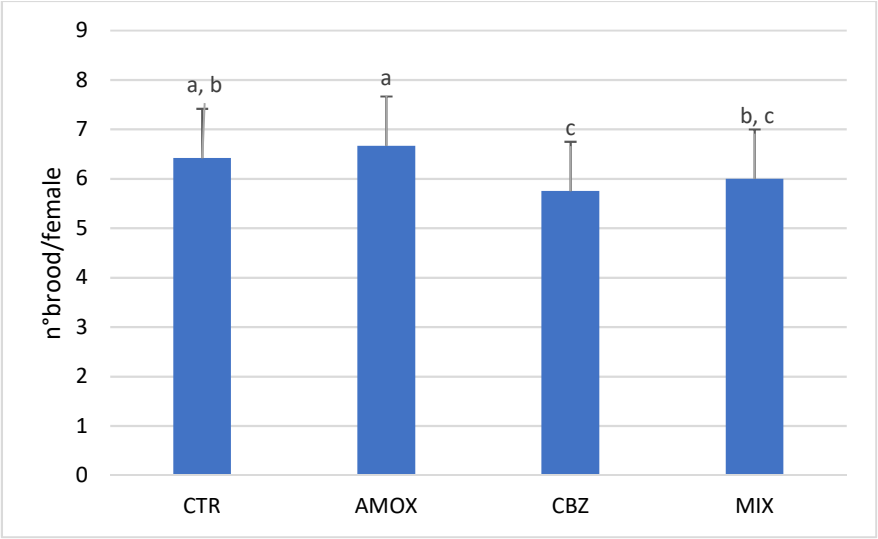

Figure 4.33: Number of broods for female.
Same letter indicate that the means are not statistically different (p>0.05).

Variation origin	SQ	gdl	MQ	F	p-Value	F crit
Inter groups	6.083333	3	2.027778	3.74359	0.017629655	2.816466
Intra groups	23.83333	44	0.541667			
Total	29.91667	47				

Table 4.31: Statistical analysis and p-value obtained on number of broods for female.

Data obtained for hatching time (time required for the offspring release) are reported in table 4.32. The graphical representation in figure 4.34 and the statistical analysis in table 4.33, show that there were no significant differences between all treated groups and the control group.

Sample	Hatching time (days)
CTR	2.1 ± 0.2
AMOX	2.1 ± 0.2
CBZ	2.3 ± 0.3
MIX	2.1 ± 0.3

Table 4.32: Hatching time.

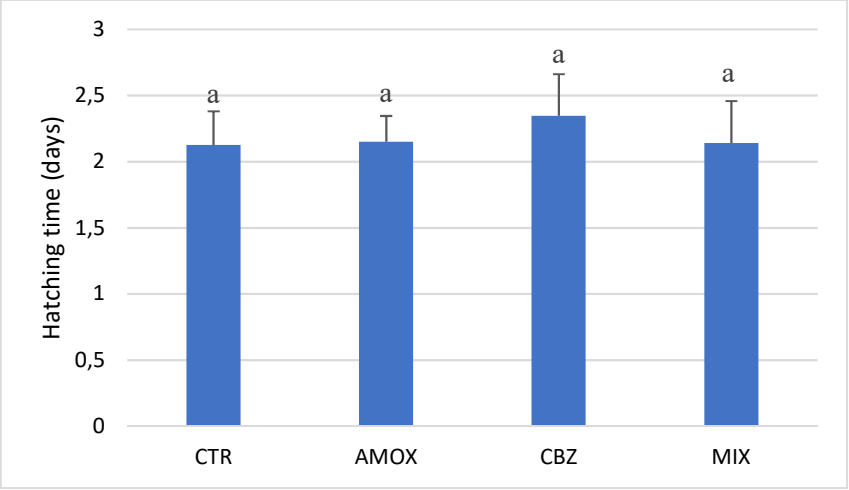

Figure 4.34: Hatching time.
Same letter indicate that the means are not statistically different (p>0.05).

Variation origin	SQ	gdl	MQ	F	p-Value	F crit
Inter groups	0,389498	3	0,129833	1,716565	0,177426668	2,816466
Intra groups	3,327944	44	0,075635			
Total	3,717442	47				

Table 4.33: Statistical analysis and p-value obtained on hatching time.

4.7 Ecotoxicological test: second generation

As in the first generation survival of *T. fulvus* was not affected by exposure to the two pharmaceutical compounds and their mixture. In the second generation the developmental time from nauplii to

copepodite was around 5 days in the control and in all treatments as in the first generation (ANOVA, p>0.05).

In relation to the other end points considered, results obtained were very different. Firstly, we consider the time taken by the females to reach maturity. Data obtained were reported in table 4.34. Statistical analysis, reported in table 4.35, shows that there is a significant difference between the control and the other samples. Particularly, the difference is between the control and the mix sample, as reported in figure 4.35.

Sample	Maturity (days)
CTR	10.7 ± 0.5
AMOX	11.1 ± 0.5
CARBA	10.9 ± 0.8
MIX	11.6 ± 0.8

Table 4.34: Appearance day of ovigerous females in treatment groups.

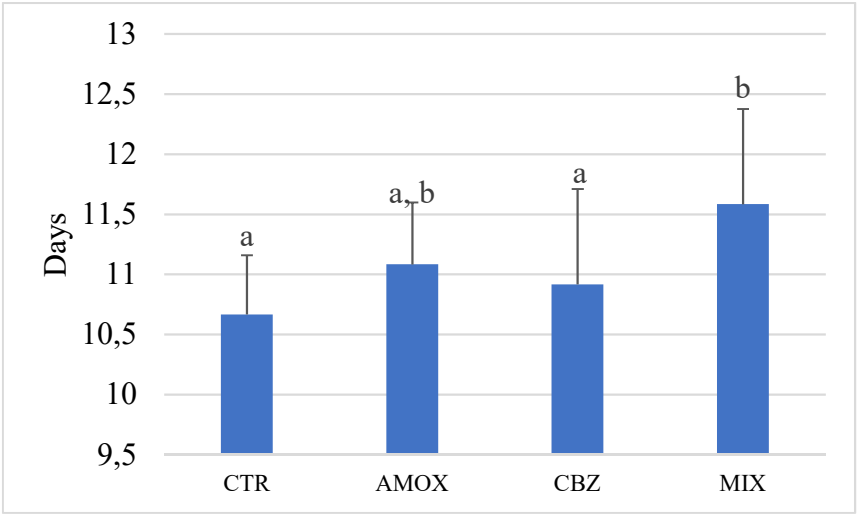

Figure 4.35: Appearance day of ovigerous females in treatment groups. Same letter indicate that the means are not statistically different (p>0.05).

Variation origin	SQ	gdl	MQ	F	p-Value	F crit
Inter groups	5.395833	3	1.798611	4.075823	0.012231	2.816466
Intra groups	19.41667	44	0.441288			
Total	24.8125	47				

Table 4.35: Statistical analysis and p-value obtained on appearance day of ovigerous females in treatment groups.

The cumulative sum of total nauplii produced by all tested females (n=12) at the end of experiment are 1784 for the control, 1332 for amoxicillin, 987 for carbamazepine and 566 in the binary mixture, figure 4.36.

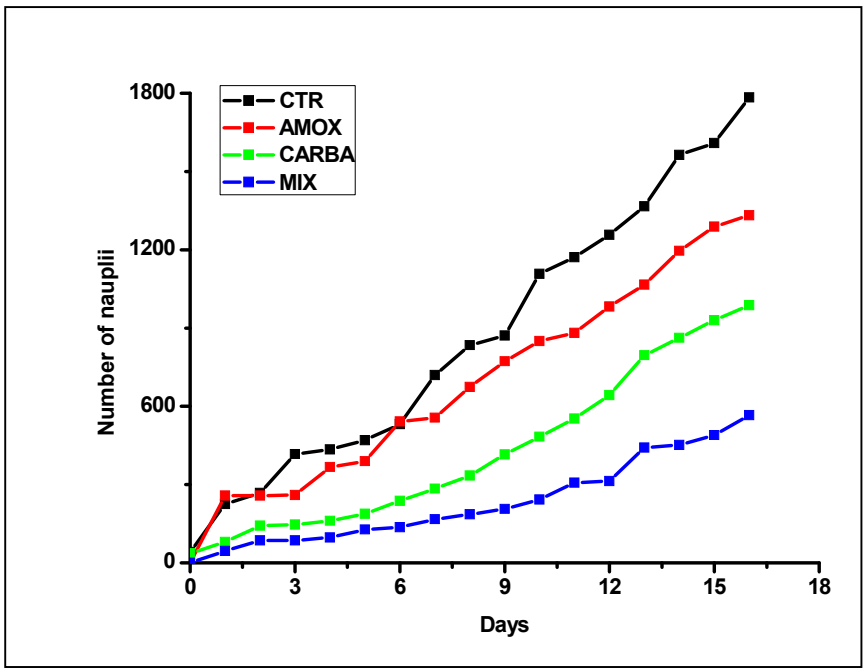

Figure 4.36: Cumulative sum of nauplii produced by females (n=12).

Unlike the first generation the mean total number of nauplii generated by each female on day 28, was reduced not only in carbamazepine, but also

in the mixture table 4.36, and figure 4.37. From the statistical analysis reported in table 4.37 it is observed that the differences were significant ($p > 0.05$).

Sample	Mean total number of nauplii/female
CTR	154 ± 32
AMOX	151 ± 47
CBZ	80 ± 35
MIX	77 ± 29

Table 4.36: Mean total number of nauplii per female on day 28.

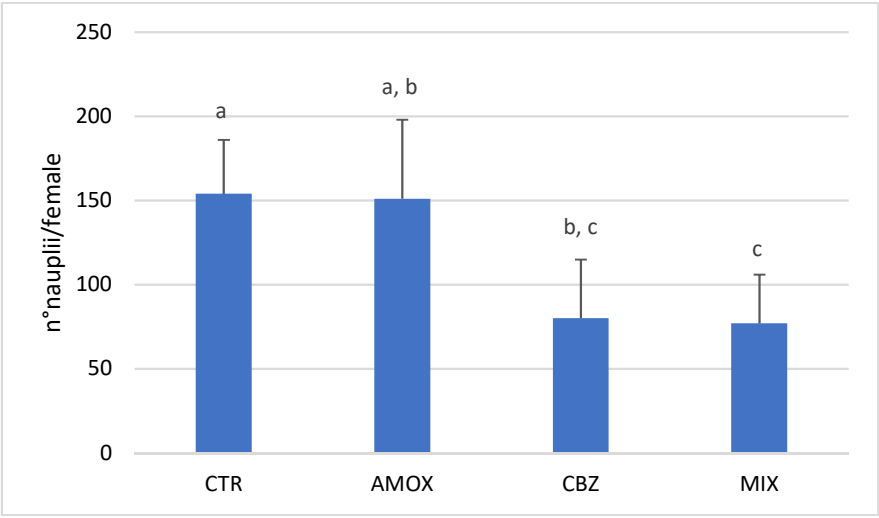

Figure 4.37: Mean total number of nauplii per female on day 28.
Same letter indicate that the means are not statistically different ($p>0.05$).

Variation origin	SQ	gdl	MQ	F	p-Value	F crit
Inter groups	66792.9	3	22264.3	6.733652	0.000775	2.816466
Intra groups	145482.6	44	3306.422			
Total	212275.5	47				

Table 4.37: Statistical analysis and p-value obtained on the mean total number of nauplii for female.

The second step was to evaluate the average number of nauplii per brood generated by female; the results obtained for each group are shown in table 4.38 and figure 4.38. As in the previous case, the statistical analysis shows that the differences in the number of births are significant, as reported by the data in table 4.39. Particularly, the significant difference is between the control and the carbamazepine sample and between the control and mix samples.

Sample	Mean number of nauplii/brood
CTR	26 ± 3
AMOX	25 ± 5
CARBA	18 ± 7
MIX	13 ± 4

Table 4.38: Average number of nauplii produced per brood.

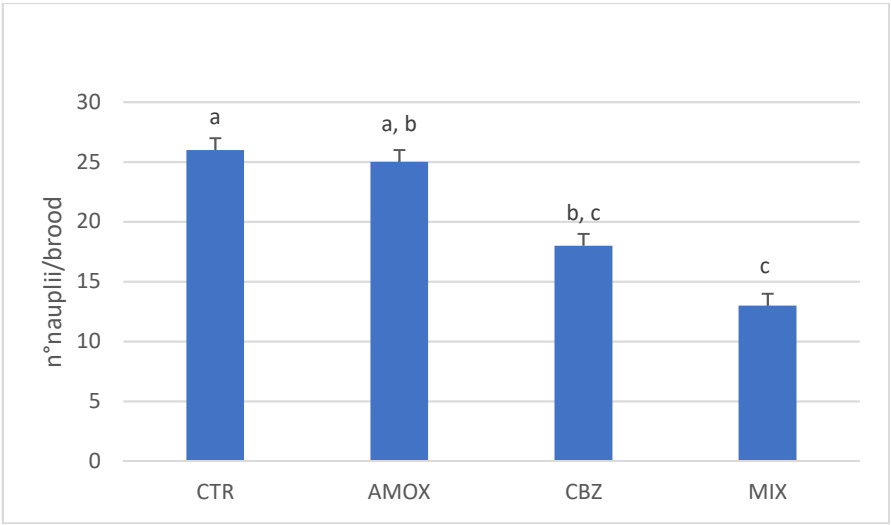

Figure 4.38: Average number of nauplii produced per brood.
Same letter indicate that the means are not statistically different (p>0.05).

Variation origin	SQ	gdl	MQ	F	p-Value	F crit
Inter groups	1323.636	3	441.2122	6.026879	0.001568	2.816466
Intra groups	3221.126	44	73.20741			
Total	4544.762	47				

Table 4.39: Statistical analysis and p-value obtained on the average number of nauplii per brood.

From the table 4.39 we can observe that between carbamazepine and binary mixed there isn't a significant difference, so we can deduce that the variation of the average number of nauplii in the binary mix is mainly determined, if not at all, by the presence of carbazepine.

The next parameter we evaluated was the number of broods for female. Data obtained was showed in table 4.40 and figure 4.39.

Sample	N° broods per female
CTR	6.6 ± 0.6
AMOX	5 ± 1
CARBA	6.1 ± 0.9
MIX	5.5 ± 0.8

Table 4.40: Number of broods for female.

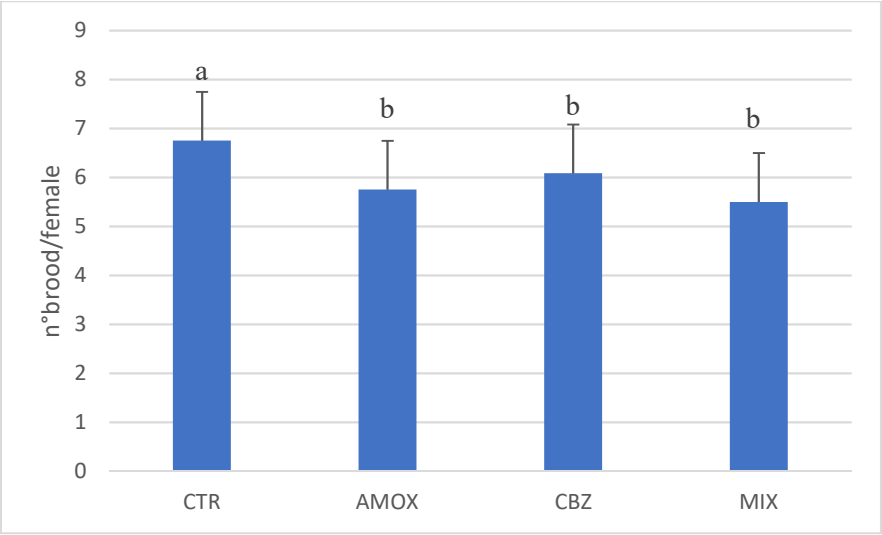

Figure 4.39: Number of broods for female.
Same letter indicate that the means are not statistically different (p>0.05).

The statistical analysis, reported in table 4.41, shows that there is a significant difference between the control and the other samples.

Variation origin	SQ	gdl	MQ	F	p-Value	F crit
Inter groups	11.16667	3	3.722222	4.988156	0.004589	2.816466
Intra groups	32.83333	44	0.746212			
Total	44	47				

Table 4.41: Statistical analysis and p-value obtained on number of broods for female

Next step was to evaluate the average hatching time; the results obtained were reported in table 4.42 and figure 4.40.

Sample	Hatching time (days)
CTR	2.0 ± 0.2
AMOX	2.3 ± 0.3
CARBA	2.1 ± 0.3
MIX	2.1 ± 0.3

Table 4.42: Average hatching time in each treatment.

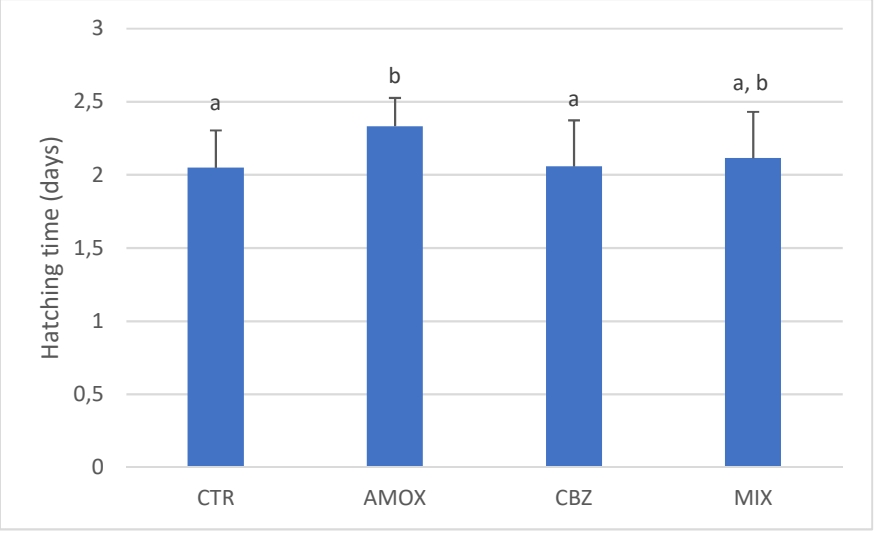

Figure 4.40: Hatching time.
Same letter indicate that the means are not statistically different (p>0.05).

The statistical analysis, reported in table 4.43, shows that there are no significant differences between the treated groups and the control.

Variation origin	SQ	gdl	MQ	F	p-Value	F crit
Inter groups	0.629153	3	0.209718	2.321853	0.08817	2.816466
Intra groups	3.974229	44	0.090323			
Total	4.603381	47				

Table 4.43: Statistical analysis and p-value obtained on the average hatching time.

4.8 Ecotoxicological test: discussion

Pharmaceuticals represent a class of emerging contaminants continuously discharged, through domestic and industrial wastewater effluents, into aquatic systems. These compounds could act as persistent substances because of their continual release from this source, as well as from their physical-chemical characteristics [45]. The potential biological activity of pharmaceuticals present in aquatic environments may induce changes in key physiological functions of exposed species, including those related to reproduction. Concerning crustaceans, the existing knowledge about the toxic effects of carbamazepine and amoxicillin is limited to a few model species, as *Daphnia magna* and *Gammarus pulex* [103,104,122-128]. The aim of this work was to investigate the chronic toxicities of two drugs, carbamazepine and amoxicillin alone and in binary mixture, across two generatios of *T. fulvus*. The reproductive capacity expressed in the various life-traits (mating, appearance of egg sacks, number of broods and size of the broods, ...) constitutes a sensitive indicator for the survival of a species and can therefore also be a useful parameter for the evaluation of the environmental risk induced by phenomena of chemical contamination. The results obtained show a clear difference between the first and second generation. The experimental results obtained show that both in the first and second generation the combination of the two drugs influences the

appearance of the first female ovigera, which appears with a delay of about one day compared to the control group, tables 4.24 and 4.34. Probably there was a synergistic effect between the two drugs because of, alone they do not determine any effect in relation to the time of maturation, instead together they succeeded in interfering significantly with the *T. fulvus* hormonal system determining a delay in maturation. The cumulative sum of the nauplii, figures 4.30 and 4.36, showed that in the first generation there are no significant effects, while in the second one the effects were observed starting from the second day. In particular, it is observed that, while on the second day we have a decrease of nauplii, compared to the control, respectively of 3.73% for amoxicillin, 47.01% for carbamazepine and 67.91% for the mix; on the last day of control we have a decrease of 25.34% for amoxicillin, 44.68% for carbamazepine and 68.27% for the mix. The appearance of alterations only in the second generation leads us to suppose that the exposure of animals to drugs, throughout their life cycle, determines not only hormonal dysfunctions, but also deeper alterations, such as genetic ones. However, at the moment this remains only a hypothesis that will have to be demonstrated. The average number of broods per female is also reduced in treatments, tables 4.30 and 4.40. In particular, in the first generation we have a 10.4% decrease for carbamazepine and 6.5% in the mix. This behavior can be explained considering that carbamazepine is a neuro-active drug, a potential endocrine disruptor in fish [125,129] and can cause inhibition of molting, delayed reproduction, and reduced fecundity in *D. similis* [84]. The interfering action of carbamazepine with the hormonal system of crustaceans has been reported by several articles, indeed, in some articles was reported that the length of DMS [130], the total number of litters, and the reproductive cycle were significantly inhibited after

exposure to carbamazepine and the intrinsic population growth rate decreased significantly [126]. The precise mode of carbamazepine action is not entirely clear in the invertebrates; some researches indicate that this pharmaceutical modulates the voltage of sodium channels in mussel cells [127,131,132], as well as induces an increment of mussel hemocyte death and an increase of superoxide anion and nitric oxide concentrations [128]. The endocrine system of crustaceans (the methylfarnesoate juvenoid hormone and the 20-hydroxyecdysone ecdysteroid hormone (20-HE)) regulates various physiological functions, of which depends the survival of the species, such as reproduction, sex differentiation, growth, and embryonic development. Carbamazepine, between 10 and 200 μg/L, act on the reproduction of daphnids by decreasing the number of juveniles produced by female, producing alterations in sex determination, and developing abnormalities in embryos exposed to this compound through the mother [45]. Another considered effect was the average hatching time, tables 4.32 and 4.42. In the control group, the average hatching time was 2.1 ± 0.2 days, in accordance with the value of 2.2 days reported in the literature [83]. In treated females, we found similar values 2.2 ± 0.2 for amoxicillin, 2.3 ± 0.3 for carbamazepine and 2.1 ± 0.3 for the mix. The same trend was recorded with the second generation (control 2.0 ± 0.2, amoxicillin 2.3 ± 0.3, carbamazepine 2.1 ± 0.3 and mix 2.1 ± 0.3).

Conclusion

In this part of thesis, new LC-MS/MS method was developed and validated for determining and quantifying 12 drugs belonging to different pharmaceutical classes: amoxicillin, erythromycin, clarithromycin, omeprazole, metformin, carbamazepine, acetylsalicylic acid, ibuprofen, diclofenac, naproxen, estradiol and ethinyl estradiol.

Optimization of chromatographic separation on a reverse phase column has predicted the use of a new triphasic gradient (water, acetonitrile and acidified water with 0.1% of formic acid) for the determination of amoxicillin, erythromycin, clarithromycin, omeprazole, metformin, carbamazepine and the use of a biphasic gradient (water, acetonitrile) for analysis of acetylsalicylic acid, ibuprofen, diclofenac, naproxen, estradiol and ethinyl estradiol. The performance of the method, in accordance with the EURACHEM guidelines, has been evaluated in terms of linear range, precision, limits of detection and quantification, recovery and measurement uncertainty. The accuracy of the method was lower than the reference value of the 30% (0.98% -11.91% repeatability, and 3.33% -15.66% intermediate repeatability), according to the method EPA. Recovery was in the 70-118% range, indicative of good accuracy of the method. The optimized and validated method allows to detect concentrations in trace of omeprazole, carbamazepine, erythromycin, clarithromycin. For these drugs the linear range (0.00l-200 µg/L), as well as the values of the limit of detection and quantification (LOD: 0.0001-0.0026 µg/L; LOQ: 0.004-0.0089 µg/L), were suitable for the use of the method in the field of trace concentrations. For each drug, all the parameters were found to be compatible to the values reported by the EPA method and those reported in the Watch list, as well as with the data reported in the literature. After optimization, method was used with

success in the analysis of selected drugs in waste water samples taken from the Potenza purification plant (Basilicata, Italy). The results obtained have confirmed that conventional wastewater treatment processes do not degrade most pharmaceuticals products.

Then, we select two drugs of those analyzed by LC-MS/MS method and we study the toxicological effects that they have on the species *Tigriopus fulvus*. The selected drugs are carbamazepine and amoxicillin, which were found in waste water treatment plant of the Potenza village (Basilicata, Southern Italy). In order to know the toxicological action that these drugs have on the species under study, we performed a chronic test on two successive generations of *T. fulvus*. The end-points we monitored were time of maturation, number of nauplii per female, average number of nauplii per brood, number of broods per female and hatching time.

The results obtained show that in the first generation the toxic effect of amoxicillin is not evident, while the presence of carbamazepine affects the number of broods. In the second generation, amoxicillin once again appears to give no visible toxic effect, while carbamazepine shows obvious toxic effects not only on the number of broods, but also on the number of nauplii generated.

From the obtained data, therefore, it can be assumed that carbamazepine is a potential endocrine disruptor not only of fish, but also of *T. fulvus* and can cause delayed reproduction, and reduced fecundity not only in *D. similis* but also in *T. fulvus.*

References

[1] M. Gavrilescu, K. Demnerovà, J. Aamand, S. Agathos, F. Fava, New biotechnology, 32 1 (2015) 147.

[2] M. Gros, M. Petrović, D. Barceló, Talanta, 70 4 (2006) 678.

[3] L. J. Carter, E. Harris, M. Williams, J. J. Ryan, R. S. Kookana, A. B. A. Bo, J. Agric. Food Chem., 62 4 (2014) 816.

[4] K. Fent, A. A. Weston, D. Caminada, Aquat. Toxicol., 76 (2006) 122.

[5] W. Chen, J. Xu, S. Lu, W. Jiao, L. Wu, A. C. Chang, Chemosphere, 93 (2013) 2621.

[6] WHO Model List of Essential Medicines 20th list (2017).

[7] A. J. Ebele, M. Abou-Elwafa Abdallah, S. Harrad, Emerging Contaminants, 3 1 (2017) 1.

[8] S. Castiglioni, R. Bagnati, D. Calamari, R. Fanelli, E. Zuccato, J. chromatogr. A, 1092 2 (2005) 206.

[9] E. Zuccato, D. Calamari, M. Natangelo, R. Fanelli, The lancet, 355 9217 (2000) 1789.

[10] Consuption for ATC I level. Federfarma (Federazione nazionale unitaria titolari di farmacia).

[11] H. Kanazawa, A. Okada, Y. Matsushima, H. Yokota, S. Okubo, F. Mashige, K. Nakahara, J. Chromatogr. A 949 1 2 (2002) 1.

[12] V. Calisto, M. R. M. Domingues, G. L. Erny, V. I. Esteves, Water res., 45 3 (2011) 1095.

[13] H. N. Mistri, A. G. Jangid, P. S. Shrivastav, J. Pharm. Biomed. Anal., 45 1 (2007) 97.

[14] Y. Jiang, J. Wang, H. Li, Y. Wang, J. Gu, J. Pharm. Biomed. Anal., 43 4 (2007) 1460.

[15] M. Petrović, M. D. Hernando, M. S. Diaz-Cruz, D. Barceló, J. Chromatogr. A 1067 1 2 (2005) 1.

[16] D. A. Vohner, J. P. M Hui, Rapid communications in mass spectrometry 12 3 (1998) 123.

[17] List of the 20 most prescribed active ingredients in Italy. Federfarma (Federazione nazionale unitaria titolari di farmacia.

[18] S. Grujic, T. Vasiljevic, M. Lause-vic, T. Ast., Rapid Communications in Mass Spectrometry: An International Journal Devoted to the Rapid Dissemination of Up to the Minute Research in Mass Spectrometry, 22 1 (2008) 67.

[19] L. Ferrando-Climent, N. Collado, G. Buttiglieri, M. Gros, I. Rodriguez-Roda, S. Rodriguez-Mozaz, D. Barceló, Sci. Total Environ. 43 8 (2012) 404.

[20] X.-S. Miao, B. G. Koenig, C. D. Metcalfe, J. Chromatogr. A 952 l 2 (2002) 139.

[21] EPA Method 1694, Pharmaceutical and Personal Care Products in Water, Soil, Sediments and Biosoilids by HPLC/MSMS, (2007).

[22] 2013/39/UE.

[23] J. Rossmann, S. Schubert, R. Gurke, R. Oertel, W. Kircha, J. Chromatogr. B 969 (2014) 162.

[24] E. Ngumba, P. Kosunen, A. Gachanja, T. Tuhkanen, Anal. Methods, 8 37 (2016) 6720.

[25] A. Werner, E. Scherwenk, W. Buchberger, J. Chromatogr. A 910.1 (2001) 69.

[26] S. Marchese, D. Perret, A. Gentili, R. Curini, F. Pastori, Chromatographia, 58 5 6 (2003) 263

[27] J. B. Quintana, T. Reemtsma, Rapid communications in mass spectrometry, 18 7 (2004) 765.

[28] M. E. Dasenaki, N. S. Thomaidis, Anal. Bioanal. Chem., 407 15

(2015) 4229.

[29] M. J. Hilton, K. V. Thomas, J. Chromatogr. A, 1015 1 2 (2003) 129.

[30] F. A. Caliman, M. Gavrilescu, Water, 37 (2009) 277.

[31] X. Wu, J. L. Conkle, F. Ernst, J. Gan., Environ. Sci. Technol., 48 (2014) 11286.

[32] B. D. Blair, J. P. Crago, C. J. Hedman, R. D. Klaper, Chemosphere 93 (2013) 2116.

[33] H.-R. Buser, T. Poiger, M. D. Müller, Environ. Sci. Technol. 32 (1998) 3449.

[34] A. L. Boreen, W. A. Arnold, K. McNeill, Aquat. Sci. 65 (2003) 320.

[35] J. C. Carlson, M. I. Stefan, J. M. Parnis, C. D. Metcalfe, Water Res. 84 (2015) 350.

[36] S. Chiron, C. Minero, D. Vione, Environ. Sci. Technol. 40 (2006) 5977.

[37] Società italiana medicina ambientale “Farmaci e ambiente: l’Ecofarmacovigilanza nel contesto globale.

[38] C. Mimeault, A. J. Woodhouse, X. S. Miao, C. D. Metcalfe, T. W. Moon, V. L. Trudeau, Aquat. Toxicol. 73 (2005) 44.

[39] G. Vernouillet, P. Eullaffroy, A. Lajeunesse, C. Blaise, F. Gagne, P. Juneau, Chemosphere, 80 (2010) 1062.

[40] B. Quinn, F. Gagné, C. Blaise, Sci. Total Environ., 389 (2008) 306.

[41] A. Bahlmann, J.J. Carvalho, M.G. Weller, U. Panne, R.J. Schneider, Chemosphere, 89 (2012) 1278.

[42] A. Almeida, V. Calisto, V.I. Esteves, R.J. Schneider, A.M.V.M. Soares, E. Figueira, R. Freitas, Aquat Toxicol, 156 (2014) 74.

[43] T.A. Ternes, Water Res., 32 (1998) 3245.

[44] Y. Zhang, S. Geissen, C. Gal, Chemosphere, 73 (2008) 1151.

[45] A. L. Oropesa, A. M. Floro, P. Palma, Environ. Sci. Pollut. Res., 23 (2016) 17311.

[46] C. G. Daughton, T. A. Ternes, Environmental Health Perspectives, 107 6 (1999) 907.

[47] M. D. Hernando, M. Mezcua, A. R. Fernández-Alba, D.Barceló, Talanta, 69 2 (2006) 334.

[48] S. Raisuddin, K. W. H. Kwok, K. M. Y. Leung, D. Schlenk, J. S. Lee, Aquat. Toxicol., 82 3 (2007) 161.

[49] M. D Ohman, H. J. Hirche, Nature, 412 6847 (2001) 638.

[50] K.-W. Lee, W. J. Shim, O. Y. Kwon, J.-H. Kang, Environ. Sci. Technol., 47 (2013) 11278.

[51] W. Schonfeld, H. A. Kirst, Macrolide Antibiotics, Series editors, Switzerland (2002).

[52] D. H. Peters, S. P. Clissold, Drugs, 44 1 (1992)117.

[53] L. Thomas, A. Lemke, D. A. Williams, FOYE'S Principi di Chimica Farmaceutica, 6 Ed, Piccin, US (2014).

[54] WHO Model List of Essential Medicines (19th List).

[55] K. Deirdre, Diseases of the liver and biliary system in children, 3 Ed., Wiley Blackwell, UK (2008).

[56] A. Jones, Chemistry: An Introduction for Medical and Health Sciences, John Wiley & Sons, UK (2015).

[57] T. D. Warner, J. A. Mitchell, Proceedings of the National Academy of Sciences of the United States of America, 99 21 (2002) 13371.

[58] World Health Organization model list of essential medicines: 21st list 2019.

[59] The Top 300 of 2019, Clin. Calc.

[60] W. Stillwell, An Introduction to Biological Membranes, 2 Ed., Elsevier BV, UK (2016).

[61] D. T. Carrell, C. M. Peterson, Reproductive endocrinology and infertility, Springer, NY (2010).

[62] B. K. Sharme, Water Pollution, Goel Publishing House, India (2005).

[63] S. K. Agarwal, Water Pollution, APH Publishing Corporation, New Delhi (2009).

[64] APAT – L'Ecotossicologia negli ambienti acquatici, Prima ricognizione dello stato dell'arte nelle Agenzie, Rapporti 71/2006.

[65] C.H. Walker, R.M. Sibly, Principles of Ecotoxiology 4 ed., CRC press Taylor & Francis Group, NY (2012).

[66] D. J. Hoffman, G. A. Burton, B. A. Rattner, Handbook of Ecotoxicology 2 ed., CRC press Taylor & Francis Group, NY (2012).

[67] D. Connell, P. Lam, B. Richardson, R. Wu, Introduction of ecotoxicology, Blackwell publishing, UK (1999).

[68] J. Paasivirta, Chemical ecotoxicology, Lewis publishers, NY (1991).

[69] B. Clasen, R. de Moura Lisboa, Soil contamination and alternatives for sustainable development, IntechOpen, 13-33.

[70] F. A. Barile, Principles of toxicology testing, CRC Press, NW (2007).

[71] M. E. Tomlin, Pharmacology & Pharmacokinetics, Springer, UK (2010).

[72] G. K. Ostrander, The handbook of experimental animals, the laboratory fish, Academic Press, USA (2000).

[73] T. H. Hutchinson, T. D. Williams, G. J. Eales, Mar. Environ. Res., 38 (1994) 275.

[74] L. Pane, G. L. Mariottini, A. Lodi, E. Giacco, Heavy metal pollution, Nova science publishers inc. NW (2008).

[75] A. Carli, L. Pane, L. Casareto, S. Bertone, C.Pruzzo, Appl. Environ. Microbiol., (1993) 1960.

[76] L. Pane, L. De Nuccio, C. Pruzzo, A. Carli, J. of Biolog. Res., 76 (2000) 37.

[77] E. Prato, I. Parlapiano, F. Biandolino, Chem. Ecology, 29 7 (2013) 635.

[78] Dgr 4170 of 30th December 2005.

[79] Regional law n. 19 of 4th April 2003.

[80] Ddg 323 of 27th June 2005.

[81] UNICHIM method 2396:2014.

[82] J. Mauchline, Advances in marine biology, the biology of calanoid copepods, Accademic Press, USA (1998).

[83] M. A. Todaro, O. Faraponova, F. Onorati, D. Pellegrini, P. Tongiorgi, Biol. Mar. Medit., 8 1 (2001) 896.

[84] O. Faraponova, E. Giacco, F Biandolino, E. Prato, F. Del Prete, A. Valenti, S. Sarcina, A. Pasteris, A. Montecavalli, S. Comin, C. Cesca, M. Francese, M. Cigar, V. Piazza, F. Falleni, I. Lacchetti, Ecotoxicol. Environ. Safety 124 (2016) 309.

[85] F. Biandolino, I. Parlapiano, O. Faraponova, E. Prato, Ecotoxicol. Environ. Safety 147 (2018) 327.

[86] O. Faraponova, M. A. Todaro, F. Onorati, M. G. Finoia, Biol. Mar.Medit. 10 2 (2003) 679.

[87] N. J. K. Simpson, Solid phase extraction, principles, techniques and applications, Marcel Dekker Inc., NY (2000).

[88] A. Żwir-Ferenc, M. Biziuk, Polish J. of Environ. Stud., 15 5 (2006) 677.

[89] D. A. Skoog, D. M. West, F. J. Holler, S. R. Crouch, Fundamentals of Analytical Chemistry, 9 Ed., USA (2014).

[90] W. J. Lough, I. W. Wainer, High performance liquid chromatography, fundamental principles and practice.

[91] E. Lundanes, L. Reubseet, T. Greibrokk, Chromatography, basic principles, sample preparation and related methods, Wiley-VCH, Germani (2014).

[92] E. Katz, R. Eksteen, P. Schoenmakers, N. Miller, Handbook of HPLC, Marcel Dekker Inc, NY (1998).

[93] J. H. Gross, Mass spectrometry, a textbook, 2 Ed., Germany (2004).

[94] R. M. Silverstein, G. C. Bassler, T. C. Morrill, Spectrometric Identification of Organic Compounds, Wiley, USA (2015).

[95] T. Cheng, Y. Zhao, X. Li, F. Lin, Y. Xu, X. Zhang, Y. Li, R. Wang, J. Chem. Inf. And Modeling 47 6 (2007) 2140.

[96] Eurachem guide, The Fitness for Purpose of Analytical Methods, 2 Ed, (2014).

[97] J. Miller, J. C. Miller, Statistics and chemometrics for analytical chemistry, 6 Ed., Edinburgh (2010).

[98] P. Araujo, J. Chromatogr. B. Anal. Technol. Biomed. Life Sci. 877 (2009) 2224.

[99] G. A. Shabir, J. Chromatogr. A, 987 1-2 (2003) 57.

[100] V. J. Barwick, S. L. R. Ellison, Analyst, 124 7 (1999) 981.

[101] M. Patriarca, F. Chiodo, F. Corsetti, B. Rossi, A. Menditto, M. Sega, M. Plassa, Quantificazione dell'incertezza nelle misure analitiche, 2 Ed. della guida Eurachem/Citac CG 4, Rapporti ISTISAN 03/30 (2000).

[102] UNI CEI ENV 13005.

[103] V. Kovacevic, A. J. Simpson, M. J. Simpson, Comp. Biochem.

Physiol. Part D, 19 (2016) 199.

[104] M. Borgatta, L. A. Decosterd, P. Waridel, T. Buclin, N. Chèvre, Sci. Total Environ. 520 (2015) 232.

[105] J. P. Williams, J. H. Scrivens, Rapid Communications in Mass Spectrometry: An International Journal Devoted to the Rapid Dissemination of Up-to-the-Minute Research in Mass Spectrometry, 19 24 (2005) 3643.

[106] H. Kuhl, Climacteric, 8 suppl 19 3 (2005) 3.

[107] M. Oettel, E. Schillinger, Estrogens and antiestrogens II, - springer, Berlin (1999).

[108] G. Evan, E. L. Sutton, Med. Cli. North Am., 99 3 (2015) 479.

[109] D. Shoupe, F. P. Haseltine, Contraception, Springer-Verlag, NY (1993).

[110] M. Petrovic, M. Gros, D. Barcelò, J. Chromatogr. A, 1124 1 2 (2006) 68.

[111] E. Gregori, M. Patriarca, M. Sega, Eurachem Guide, Suitability for the purpose of analytical methods. Guide for laboratories on method validation and related topics, 2 Ed., (2014).

[112] S. Balazamo, V. Ubaldi, M. Peleggi, P. Dellavedova, E. Calabretta, L. Colzani, S. De Martin, I. Martinuzzi, P. Paris, M. Potalivo, M. G. Simeone, M. Vitelli, Primo monitoraggio delle sostanze del1'Elenco di Controllo (Watch List), ISPRA Rapporti 260/2017, Marzo (2017).

[113] B. Magnusson, U. Ömemark (eds.) Eurachem Guide: The Fitness for Purpose of Analytical Methods - A Laboratory Guide to Method Validation and Related Topics, 2 Ed., (2014).

[114] Analytical Methods Committee, Analyst 119 (1994) 2363.

[115] A. L. N. van Nuijs, I. Tarcomnicu, W. Simons, L. Bervoets, R. Blust, P. G. Jorens, H. Neels, A. Covaci, Anal. Bioanal. Chem., 398 5 (2010) 2211.

[116] F. T. Peters, O. H. Drummer, F. Musshoff, Forensic science international, 165 2 (2007) 216.

[117] C. Afonso-Olivares, Optimization of a solid phase extraction combinated with liquid chromatography tandem mass spectrometry procedure to simultaneous determination of pharmaceuticals compounds in treated water samples, (2013).

[118] Guide to the Expression of Uncertainty in Measurement ISO, Geneva (1993).

[119] UNI CEI EN ISO/IEC 17025:2018.

[120] 1° semester 2018, List of the 50 best-selling non-prescription medicines at pharmacies open to the public and commercial establishments pursuant to art. 5 of the Law Decree 223/2006, Ministero della Salute.

[121] World Health Organization, Pharmaceuticals in drinking-Water (2012).

[122] H. Chen, X. Gu, Q. Zeng, Z. Mao, Int. J. Environ. Res. Public Health, 16 (2019) 209.

[123] C. Rivetti, B. Campos, C. Barata, Aquat. Toxicol., 170 (2016) 289.

[124] J. Forget-Leray, I. Landriau, C. Minier, F. Leboulenger, Ecotoxicol. Environ. Safety 60 (2005) 288.

[125] A. Josa, G. Repetto, J. C. Rios, M. J. Hazen, M. L. Molero, A. del Peso, M. Salguero, P. Fernandez-Freire, J. M. Perez-Martın, A. Camean, Toxicol. In Vitro 17 (2003) 525.

[126] M. Lurling, E. Sargant, I. Roessink, Life-History Consequences for Daphnia pulex Exposed to Pharmaceutical Carbamazepine, Wiley Periodicals, Inc., (2006) 172.

[127] H. J. De Lange, W. Noordoven, A. J. Murk, M. Lurling, E. T. H. M. Peeters, Aquat. Toxicol. 78 (2006) 209.

[128] A. G. Trovo, R. F. Pupo Nogueira, A. Aguera, A. R. Fernandez

Alba, S. Malato, Water Res., 45 (2011) 1394.

[129] S. Yan, M. Wang, J. Zha, L. Zhu, W. Li, Q. Luo, J. Sun, Z. Wang, Environ. Sci. Technol., 2 (2018) 886.

[130] Y. Tian, X. Xia, J. Wang, L. Zhu, J. Wang, F. Zhang, Z. Ahmad, Bulletin of Environ. Contamination Toxicol., 103 (2019) 723.

[131] L. Martin-Diaz, S. Franzellitti, S. Buratti, P. Valbonesi, A. Capuzzo, E. Fabbri, Aquat. Toxicol., 94 (2009) 177.

[132] P. Tsiaka, V. Tsarpali, I. Ntaikou, M.N. Kostopoulou, G. Lyberatos, S. Dailianis, Ecotoxicol., 22 8 (2013) 1208.

Concluding remarks

The overall aims of this research were the development of different methods for the detection of some emerging pollutants and the evaluation of toxic effects that some of these molecules produce on *Tigriopus fulvus*. In the Part A of this work two modified electrodes, the first one based on polyvinyl alcohol (PVA) structured with particles of oxidized graphene (GO), and the second one on betaine-Pt on glassy carbon, were developed and characterized by voltammetric and spectroscopic techniques.

PVA based electrode was tested for the determination of few emerging pollutants, i.e. paracetamol, ibuprofen, acetylsalicylic acid, piroxicam and nimesulide, showing a good electrocatalytic character in a neutral environment. In addition, DPV (Differential Pulse Voltammetry) analysis showed interesting analytical performances in wide ranges of potentials usefull for analytical purposes, i.e. paracetamol -0.1 V ÷ 1.1 V, acetyl salicylic acid. -0.5 V ÷ 1.2 V, piroxicam. 0.2 V ÷ 0.7 V, nimesulide -1.4 V ÷ 0.7 V and ibuprofen 0 V ÷ 1.4 V.

A preliminary evaluation of the performances of betaine-Pt based electrode in acidic conditions showed good electroanalytical response, especially with respect to a classical unmodified graphite electrode.

In the second part of the work, a new LC-MS/MS method was optimized, validated and used for determining 12 drugs (amoxicillin, erythromycin, clarithromycin, omeprazole, metformin, carbamazepine, acetylsalicylic acid, ibuprofen, diclofenac, naproxen, estradiol and ethinyl estradiol) in water samples collected in a Potenza purification plant (Basilicata, Southern Italy).

For each drug, all the parameters were found to be compatible to the values reported by the EPA:1694 method and those reported in the

Watch list's procedure (2017), as well as with the data reported in the literature. The results confirmed that pharmaceuticals occurring in municipal wastewater are not efficiently eliminated by conventional wastewater treatment processes. Then, carbamazepine and amoxicillin, which were found in waste water treatment plant of the Potenza village (5µg/L carbamazepine and 2µg/L amoxicillin) were used to evaluate the toxicological effects on the species *Tigriopus fulvus*. In detail, a chronic test on two successive generations of *T. fulvus* showed that carbamazepine could be considered a potential endocrine disruptor since a delayed reproduction, and a reduced fecundity in *T. fulvus* was observed.

In conclusion, the results of the present study confirmed that pharmaceuticals occurring in municipal wastewater are not efficiently eliminated by conventional wastewater treatment processes. In addition, thanks to toxicity study on *T. fulvus*, carbamazepine could be considered a potential endocrine disruptor since a delayed reproduction and a reduced fecundity in *T. fulvus* was observed.

Appendix A

IUPAC name of analyzed molecules

Acetylsalicylic acid: 2-(acetiloxy)benzoic acid

Amoxacillin: (2S,5R,6R)-6-[[(2R)-2-amino-2-(4-hydroxyphenyl)acetyl]amino]-3,3-dimethyl-7-oxo-4-thia-1-azabicyclo[3.2.0]heptane-2-carboxylic acid

Carbamazepine: benzo[b][1]benzazepine-11-carboxamide

Clarithromycin: 3R,4S,5S,6R,7R,9R,11R,12R,13S,14R)-6-[(2S,3R,4S,6R)-4-(dimethylamino)-3-hydroxy-6-methyloxan-2-yl]oxy-14-ethyl-12,13-dihydroxy-4-[(2R,4R,5S,6S)-5-hydroxy-4-methoxy-4,6-dimethyloxan-2-yl]oxy-7-methoxy-3,5,7,9,11,13-hexamethyl-oxacyclotetradecane-2,10-dione

Diclofenac: 2-[2-(2,6-dichloroanilino)phenyl]acetic acid

Erythromycin: (3R,4S,5S,6R,7R,9R,11R,12R,13S,14R)-6-[(2S,3R,4S,6R)-4-(dimethylamino)-3-hydroxy-6-methyloxan-2-yl]oxy-14-ethyl-7,12,13-trihydroxy-4-[(2R,4R,5S,6S)-5-hydroxy-4-methoxy-4,6-dimethyloxan-2-yl]oxy-3,5,7,9,11,13-hexamethyl-oxacyclotetradecane-2,10-dione

Estradiol: (8R,9S,13S,14S,17S)-13-methyl-6,7,8,9,11,12,14,15,16,17-

decahydrocyclopenta[a]phenanthrene-3,17-diol

Ethinylestradiol: (8R,9S,13S,14S,17R)-17-ethynyl-13-methyl-7,8,9,11,12,14,15,16-octahydro-6H-cyclopenta[a]phenanthrene-3,17-diol

Ibuprofen: 2-[4-(2-methylpropyl)phenyl]propanoic acid

Metformin: 3-(diaminomethylidene)-1,1-dimethylguanidine

Naproxen: (2S)-2-(6-methoxynaphthalen-2-yl)propanoic acid

Nimesulide: N-(4-Nitro-2-fenossifenil)metansolfonammide

Omeprazole: 6-methoxy-2-[(4-methoxy-3,5-dimethylpyridin-2-yl) methylsulfinyl]-1H-benzimidazole

Paracetamol: N-(4-hydroxyphenyl)acetamide

Pyridoxine: 4,5-bis(hydroxymethyl)-2-methylpyridin-3-ol

Piroxicam: 4-hydroxy-2-methyl-1,1-dioxo-N-pyridin-2-yl-1λ6,2-benzothiazine-3-carboxamide

Thiamine: 2-[3-[(4-amino-2-methylpyrimidin-5-yl)methyl]-4-methyl-1,3-thiazol-3-ium-5-yl]ethanol

Scientific production

1. D. Coviello, M. Contursi, R. Toniolo, I. G. Casella, “Electrochemical and spectroscopic investigation of a binary Ni-Co oxide active material deposited on graphene/polyvinyl alcohol composite substrate” Journal of Electroanalytical Chemistry, 791 (2017) 117-123. (DOI: 10.1016/j.jelechem.2017.02.048)

2. D. Coviello, I. G. Casella, “Electrochemical performance of binary Ni-Co particles deposited on graphene oxide/polyvinyl alcohol substrate in alkaline medium” Electrochimica Acta, 261 (2018) 104-112. (DOI: 10.1016/j.electacta.2017.12.082)

3. R. Pascale, G. Bianco, D. Coviello, M. C. Lafiosca, S. Masi, I. M. Mancini, S. A. Bufo, L. Scrano, D. Caniani, “Validation of a LC-MS/MS method for the determination of drugs in watsewater using a three-phase solvent system”, accepted for publication by Journal of Sparation Science in 31/10/2019. (DOI: 10.1002/jssc.201900509)

Acknowledgments

I thank Prof. I. G. Casella† with whom I started this PhD experience. I will never forget the great culture and immense humanity that characterized you.

I thank Prof. Giuliana Bianco for having welcomed me into her research group.

I thank Dr. Michela Contursi for being a solid point of reference in all these years.

I thank Dot. Ermelinda Prato, Dot. Isabella Parlapiano and the CNR-IRSA of Taranto for the support provided to me during the progress of part C of this work.